Design and optimization of the ECOSat satellite requirements and integration

A trade study analysis of vibrational, thermal, and integration constraints

by

Justin Thomas Curran

B.Eng., University of Victoria, 2013

A Thesis Submitted in Partial Fulfillment of the

Requirements for the Degree of

Master of Applied Science

in the Department of Mechanical Engineering

© Justin Thomas Curran, 2014

University of Victoria

All rights reserved. This thesis may not be reproduced in whole or in part, by photocopy or other means, without the permission of the author.

Supervisory Committee

Design and optimization of the ECOSat satellite requirements and integration

A trade study analysis of vibrational, thermal, and integration constraints

by

Justin Thomas Curran

B.Eng., University of Victoria, 2013

Supervisory Committee

Dr. Afzal Suleman (Department of Mechanical Engineering)
Supervisor

Dr. Nikolai Dechev (Department of Mechanical Engineering)
Academic Member

Supervisory Committee

Dr. Afzal Suleman (Department of Mechanical Engineering)
Supervisor

Dr. Nikolai Dechev (Department of Mechanical Engineering)
Academic Member

ABSTRACT:

This thesis presents the design of a working and testable satellite with particular emphasis on the electrical, mechanical, and thermal modelling and performance issues for the ECOSat project in the framework of the Canadian Satellite Design Competition.

In order of importance, based on the design challenges for the satellite structure were the dynamics modelling and analysis, thermal modeling and analysis, and assembly and integration modeling. Both the dynamics and thermal modeling of the satellite were completed using Finite Element Analysis (FEA) in NX with the NASTRAN solver.

The dynamic analysis study was performed first since it has the primary design driver for the structure. These frequencies are of concern due to the 90 Hz or greater fundamental frequency requirement for each axis. The dynamic modes of the satellite structure had the largest influence not only on the design of the structure but also its interface to the electronic systems as these had to meet the required testing qualification levels. It was found that the first fundamental frequency appeared near 200 Hz in the XY plane of the structure.

The second study performed was on the thermal modeling of the satellite both for extreme operating conditions in “Hot” and “Cold” cases. Operational limiting cases were identified for the batteries in the cold and hot case study, and the power amplifier for the transmitter was identified for the hot case study. For the batteries to perform satisfactorily for the cold and hot case problem, a metal bracket with an electric heater was added to the design. The heaters were added to the design as a resistive heating

element, the additional thermal coupling from the bracket improved heat transfer during the hot case. A trade study analysis was conducted for the power amplifier. Here, a bi directional heat spreader made of pyrolytic graphite attached to a frame member with high thermal inertia was chosen as the optimal solution.

Finally, the third study performed tested the interface and clearance requirements of the satellite. The synergistic integration of the electrical and mechanical systems required significant attention in order to ensure the successful assembly, integration, and testing of the two systems. The investigation focused on the cabling assemblies of the satellite. Several design iterations were required for the power regulation, transmitter, receiver, modem, and onboard computer systems. Detailed assembly drawings were created for the cabling assembly fabrication prior to the final integration of the electrical and mechanical systems.

The performance simulations show that the satellite systems meet or exceed the required launch qualification tests as well as the thermal cycling requirements for all systems and their components to operate within the manufacturer specified values. Once completely assembled and launched into orbit, the satellite should be able to perform and within its operational and mission requirements in both a sun synchronous or polar orbit at a range of altitudes.

ACKNOWLEDGMENTS

I would like to thank Dr. Afzal Suleman, who provided this unique opportunity to develop and work on the ECOSat project and continue on to complete a MASc. at the University of Victoria. I would also like to thank Larry Reeves for creating the Canadian Satellite Design Challenge and providing myself and all the other participants with the opportunity to pursue a career in the space industry.

Special thanks also goes to all the members of the ECOSat team, it would not have been possible without their dedication and commitment in particular I would like to thank: Nigel Syrotuck, Cass Hussmann, Devin Peltier, Kris Dolberg, Spencer Davis, and Jarrah Bergeron for their expertise and dedication they were and are critical to the current and future success of the project.

TABLE OF CONTENTS

Abstract: i
Acknowledgments iii
Table of Figures viii
List of Tables xi
Table of Equations xi
Acronyms xii
1 Introduction 1
1.1 Background 1
1.1.1 The Canadian Satellite Design Challenge 1
1.1.2 The ECOSat Project 1
1.1.3 Satellite Requirements 2
1.1.4 Satellite Orbital Parameters 3
1.2 Thesis Overview 3
1.2.1 Section Organization 4
1.3 My Contributions 5
2 Vibrational Modeling and Qualification 6
2.1 Summary 6
2.2 Introduction 6
2.3 Project Goals 7
2.4 NX Modeling and Assembly 8
2.4.1 Modeling Details 9
2.4.2 Add Component 10
2.4.3 Part Idealization 12
2.4.4 Modeling Problems 12
2.4.5 Finite Element Model 13

2.4.6 3D Meshes 14
2.4.7 2D Meshes 14
2.4.8 1D Elements 16
2.4.9 Additional Objectives 19
2.4.10 Grouping 22
2.4.11 Simulation 23
2.4.12 Constraints 24
2.4.13 Solver Properties 25
2.4.14 Solution Properties 26
2.5 Pre Environmental Testing Simulation Results 27
2.5.1 Constrained at Rail Ends 27
2.5.2 Constrained at Rail Sides 31
2.5.3 Constrained at Rail Ends with PCB's 32
2.6 Previous Vibration Testing Results 34
2.7 2014 Vibration Testing Results 34
2.8 Post Environmental Testing Simulation Results 36
2.9 Conclusion 38
3 Thermal Modeling and Transfer Selection: 39
3.1 Summary 39
3.2 Introduction 40
3.3 Problem Specification: 40
3.3.1 Model Definition 43
3.4 Heat Transfer Methods 45
3.4.1 Bidirectional Heat Transfer 45
3.4.2 Unidirectional Heat Transfer 45
3.4.3 Variable Conductance Heat Pipes 46
3.5 Heat Transfer Method Selection 49

3.5.1 Heat Spreader Material Selection.. 50
3.6 Manufacturer Specific PGS Selection.. 59
3.6.1 Momentive 59
3.6.2 Mint*eq* 60
3.6.3 Panasonic 61
3.6.4 Manufacturer Selection 61
3.7 Testing.. 62
3.8 Conclusion 65
4 Heat Spreader Implementation and Optimization: 67
4.1 Summary 67
4.2 Introduction.. 67
4.3 Problem Specification 68
4.4 Heat Spreader Material Selection 68
4.5 Solid Model.. 69
4.5.1 Additional Modeling 70
4.5.2 Optimization Caveat 70
4.6 Finite Element Model 70
4.6.1 3D Meshes 70
4.6.2 2D Meshes 71
4.7 Simulation Model.. 71
4.7.1 Thermal Load.. 71
4.7.2 Thermal Couplings.. 71
4.7.3 Thermal Constraints.. 73
4.8 FEA Results 74
4.8.1 Initial Findings No PGS 74
4.8.2 Initial Findings with PGS.. 75
4.8.3 Optimization Results.. 77

4.9 Conclusion 80
5 Solid Modeling for Integration 81
5.1 Solid Modeling Summary 81
5.2 Introduction 82
5.3 Electrical Component Creation 83
5.4 Library Creation 88
5.5 Routing 93
5.5.1 Drag and Drop 93
5.5.2 From-To List 96
5.6 Route Checking 98
5.7 Manufacturing Drawings 99
5.8 Conclusion 100
5.8.1 Problems Encountered 100
6 Final Remarks and Future Work 103
6.1 Final Remarks 103
6.2 Future Work 104
7 References 106
Appendix A Random Vibration Specification 109
Appendix B Thermal Vacuum Profile 110
Appendix C 2012 Vibration Testing Results 111
Appendix D 2014 Vibration Testing Results 114

TABLE OF FIGURES

Figure 2.1: Satellite structure with Internal PCB's 7
Figure 2.2: NX Structural Model 8
Figure 2.3: Concentric Constraint 9
Figure 2.4: Center Axis Constraint 10
Figure 2.5: Positioning by Constraint 11
Figure 2.6: Component Preview 11
Figure 2.7: Part Idealization 12
Figure 2.8: 3D Element Mesh 13
Figure 2.9: PCB Assembly with Bolt Connections 15
Figure 2.10: Laminate Structure of PCB with 4 layers 16
Figure 2.11: Bolt Connection Dialogue 17
Figure 2.12: Section Evaluation 18
Figure 2.13: Beam Collector 19
Figure 2.14: Threaded Bolt Spider Connection 20
Figure 2.15: Standoff Illustration 21
Figure 2.16: Spider Connection 21
Figure 2.17: Sub Grouping 22
Figure 2.18: Model Groups 23
Figure 2.19: Satellite Deployment Pod 24
Figure 2.20: Simulation Model with Constraints 25
Figure 2.21: Solution Properties 26
Figure 2.22: Bulk Element Data 27
Figure 2.23: Simulation Model with Constrained Rail Ends and Boundary Conditions 28
Figure 2.24: Mode 1, 306 Hz 28
Figure 2.25: Mode 2, 310 Hz 29
Figure 2.26: Mode 3, 406 Hz 29
Figure 2.27: Mode 4, 465 Hz 30
Figure 2.28: Mode 5, 701 Hz 30
Figure 2.29: Fully Constrained Structure 31
Figure 2.30: Mode 1, 979Hz 32
Figure 2.31: Structure with PCB and Constrained Rail Ends 33
Figure 2.32: Mode 1, 1.002 Hz 33

Figure 2.33: No 3D Elements ... 36
Figure 2.34: Current Bulk Element Data ... 37
Figure 3.1: Satellite External structure ... 43
Figure 3.2: Satellite Internal Structure ... 44
Figure 3.3: Thermosyphon ... 46
Figure 3.4: Variable Conductance Heat Pipes ... 47
Figure 3.5: Heat Conduction of Each Material in the AB Plane ... 50
Figure 3.6: Thermal Conductivity of PGS with Temperature ... 54
Figure 3.7: Specific Heat and % Thermal Expansion in the AB plane of Pyrolytic Graphite Vs Temperature ... 55
Figure 3.8: Momentive PGS Properties ... 59
Figure 3.9: Minteq PGS Properties ... 60
Figure 3.10: Panasonic PGS Properties ... 61
Figure 3.11: Heat Transfer Experiment ... 62
Figure 3.12: Experiment Heating for 10 Sec ... 63
Figure 3.13: Experiment Cooling for 20 Sec ... 63
Figure 3.14: Heat Spreader Experiment ... 64
Figure 4.1: Solid Model of Electronic Component Mounting ... 69
Figure 4.2: Simulation model with Constraints, Couplings, and Loads ... 74
Figure 4.3: Nodal Thermal Results no PGS ... 75
Figure 4.4: Temp Results with 17um PGS ... 76
Figure 4.5: Temp Results with 100um PGS ... 76
Figure 4.6: Nodal Temperature Design Cycle 2 ... 78
Figure 4.7: Heat Spreader plot of Temperature vs Width ... 79
Figure 4.8: Final Nodal Temperature Plot ... 79
Figure 5.1: Printed Circuit Board Stack Before ... 81
Figure 5.2: Printed Circuit Board Stack After ... 81
Figure 5.3: Solid Part Model ... 83
Figure 5.4: C-Point Added ... 85
Figure 5.5: Mate References Added ... 86
Figure 5.6: Mate Referenced Non Cable Part ... 88
Figure 5.7: Design Library ... 88
Figure 5.8: Cable Library Excel ... 90
Figure 5.9: Core Library ... 91

Figure 5.10: Library Information and Format ... 92
Figure 5.11: Opened Existing XML Library ... 93
Figure 5.12: Drag and Drop Routing ... 94
Figure 5.13: Spline Placement ... 95
Figure 5.14: Spline Errors ... 95
Figure 5.15: Route with Two End Points ... 96
Figure 5.16: From-To Dialogue ... 97
Figure 5.17: From-To List Excel ... 97
Figure 5.18: Spline Evaluations ... 98
Figure 5.19: Annotation Schematic ... 99
Figure 5.20: RG174u Cable ... 99
Figure A.1: Random Vibration Specification ... 109
Figure B.2: Thermal Vacuum Test Profile ... 110
Figure C.3: X Plane Frequency Response ... 111
Figure C.4: Y Plane Frequency Response ... 112
Figure C.5: Z Plane Frequency Response ... 113
Figure D.6: 1st X-Axis Low Level Sine Response ... 115
Figure D.7: X-Axis Random Vibration Response ... 116
Figure D.8: 2nd X-Axis Low Level Sine Response ... 117
Figure D.9: 1st Y-Axis Low Level Sine Response ... 118
Figure D.10: Y-Axis Random Vibration Response ... 119
Figure D.11: 2nd Y-Axis Low Level Sine Response ... 120
Figure D.12: 1st Z-Axis Low Level Sine Response ... 121
Figure D.13: Y-Axis Random Vibration Response ... 122
Figure D.14: 2nd Z-Axis Low Level Sine Response ... 123

LIST OF TABLES

Table 3-1: Hot Case 42
Table 3-2: Cold Case 42
Table 3-3: Heat Transfer Method Selection Matrix 49
Table 3-4: Heat Spreader Material Selection 50
Table 3-5: Pyrolytic Graphite Calculated and Empirical Properties 53
Table 4-1: PGS Thermal Conductivity by Thickness 70
Table 4-2: Optimization Spreadsheet 77
Table 4-3: Final Optimization 78
Table D-1: Sensor Legend 114

TABLE OF EQUATIONS

Equation 3.1: Thermal Conductivity of PGS in the C plane 56
Equation 3.2:Thermal Conductivity of PGS in the AB plane 56
Equation 3.3: Specific Heat Capacity of PGS 56
Equation 3.4: Modulus of Elasticity of PGS 56
Equation 3.5: Thermal Expansion of PGS relative to Alpha in the AB Plane at 300K 56
Equation 3.6: Absolute Thermal Expansion of PGS in AB plane 57
Equation 3.7: Thermal Expansion of PGS relative to Alpha in the C Plane at 300K 57
Equation 3.8: Absolute Thermal Expansion of PGS in C plane 57
Equation 3.9: Ultimate Tensile Strength of PGS 57
Equation 4.1: Fourier's Law 71
Equation 4.2: Coefficient of Heat Transfer 72
Equation 4.3: Aluminum Standoff to PCB Heat Transfer Coefficient 72
Equation 4.4: Aluminum Standoff to Plate Heat Transfer Coefficient 72
Equation 4.5: IC to PCB Heat Transfer Coefficient 73
Equation 4.6: Pyrolytic Graphite to IC Heat Transfer Coefficient 73

ACRONYMS

1d	One Dimensional
2d	Two Dimensional
3d	Three Dimensional
Al	Aluminum
CAD	Computer Aided Design
CHP	Conventional Heat Pipe
COPUOS	Committee on the Peaceful Uses of Outer Space
CSDC	Canadian Satellite Design Challenge
Cu	Copper
DFL	David Florida Lab
FEA	Finite Element Analysis
FHP	Flat Heat Pipe
GPS	Global Positioning System
GVT	Ground Vibration Testing
HS	Heat Spreader
ISS	International Space Station
IC	Integrated Circuit
ITU	International Telecom Union
LEO	Low Earth Orbit
LHP	Loop Heat Pipe
LLS	Low Level Sine
LTDHP	Liquid Trap Diode Heat Pipe
MASc	Masters of Applied Science
NCG	Non Condensable Gas
PCB	Printed Circuit Board
PGS	Pyrolytic Graphite Sheet
RF	Radio Frequency
RHP	Rotating Heat Pipe
RVT	Random Vibration Test
SiC	Silicon
TS	Thermosyphon
UVic	University of Victoria
VCHP	Variable Conductance Heat Pipe
VTDHP	Vapor Trap Diode Heat Pipe

1 INTRODUCTION

1.1 BACKGROUND

1.1.1 The Canadian Satellite Design Challenge

The Canadian Satellite Design Challenge (CSDC) is a Canada-wide competition for teams of university students to design and build a small operational science research satellite known as a "3U- CubeSat " or "triple- CubeSat ". These satellites measure 34cm x 10cm x 10cm, and have a maximum mass of 4kg. The satellites undergo full launch and space environment qualification, with the goal of launching the winning satellite into orbit to conduct scientific research. The anticipated next launch date is in 2015 or 2016.

Beyond the primary goal of designing and building a CubeSat, the CSDC has objectives to:

1. Enhance space-related knowledge and capacity at Canadian universities;
2. Increase academia-industry co-operation in space-related research and development; and,
3. Expose participants to the management processes of a large engineering project.

The CSDC also has an educational outreach component, requiring teams to deliver presentations to schools and the public. These presentations are intended to raise awareness and understanding of space activities, as well as to inspire younger students to pursue higher education or careers in science and engineering fields.

The CSDC is a re-occurring competition for post-secondary students. The first CSDC began in January, 2011, and was completed in September 2012, the 50th anniversary of the launch of Alouette-I, Canada's first satellite; the first competition was won by the team from Concordia University in Montréal. The second CSDC began in October 2012, and completed in May 2014; the second competition was won by the University of Victoria. [1] The third CSDC began in October 2014, and will be concluded in the spring of 2016.

1.1.2 The ECOSat Project

The ECOSat satellite is the University of Victoria (UVic) design submission to the CSDC. The team is made up of twenty to thirty students from different backgrounds, primarily engineering, but also computer science, physics, math, and business. The project handles not only all the technical aspects of the satellite design such as power, communications, payload, data handling, attitude determination and control, but also tries to be involved in the community by actively working with local schools and small organizations

to promote educational outreach and space awareness. [2] Though small in size, the three unit CubeSat must have the same functionality of larger commercial satellites. It is an extensive but very rewarding challenge for students and volunteers.

The author of this paper had the good fortune of being presented with the opportunity to lead the design of the ECOSat project as the Chief Engineer throughout his undergraduate degree and his masters. This MASc. Thesis consists of the work developed during the author's time with the ECOSat team in developing the complete satellite.

1.1.3 Satellite Requirements

The requirements for the ECOSat project must meet the industry standard levels for satellite testing this in part to a number of factors. For satellites of this size they are always a secondary or "piggyback" payload from the launch provider perspective they are essentially ballast for the craft and a means of generating additional revenue from a launch. Due to the fact that the primary payload has paid for the use of the launch vehicle they want to be assured that there is no possibility that any secondary payload could be a potential risk to the launch vehicle or to the other payloads on board.

Some of the requirements which must be met pertain to off-gassing issues, vibrational frequencies and modes, the energization of systems and components, and storage requirements for payloads. Additional requirements pertain to agreements which have been reached with other nations such as regulatory bodies like the International Telecom Union (ITU) for radio frequency allocations [3], the Committee on the Peaceful Uses of Outer Space (COPUOS) for issues of space debris, de orbit time after mission completion, and liability for interference with other nations [4].

Additional requirements have also been imposed on the satellite as part of the CSDC, the following is some of the requirements pertaining to the work conducted in this thesis:

- The spacecraft shall be designed to accomplish its mission purpose and to maintain spacecraft health during the design lifetime of its mission.
- The spacecraft shall be passive and self-contained (i.e., electrically OFF, no charging of batteries, no telemetry, and no other support) from the time it is loaded into the launch dispenser until after its deployment on-orbit. This may encompass duration of several months.
- The satellite must have a mass not exceeding 4kg.
- The center of mass of the satellite must be within a 2cm sphere of the geometric center of the satellite.
- The spacecraft shall be able to withstand a quasi-static acceleration of 12g.

- The spacecraft shall be able to withstand the qualification level launch random vibration environment shown in Appendix A: Random Vibration Specification
- The spacecraft shall have a fundamental frequency greater than or equal to 90 Hz in each axis.
- The spacecraft shall be able to withstand a maximum depressurization of -5 kPa/s.
- The spacecraft shall satisfy the following low-out gassing requirements to prevent contamination of other spacecraft during integration, testing, and launch.
    - Total Mass Loss ≤ 1.0%.
    - Collected Volatile Condensable Material ≤ 0.1%.

Additional requirements specified by the competition can be found in Design, Interface, and Environmental Testing Requirements document. [5]

1.1.4 Satellite Orbital Parameters

The satellite is designed to operate in a Low-Earth Orbit (LEO), between 400 km and 800 km. At the design and implementation phase of the satellite the launch has not been procured, and more specific orbit parameters cannot be given; thus, the mission and satellite have been designed such that it can operate in both a sun-synchronous orbit at different Equator Crossing Times and in the orbit of the International Space Station (ISS).

1.2 THESIS OVERVIEW

The work comprised in this thesis stems from the involvement on the ECOSat satellite design project at the University of Victoria. This project has been actively participating in the Canadian Satellite Design Challenge since January 2011 due to the nature of the expedited timeline of the competition, and the involvement with a volunteer based student team the project has faced many challenges and difficulties. Some of these difficulties steam from the composition of the team members and the turbulent nature of their participation due to the co-op program integration within the engineering program. Some other issues are ones of resources and funding since any activity which requires high levels of integration with many systems and components has high costs both monetarily and temporally. The elevated turn-over rate of team members, short timelines and limited resources coupled together required the team to make several design decisions which could not be properly researched at the time.

A large part of the work in this thesis was dedicated to investigating these decisions and ensuring the underlying assumptions made were sound and factual. Part of this work was to ensure that the integration of all system components would be successful. One of the difficulties with such work is that many of the

components cannot be verified for integration until all systems are finished because of this there was a great effort put into the modeling of the satellite systems.

The introduction section of this document outlines some of the requirements and regulations that forced design decisions as well the driving factors behind the use of particular software packages, and why emphasis was heavily weighted on specific aspects of the project during the design and modeling phases.

1.2.1 Section Organization

The sections in this document were arranged in the order of importance from a design perspective, which is also the chronological order in which they were executed. The vibration analysis study covered in Vibrational Modeling and Qualification section was conducted first since it has the largest bearing on the mechanical design of the structure and how this is related to the fundamental frequencies in each axis. These frequencies are of concern due to the 90 Hz or greater fundamental frequency requirement for each axis. [5]

The second study performed was on the thermal modeling of the satellite both for extreme operating conditions in “Hot” and “Cold” cases, as well as looking at specific studies on high power dissipation devices. This study was needed in order to verify the safe operation of individual components and systems to ensure they do not exceed manufacturer specified values. If risk cases are identified appropriate design changes would be required such as the addition of heaters or heat sinks.

The third study performed was for the interface and clearance requirements for the satellite. This section was the final study since the primary design concerns and verification had been conducted what remained was hopefully only small design changes in order to accommodate issues pertaining to assembly and integration of the satellite. Many of the mechanical assembly issues had been foreseen and dealt with during the structural design phase. However it was the marriage between the electrical and mechanical systems which required significant attention in order to guarantee the successful assembly and integration of the two systems once the satellite was completed. This consists of all the additional cabling for charging, solar cells, Communication systems, and RF Coaxial Cable.

1.3 MY CONTRIBUTIONS

Due to the complexity of the ECOSat project and the need for a team structure to accomplish an undertaking of this magnitude it is important to distinguish the work of the team and its members from that of the author of this thesis. The work used by the author is entirely of his own creation, all the models used in the NX environment for analysis were modeled by the author and created for his express use in this project. The basis and configuration of the models is derived from the work of other team members. The following works were performed in its entirety by the author:

- NX Solid Modeling
- NX Thermal Simulation
- NX Vibration Simulation
- Simulation Analysis
- SolidWorks Cable Assembly Modeling
- Electrical Route Planning
- Electrical Design Changes from Simulation Analysis
- Cable fabrication
- Assembly and Integration Planning
- Travel Planning
- Satellite Transportation

2 VIBRATIONAL MODELING AND QUALIFICATION

2.1 SUMMARY

The vibration analysis study covered in this section was conducted first since it has the largest bearing on the mechanical design of the structure and the mechanical structure has the strongest influence on the fundamental frequencies in each axis. These frequencies are of concern due to the 90 Hz or greater fundamental frequency requirement for each axis set out by the CSDC. [5]

The modeling of the vibrational modes of the satellite structure has the biggest impact on not only the design of the mechanical structure but also its interface to the electronic systems if it did not meet the required testing qualification levels.

The modeling and simulation of the ECOSat satellite structure and electronic circuit boards was successful in approximating the fundamental frequencies. The previous testing results were an excellent resource for the verification and qualification of the pre-environmental testing model. The use of these previous testing results for the current satellite structure

It was found from the simulations prior to testing in May 2014 that the first fundamental frequency appeared near or greater than 200 Hz in the XYZ axes of the structure. The results obtained showed strong correlation to the results from testing at the David Florida Lab (DFL) as depicted in Appendix D 2014 Vibration Testing Results. Several peaks can be seen in the range of 187 to 400 Hz in all three axes from the vibrational response data, this shows correlation to the simulation results.

2.2 INTRODUCTION

The goal of this project is to accurately model the satellite structure and its subsystems using the NX FEA environment in order to perform a preliminary qualification of the satellite mechanical structure prior to design finalization. This qualification testing is required in order to meet the vibrational requirements for satellite launch providers.

The first requirement for this study will be to create an accurate representation of the physical satellite structure using the NX modeling environment. This will be achieved through the use of 3d, 2d, and 1d mesh types as well as modeling the bolt connections between assembly members in order to accurately model the relationships between solid bodies. This will require the creation of custom materials for representing the novel materials in the satellite design. The largest obstacle to tackle after initially verifying that the model has the correct geometry in the NX environment will be defining the connection

points for the assembly. Spider bolt connections will be used in the model for constraining and attaching all assembly parts together this should more accurately model the simulation and modeling design trade-offs. The use of bolt connection tools allows the designer to not only select multiple bolt location simultaneously it also has the ability to change all connections referenced to a single design point thereby making the simulation of multiple design options easier.

After initial simulation results are obtained they will be compared to vibrational testing results from a previous testing campaign with a similar mechanical configuration. The comparison of the previous testing results to simulations will aide in verifying that the satellite model is an accurate depiction of the physical structure.

2.3 PROJECT GOALS

To model the physical connections in the satellite between structural members and the connections between the printed circuit boards to the external structure. These models which have been created in SolidWorks with intricate detail will first be simplified and imported into the NX modeling environment to be rebuilt as an assembly project. The assembly created in NX will be used for the analysis of the normal modes and vibrational frequencies of the structure and internal printed circuit board stack. The internal print PCB stack is depicted in Figure 2.1 shows some of the details of the PCB stack and structural members prior to simplifying the internal structure for modelling. The external structural components and enclosure have been excluded from the pictures below in order to see the internal printed circuit board stacks more clearly.

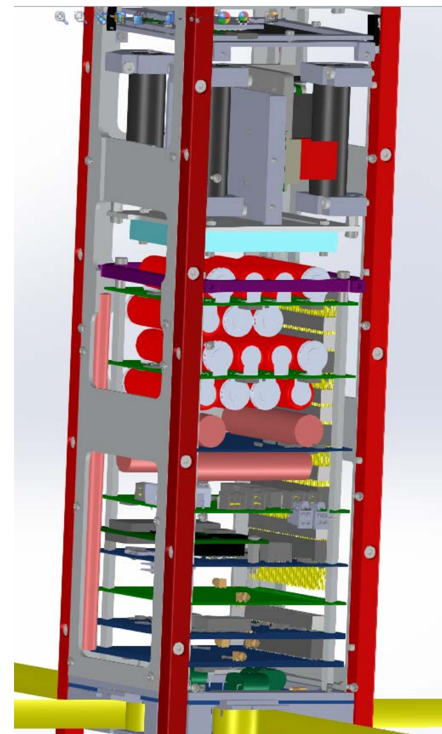

Figure 2.1: Satellite structure with Internal PCB's

2.4 NX Modeling and Assembly

The first step after deciding which structural components would be critical for analyzing the vibrational and normal modes of the satellite was to save them as separate solid part files so that they may be imported into NX. Currently the 7.5 version of NX that was used for the analysis does not support the importation of SolidWorks Assembly files only simple part files without features. In Figure 2.2: NX Structural Model it can be seen that although the part is very similar to the depiction of the SolidWorks part model it is missing significant detail such as the components for each printed circuit board, the fasteners between structural members, the standoffs that link each printed circuit board to one another, their upper and lower mounts, as well as the payload section is currently absent from the model however a few of the supporting structural members for the payload will be added later for further model refinement.

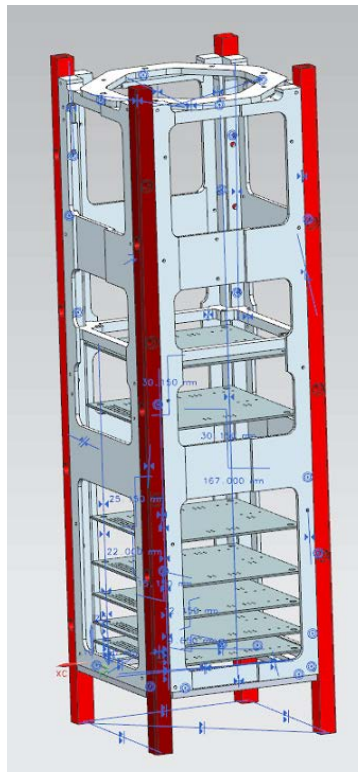

Figure 2.2: NX Structural Model

2.4.1 **Modeling Details**

2.4.1.1 Concentric Mates:

One of the key differences when creating assembly models in NX versus the SolidWorks environment is when creating concentric constraints or mates, the two concentric entities must be the two closest such references as seen in Figure 2.3: Concentric Constraint if either of the edges were selected that are not the closest edge reference to the constraint it would result in a broken constraint. This led to many difficulties in creating the assembly especially when creating models with concentricity which were separated by a specific distance since the NX environment expects the mates to also be coincident for concentricity constraint to be valid.

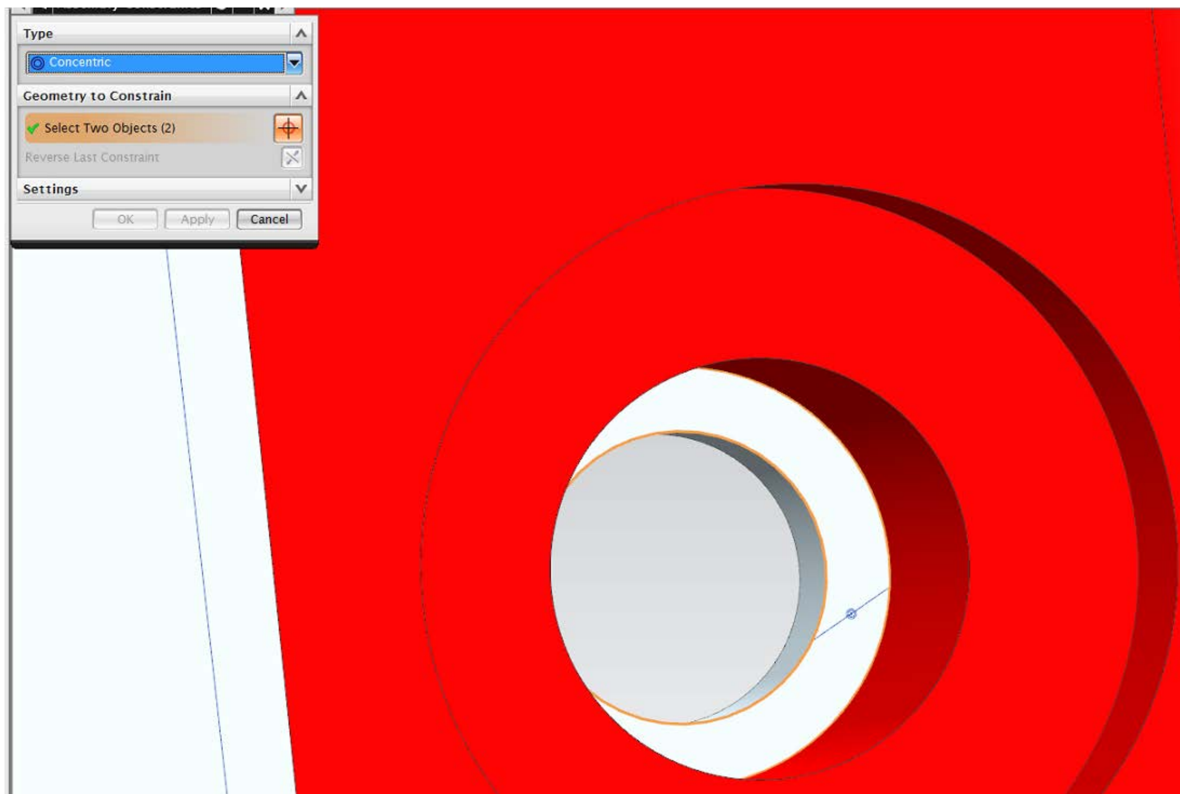

Figure 2.3: Concentric Constraint

It can be seen in Figure 2.2: NX Structural Model that the holes for the printed circuit boards have been aligned. In order to properly align circular features to be concentric in NX you must use the “Touch Align” constraint which seems unintuitive, under the “Touch Align” type constraint you can select the sub option to “Infer Center/Axis” which can be seen in Figure 2.4: Center Axis Constraint once the top and bottom members for printed circuit board stack were aligned, each subsequent board was then aligned to the bottom structural mount of the printed circuit board stack.

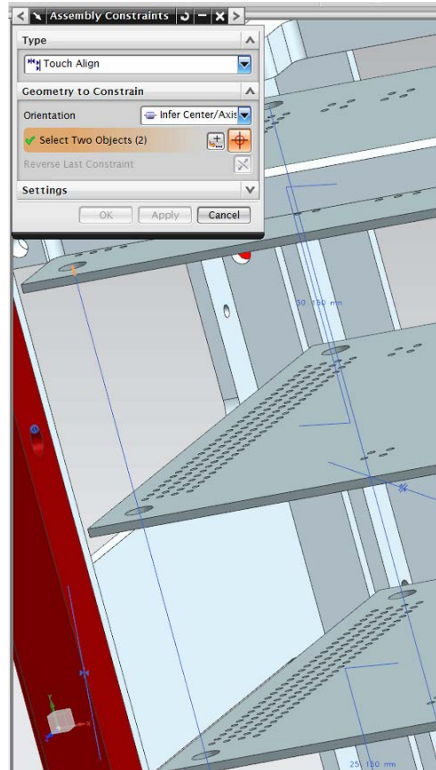

Figure 2.4: Center Axis Constraint

2.4.2 Add Component

When adding additional components to the assembly it was discovered that it was possible to position the part via constraint rather than simply placing the component haphazardly on the document and then constraining the part once already inserted into the model. This often led to much more difficulty in properly constraining the part to the assembly model. It was also discovered through heavy use of NX and creating multiple assemblies that it was also possible to reuse parts that had been placed in the assembly, as well as it was possible add multiple parts concurrently after finishing constraining one part. Additionally when using the position by constraint method as shown in Figure 2.5: Positioning by Constraint not only does it give you the option for previewing the part but it also allows you to use the "Component Preview" window to select features to perform the constraints with as seen in Figure 2.6: Component Preview. This feature is incredibly handy since it makes it possible to have the assembly model oriented in one view and to be able to independently change the viewing orientation of the part to be added to the assembly. This can greatly simplify and expedite the assembly process as well as making visually confirming that the part is being constrained properly.

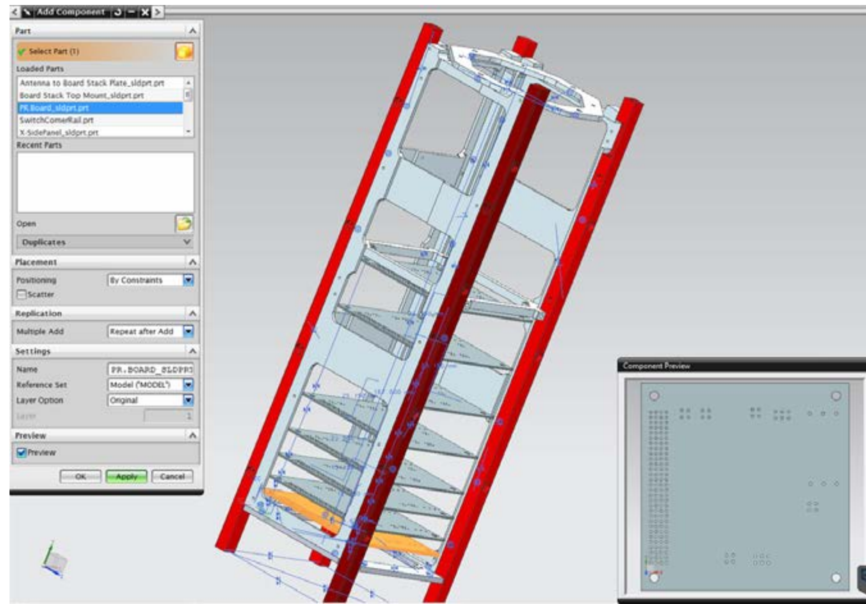

Figure 2.5: Positioning by Constraint

In Figure 2.6: Component Preview the part that is being added to the assembly can also be seen in the "Main Assembly" window. This makes it very easy and quick for the user to ensure that the part is properly mating to the assembly structure since which every additional constraint the part which is being added will move in reference to the newly defined constraint.

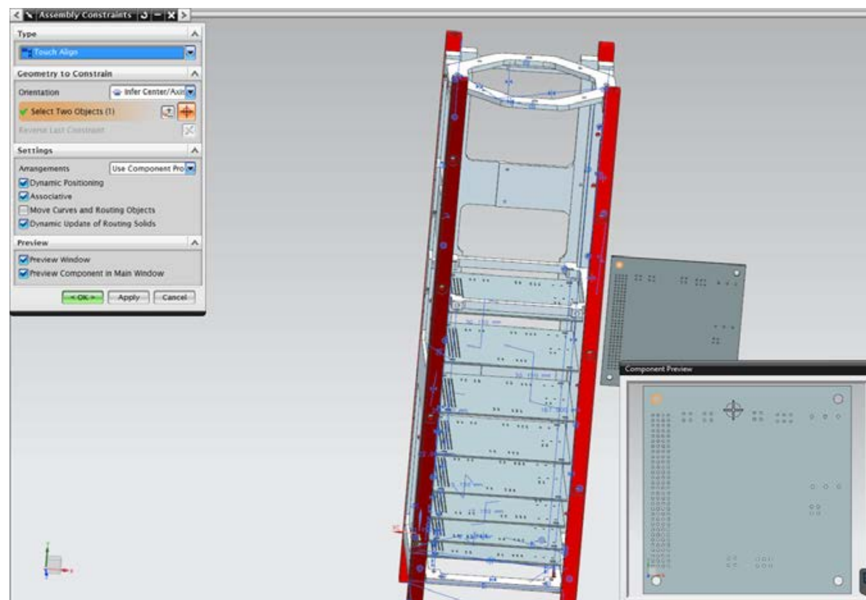

Figure 2.6: Component Preview

2.4.3 Part Idealization

Once the primary structural elements were added to the model it was necessary to remove non critical features from the assembly to further simplify the structure so that simulations could be conducted in a timely manner. In Figure 2.7: Part Idealization it can be seen that the holes with a diameter less than 2mm have been removed from the idealized modeled parts. The selection of a hole size less than or equal to 2mm was such that this provided the elimination of holes for soldering but still retained the holes for physically connecting the printed circuit boards to one another via standoffs which for this model is represented as bolt connections.

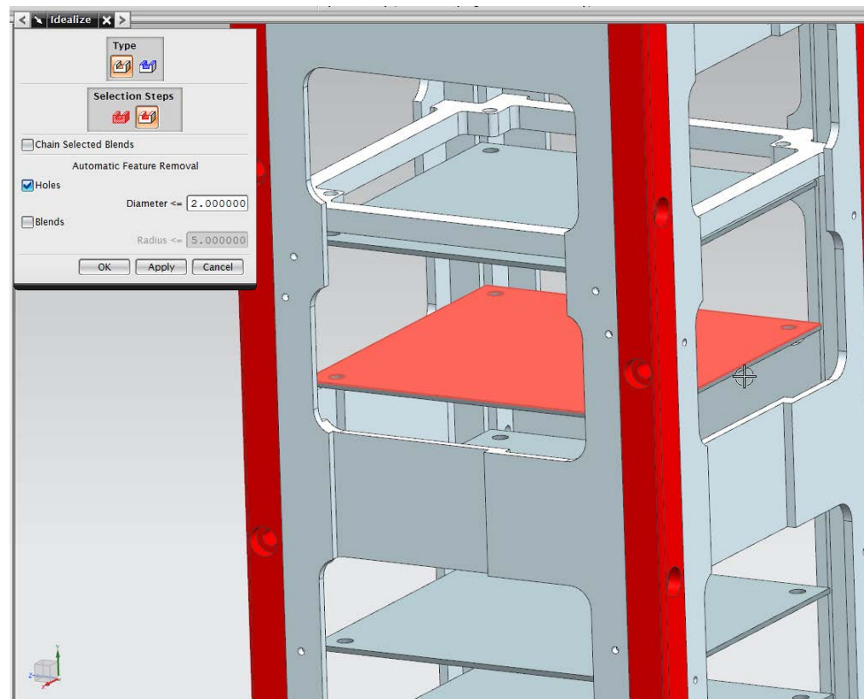

Figure 2.7: Part Idealization

The other features in the model which could have possibly been suppressed or idealized would have been the recessed feature in the face of the side panels. However it was a point of interest for the study to observe how these would behave under stress to investigate if this would be a systemic weakness in the design of the side panel structure.

2.4.4 Modeling Problems

For the idealization of the parts in the model the main difficulty in creating the idealized part was neglecting to delete the original un-idealized body prior to entering the FEM state of NX which resulted in two bodies being present in the model with intersecting solid bodies. To rectify the problem it required

re-entering the idealized part and deleting the bodies form the model and prompting the idealized body in order to link it to the original part from the modelling mode of NX.

Working in the NX environment was quite difficult transitioning between the different modes primarily going from the modeling stage to simulation and finite element mode back to modeling seemed to pose many difficulties. After becoming familiar with the NX it was discovered how to effectively manage mode state switching. It comes down to a two part process, the first step is to use the Simulation file view pane, by using the pane to transition between Simulation, Finite Element Modeling, Part Idealization, and Modeling it allows the user to switch between the various modes. The second step is ensuring the model is in the correct state, the user must transition to the "Idealized Part or Part" view in order to be able to switch modes in the NX environment.

2.4.5 Finite Element Model

The finite element mesh creation for the part was a very time consuming aspect of the project it combined 3D, 2D, 1D, and 0D element meshes. For the initial attempt at generating results and investigate the modal and vibrational response of the system a model with pure 3D elements was created. The initial mesh size which was calculated by NX was used for the simulation the software calculated approximately a 4mm mesh size for the side panels and rails and a 2mm mesh size for the top and bottom plate.

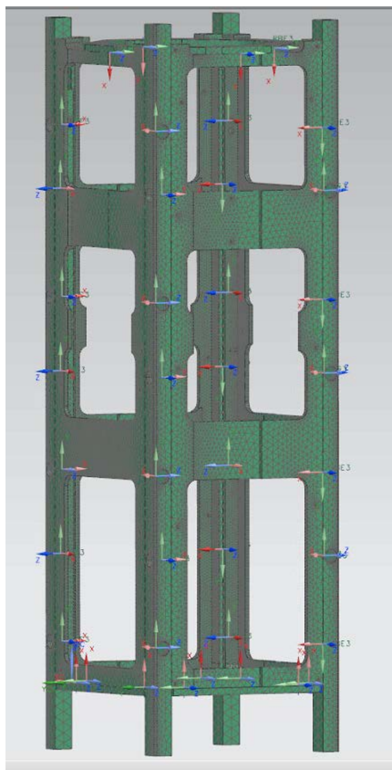

Figure 2.8: 3D Element Mesh

An iterative approach was chosen for the mesh creation and simulation of the model, the first attempts at simulating the structure consisted of a single side panel with no rails and then progressing to more complicated structures with multiple constraints and multiple solid bodies.

2.4.6 3D Meshes

The side panels, rails, and upper PCB mount used 3D meshes for the simulation and modeling of the parts, initially the top and bottom plates were also modeled as 3D meshes but this led to very large simulation files coupled with long solution times.

The mesh for the side panels was refined from its initial approximation of 4mm to 2mm and then 1.5 mm, further mesh refinement was attempted but mesh sizing close to or below 1mm causes the computer to fail and crash even with a large memory allotment and a scratch drive provided for the software. On average simulation would run for approximately 30 to 45 minutes on a computer designed for CAE and FEA processing with 32GB of DDR3 Ram available, a CAD Graphics card, and the latest i7 processor.

2.4.7 2D Meshes

The top and bottom plate elements were selected to be molded as plate elements since they are planar pieces with simple features such as holes, this aided in reducing the simulation time and the element numbers for simulation. The top and bottom plates also have small thicknesses in order to properly simulate their physical properties a minimum of 3 to 4 elements through the thickness of the material should be used for modeling purposes. CQUAD 8 was used for the 2D element creation with an initial ~2mm mesh size the subdivision and paver meshing methods were experimented with.

2.4.7.1 Subdivision meshing method

With the Subdivision meshing method, the software uses a recursive subdivision technique to generate the mesh on the selected faces. With recursive subdivision, the software repeatedly divides and then subdivides the selected geometry to create the mesh. With this method, once the software has generated the initial set of elements, it then performs a series of cleaning and smoothing operations to improve the overall quality of the mesh

2.4.7.2 Paver meshing method

With the Paver meshing method, the software uses a hybrid technique to generate the mesh on the selected faces. With the Paver method, the software combines a paving technique with a recursive subdivision technique to produce more structured, boundary conforming free meshes with good quality. This hybrid approach allows the software to create a more structured mesh around the surface's outer boundary as well as around any interior holes while still generating a free mesh on the rest of the surface.

After trying both methods in the design the Subdivision was used for the surfaces since it generated fewer failed elements that were skewed or had angles to large based on the element evaluation a total of 13 elements failed for the 2D elements with a mesh size of 0.5mm. As the model increased in complexity further model refinement and complexity was added the printed circuit boards were added to the internal structure along with bolt connections attaching each board to the upper and lower support mount as seen in Figure 2.9: PCB Assembly with Bolt Connections.

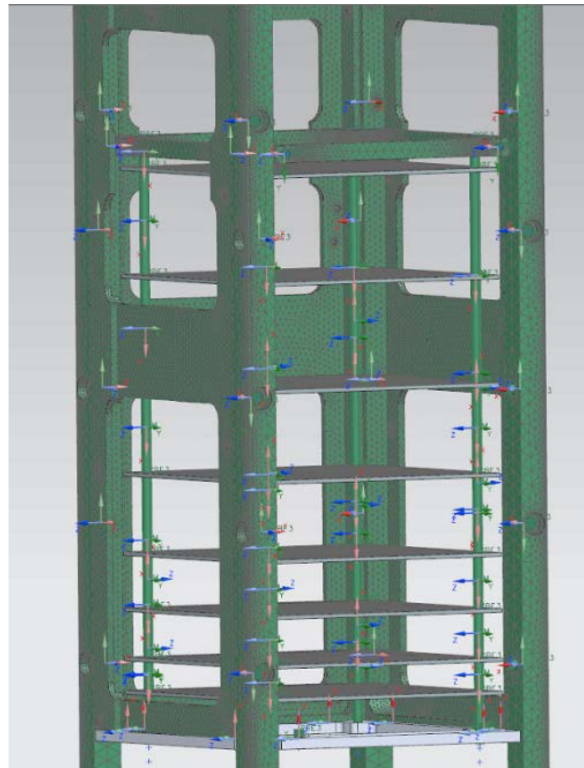

Figure 2.9: PCB Assembly with Bolt Connections

2.4.7.3 Material

The "Material Properties" window in NX is used for assigning materials to model elements; if the materials are assigned to the physical solid bodies then they will be inherited by the Finite Element Meshes. Additionally the materials can be assigned to individual meshes, or mesh collectors.

In order to properly model the vibrational states of the satellite a custom material was needed to be created in order to define the material for the printed circuit board stack. PCBs are made of two different materials: FR-4 (fiberglass-reinforced epoxy) and copper (metal). The layers of copper between the FR-4 connect the electronic components with each other. They are very thin, mostly 18 or 35 micrometer. PCBs are laminates of layered fiberglass reinforced epoxy and copper you can create a laminate, as

shown in Figure 2.10: Laminate Structure of PCB with 4 layers the purple is depicting the Copper and the Red is a specific type of fiberglass known as Flame Retardant-4 (FR-4).

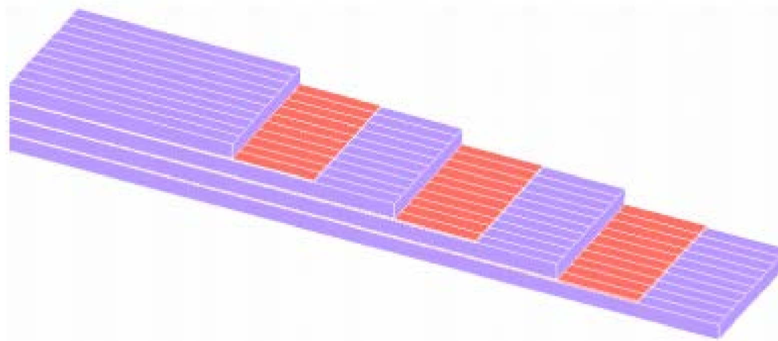

Figure 2.10: Laminate Structure of PCB with 4 layers

The material that will be used for the final design is FR-4 which is a standardized circuit board substrate. FR-4 is a fiberglass-reinforced epoxy. This means that FR-4 is a polymer with a fiberglass woven through the matrix structure of the polymer. The fiberglass is orientated in the PCB plane, so FR-4 is much stronger in the plane than in the thickness direction, therefore it is an orthotropic material. The relevant material properties of FR-4 were obtained from experimental research. [6]

2.4.8 1D Elements

For simulating the connection of the side panels and rails 1D bolt connections were made using the "Bolt Connection" tool for creating spider connections on either mesh surface linked by a 1D beam element. This allowed the user to create bolt connection for all locations where there were bolts traveling in the same direction through the same plane. The bolt connections must all have the same connection vector when creating the collector in order to constrain the degrees of freedom of the connected elements properly. If elements on perpendicular faces are selected or elements on parallel faces with reverse direction the bolt connection will not properly constrain the parts. In Figure 2.11: Bolt Connection Dialogue the orange highlighted bolt connection are illustrate the previous description of the connections in a plane with the same normal vector. In the case of the satellite the bolts are all connected into a tapped hole for weight reduction and simplified assembly. If a bolt and nut connection was used the model would show a spider connection on both faces of the connecting meshes.

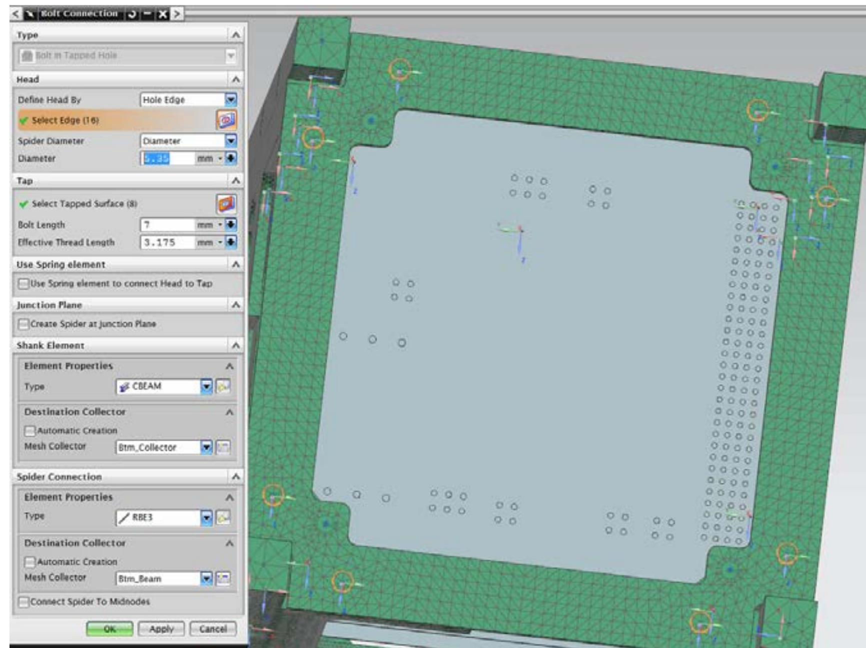

Figure 2.11: Bolt Connection Dialogue

2.4.8.1 Bolt Collector

For each bolt connection set a collector is required in order to define the physical properties that the bolt connection is representing, this represents the material and the type of connection element. The first step is creating a name for the collector and a beam property.

If a Beam Property has not been created to select from the dropdown menu one will need to be created so that a physical representation is available for simulation. In the above figure an M3Bolt beam has already been created with the following properties.

2.4.8.1.1 Section Type

There are two options for the user to select either “Constant” or “Tapered” if a constant section type is select there is only a “Fore Section” option presented to the user since this is specifying that the bolt has the same cross sectional area for both the fore and aft section of the bolt. Constant bolt areas were used exclusively in this simulation since this is an accurate representation of the physical implementation of the bolt used for the assembly. If a tapered section type is selected the user is able to define separate cross sectional area’s for the fore and aft sections of the bolt. The cross sectional menu provides the user with a visual representation in the “Illustration” window for the “DIM1” value, in the case of a ROD element it is representing the radial diameter of the bolt shaft. Since the model is using M3 bolts the radial dimension is defined as 1.5mm.

Once the dimension has been selected and inputted the user is able to "Evaluate Section Properties" this performed a calculation of the cross sectional area and provides the user with the information presented in Figure 2.12: Section Evaluation which the user can then use to cross reference against the physical bolts that are being simulated in the design and correct the dimensions in order to accurately reflect the area, shear factors, and any other important properties for the purpose of the analysis.

```
Section dimensions:

DIM1                    : = 1.5  (mm)

Section properties:

Area                               =      7.068583385 (mm^2)
Centroid,            Z             =      0.000000000 (mm)
Centroid,            Y             =      0.000000000 (mm)
Shear Center,        Z             =      0.000000000 (mm)
Shear Center,        Y             =      0.000000000 (mm)
Eccentricity,        Z             =      0.000000000 (mm)
Eccentricity,        Y             =      0.000000000 (mm)
Moment of Inertia,  Iz             =      3.976078106 (mm^4)
Moment of Inertia,  Iy             =      3.976078106 (mm^4)
Moment of Inertia,  Iyz            =      0.000000000 (mm^4)
Torsional Constant, K              =      7.952156212 (mm^4)
Warping Constant,   Cw             =      0.000000000 (mm^6)
Shear Factor along y axis,  K1      =      0.857215602
Shear Factor along z axis,  K2      =      0.857207946

Location of stress recovery points (extreme fibers):

    Stress Recovery Point, C(z)  =       0.000000000 (mm)
    Stress Recovery Point, C(y)  =       1.500000000 (mm)
    Stress Recovery Point, D(z)  =       1.500000000 (mm)
    Stress Recovery Point, D(y)  =       0.000000000 (mm)
    Stress Recovery Point, E(z)  =       0.000000000 (mm)
    Stress Recovery Point, E(y)  =      -1.500000000 (mm)
    Stress Recovery Point, F(z)  =      -1.500000000 (mm)
    Stress Recovery Point, F(y)  =       0.000000000 (mm)

This section is referenced 2 times
```

Figure 2.12: Section Evaluation

2.4.8.1.2 Material

The material type prompts the user with the standard material property window for selecting materials from the NX library or from one that the user created for a custom material.

2.4.8.1.3 Non-Structural Mass

The non-structural mass is for specifying a mass loading on the component that is not due to the material properties of the model.

2.4.8.2 Beam Collector

In the case of the “Bolt Connection” dialogue the “Beam Collector” is for containing the spider elements for connecting to the meshes of the two sided surface. The spider bolt connection is responsible for transferring the loading to the surrounding meshing to represent the force applied from the bolt head.

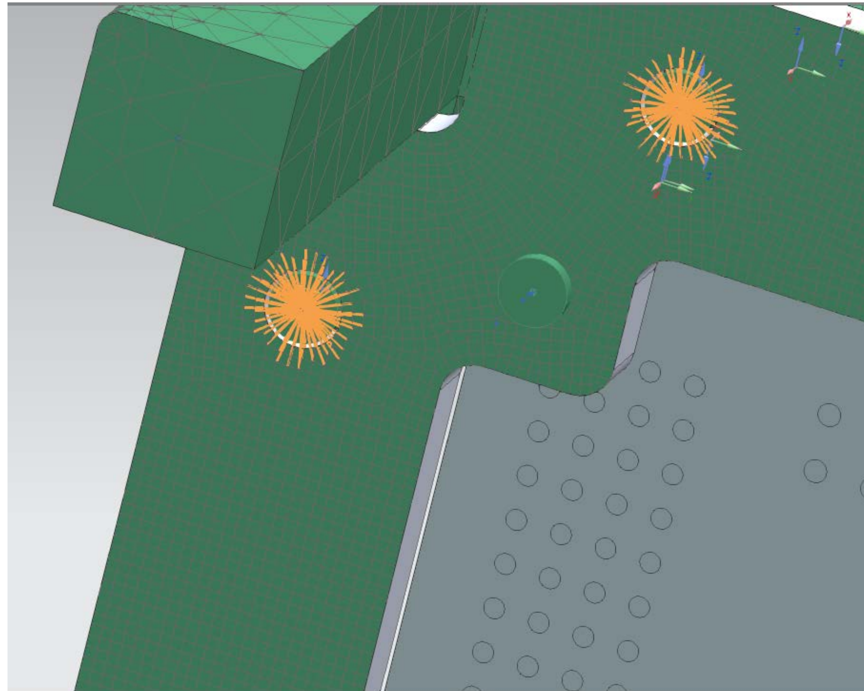

Figure 2.13: Beam Collector

2.4.9 Additional Objectives

2.4.9.1 Bolt Connection Grouping

When originally working with the bolt connection tool all fasteners were selected and incorporated into a single collector group this had the unfortunate outcome that the degrees of freedom were only properly constrained for the connection selected in the first plane. When creating bolt hole connections the NX environment creates a local coordinate system based on the circular surfaces selected where the Z axis is defined as the vector passing through the center axis of the circularly connected faces.

2.4.9.2 Mesh Collector Creation

When creating mesh collectors and bolt-hole connections the material for the connection and the fore and aft section of the bolt shank are not created. This resulted in numerous errors when simulating the model and took some research in order to determine the cause of the discrepancy when simulating. Intuitively it was thought that the shaft size would have been determined for the beam element based on the hole diameter of the circular face that was being modeled.

2.4.9.3 Bolt Length/Effective Thread Length

When initially modeling the bolt connection not much attention was paid to the length of the bolt and the length was specified such as to meet the actual physical implementation of the satellite fasteners. This resulted in a number of errors where the spider mesh was not making a connection to the surface of the mesh in the cylindrical faces for representing the threaded bolt connection. The problem arises when the bolt length coupled with the effective thread length protrudes too far beyond the surface of the mesh it does not create a spider mesh connection to the 2d or 3d element mesh linking the bolted surfaces. The orange highlighted elements show in Figure 2.16: Spider Connection depicts the spider connection to the 2d element surface.

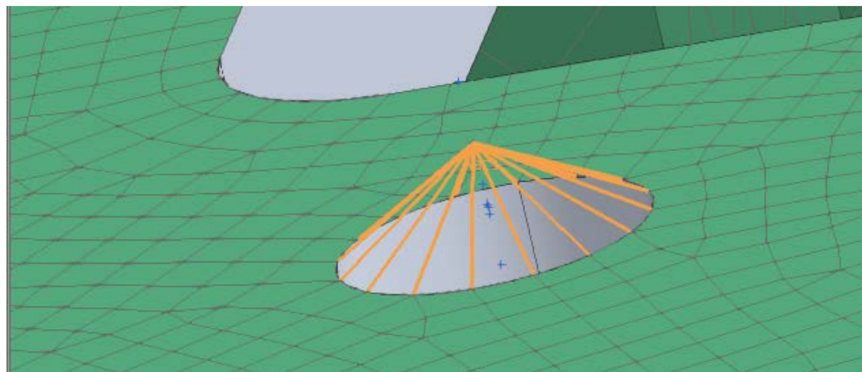

Figure 2.14: Threaded Bolt Spider Connection

2.4.9.4 Multiple Connected Bolt Segments

When initially attempting to connect multiple PCB boards to one another using coupled bolts, i.e. trying to model the connection of standoffs as see in Figure 2.15: Standoff Illustration where the male threading of one standoff passes through the thickness of a PCB connecting to the female threading of the standoff on the opposite face of the PCB. The first attempt used multiple bolt connection where the head of one bolt appeared on the top side of the board with the nut of the bolt connection from the board connection above appearing on the opposite trying to imitate the compressive and tensile nature of the standoffs. However with overlapping geometry for the bolt heads and nuts of differing bolt connection the simulation did not work and another approach was required.

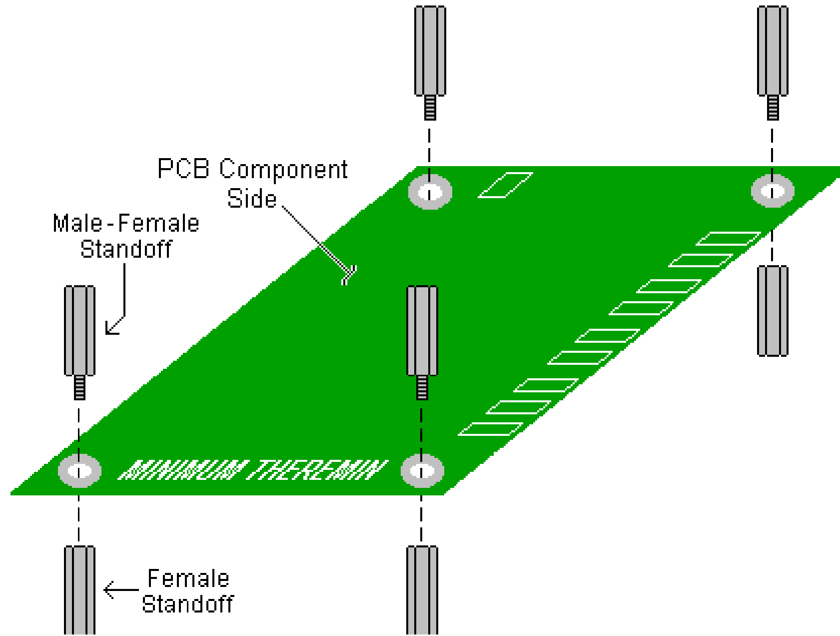

Figure 2.15: Standoff Illustration

The solution to the initial problem of how to model the stacking configuration of the standoffs with the female and male threading coupled connection came by further investigating the modeling options for bolt connections. Under the "Bolt Connection" method there is a "Junction Plane" option for specifying additional planes that the bolts pass through to be connected to. The use of this option results in creating "Spider Junctions" at each intermediate PCB plane providing a rigid connection to the simulated standoff bolt. In Figure 2.16: Spider Connection the connection to the 2D PCB plane can be seen by the thin green lines representing the "Spider Connection" or beam elements that join each PCB to the standoff "Simulated Bolt" passing through each printed circuit board.

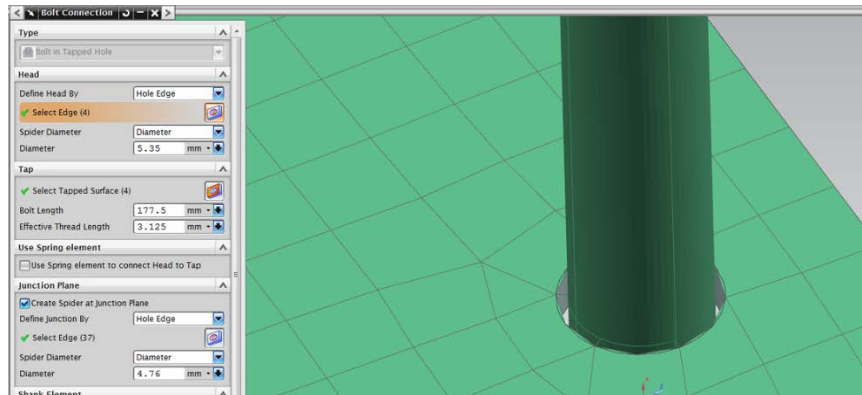

Figure 2.16: Spider Connection

2.4.10 **Grouping**

Often when working in the modeling environment it is required to hide and show a number of parts to select the correct surface for creating finite elements, constraints, loads and other simulation properties. As can be seen in Figure 2.17: Sub Grouping all the 3D element meshes are grouped into a single section. The caveat to this is there is no ability to create subgroups in which you could place individual mesh groups such as grouping the rails or the side panels, or grouping via face orientation.

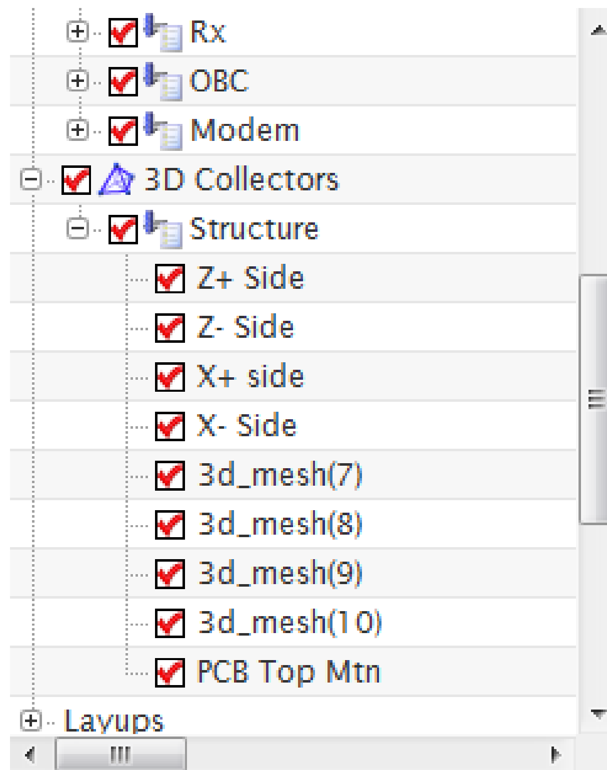

Figure 2.17: Sub Grouping

It was discovered however that it is possible to create groups for encapsulating any type of object whether it be a polygon body, mesh, load, idealized part or other model. This provides the user with the ability to easily hide multiple entities to greater facilitate the modeling process by making it a simple process to hide parts by groups. In Figure 2.18: Model Groups it can be seen that by simply selecting the “Rails” group from the group selection window on the left hand pane that the correct entities are selected in the modeling window. By right clicking on the groups a context menu appears as shown in Figure 2.18: Model Groups which presents the user with a number of possibilities for manipulating entities in the main modeling window such as:

2.4.10.1.1 Show Only

This will make the part selected the only one visible in the main modeling window

2.4.10.1.2 Show

This will display the part with any other current displayed parts in the modeling window which is useful for displaying parts that were hidden previously for performing other modeling operations.

2.4.10.1.3 Hide

This will cause the selected parts to be hidden from the main modeling window.

The remaining options are for manipulating the representation of the group e.g. Renaming the group, copying the group, deleting the group, editing the group which is performs the same options as the individually mentioned group options here. As well as the “Add to Group” and “Remove from Group” options which allows the user to select polygon or element bodies in the main modeling window and perform the corresponding action related to the group. The information window lists the name of the group, the group number and the number of entities contained in the group.

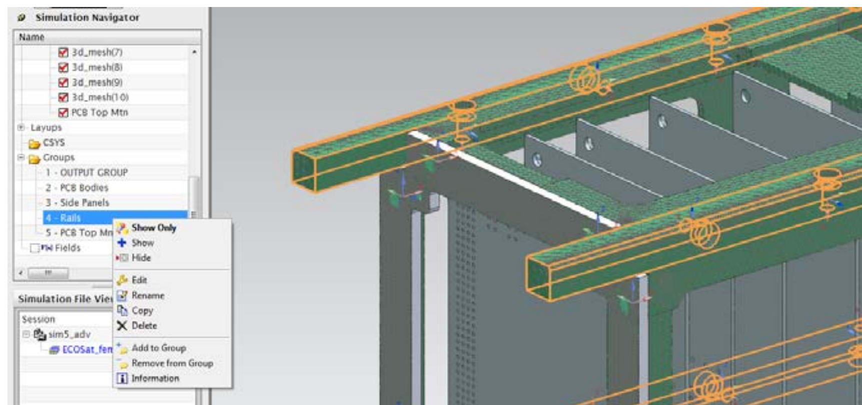

Figure 2.18: Model Groups

2.4.11 **Simulation**

The simulation portion of the design posed its own unique set of challenges beyond the ones discovered in the solid modeling and finite element modeling sections of the project. The project focused around the vibrational and normal modes of the satellite which results in no loads being applied to the system. However in order to properly model the vibrational states of the satellite there must be constraints applied to the model. Defining the constrained surfaces of the model was quite straight forward, however choosing the correct type of constraint required careful consideration of how the satellite might move in the launch module.

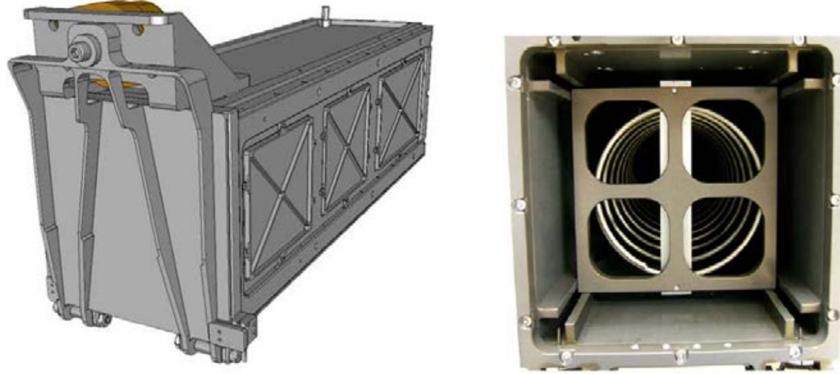

Figure 2.19: Satellite Deployment Pod

2.4.12 Constraints

From Figure 2.19: Satellite Deployment Pod it can be seen that the satellite will be constrained to translation motion on the rails which prevents the satellite from translating in the X and Y directions but can slide in the Z direction. I variety of constraint conditions were applied to see how variations in constraints effect the modal and vibrational response of the structure. As can be seen in the side pane of Figure 2.20: Simulation Model with Constraints several constraints have been created and tested in order to better estimate the real world response. The constraints range from limiting all six degrees of freedom to, simple translation, to enforced maximum displacements.

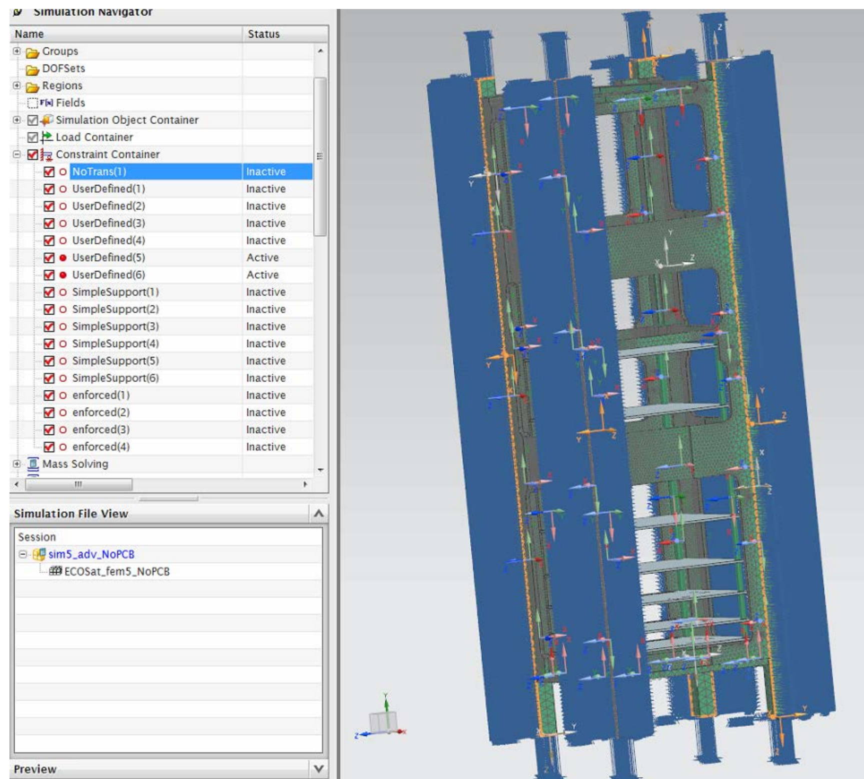

Figure 2.20: Simulation Model with Constraints

2.4.13 **Solver Properties**

As the model became increasingly complex simulations increased execution time and results also began showing some errors. Upon further investigation of the solver properties and the use of the help files for the NX environment it was possible to optimize the solver parameters.

2.4.13.1 Solver Options

The Memory for the solver was increased however it should be noted that the specified memory is per operating core in the computer this resulted in a number of crashes during the initial simulations. Since the maximum available memory was being specified the computer was running out of memory, since that was the allocation being made to each individual core the operating system would run out of free memory, become unstable and crash. The increase in available memory to the Nastran solver greatly reduced the simulation time of the program.

The scratch directory was also required to be specified as the model complexity increases the program required increasingly large amounts of RAM since more was not available a hard disk directory was required in order to deal with the memory over run issues. The directory was created on a solid-state drive so that the solution could be completed as swiftly as possible since the data writes to the drive have a significant overhead on operations.

2.4.13.2 Bulk Options

The bulk options for the Nastran solver control the precision in which the results are tabulated. The field format specifies the digit precision between 8 or 16, the either options uses 8 digit precision for cards that have a small field and 16 digit precision for cards that have a large field. Specifying large format forces all cards to 16 digit precision, and specifying small format forces all cards to 8 digit precision.

Exponential format has two options NASTRAN and Standard, the NASTRAN format preserves greater precision and accuracy by having a larger exponential format.

The Real Filter Value truncates all the matrix values to 0 if they fall below the filter value. The value was reduced to 1e-18 to provide further accuracy.

2.4.14 Solution Properties

The solution was setup to investigate the primary vibrational frequencies and modes for each axis of the satellite structure, the range of frequency interest was sent from 0Hz to 1 kHz. The requirements for the structure are to have the primary vibrational frequencies for each axis above 90 Hz. The solution properties can be seen below in Figure 2.21: Solution Properties the Lanczos eigenvalue extraction method since it combines the best of both transformation and tracking methods for eigenvalue extraction which typically yields a fast and efficient solution for mode simulation.

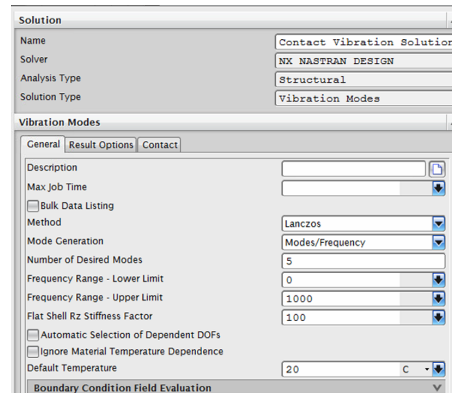

Figure 2.21: Solution Properties

2.5 PRE ENVIRONMENTAL TESTING SIMULATION RESULTS

The refined finite element model for the study is shown below in Figure 2.22: Bulk Element Data the final model contains over one million elements; the breakdown for each individual type can be seen in the figure.

NAME	NUMBER
BCRPARA	16
BCTADD	1
BCTSET	1
BSURFS	16
CBEAM	48
CORD2R	1
CQUAD8	2095
CTETRA	328276
CTRIA6	136
EIGRL	1
GRID	638652
MAT1	2
MATT1	2
PARAM	4
PBEAM	1
PSHELL	2
PSOLID	2
RBE3	96
SPC	738
SPCADD	1
TABLEM1	3

Figure 2.22: Bulk Element Data

2.5.1 Constrained at Rail Ends

The model for simulation was developed with the rail ends constrained and contact boundary conditions developed to prevent the material from passing through the contact planes for each incident surface. The Simulation model with the constrained rail ends and the surface contact boundary conditions can be seen in Figure 2.23: Simulation Model with Constrained Rail Ends and Boundary Conditions.

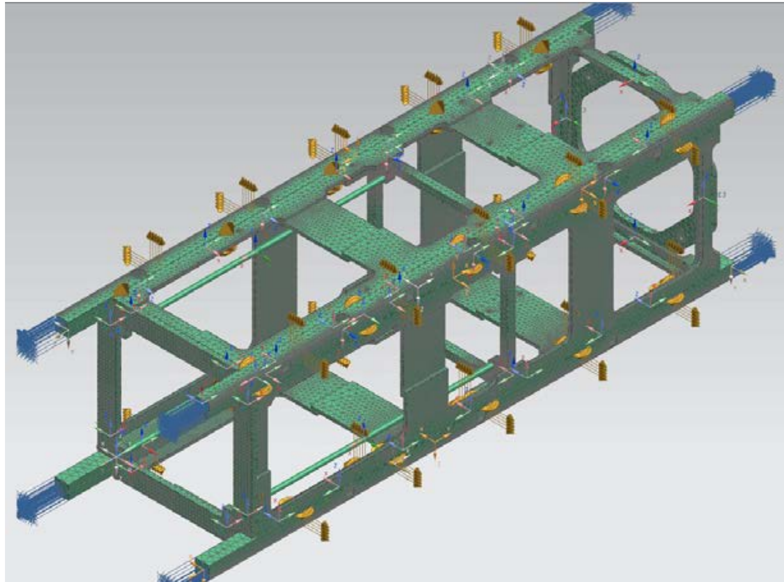

Figure 2.23: Simulation Model with Constrained Rail Ends and Boundary Conditions

2.5.1.1 Results

The deformation of the structure can be seen in the displacement of the structure exceeds prediction but the mode and frequency are on the correct order of magnitude.

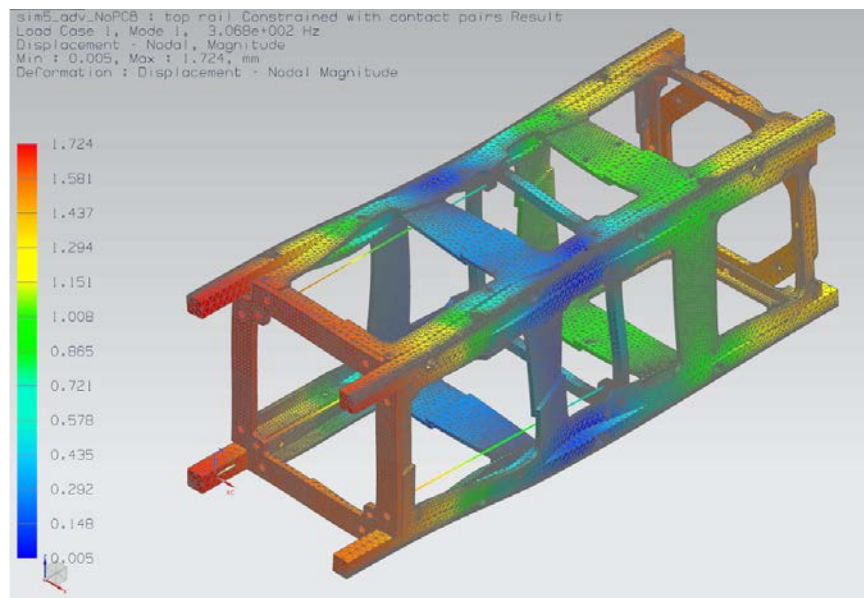

Figure 2.24: Mode 1, 306 Hz

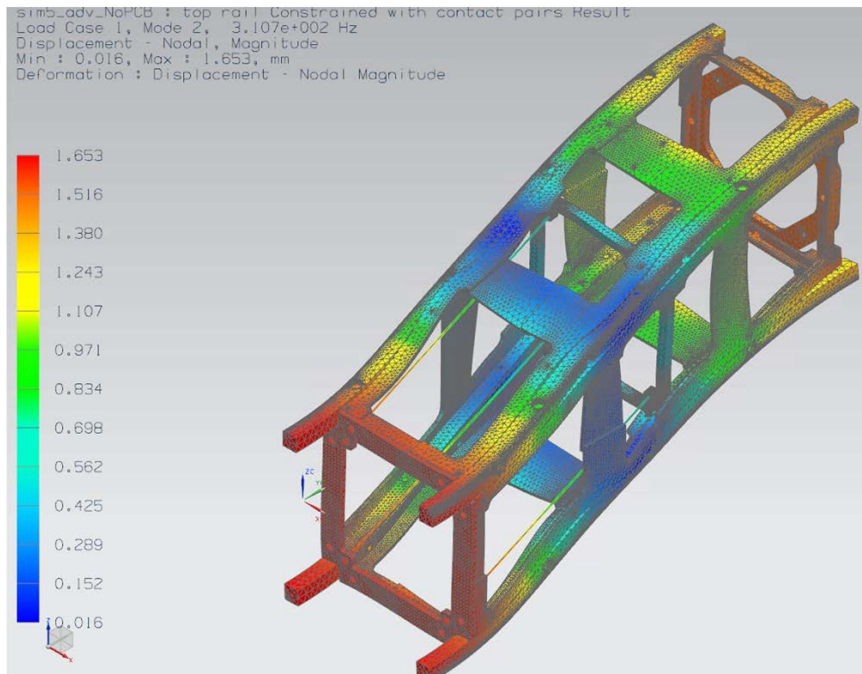

Figure 2.25: Mode 2, 310 Hz

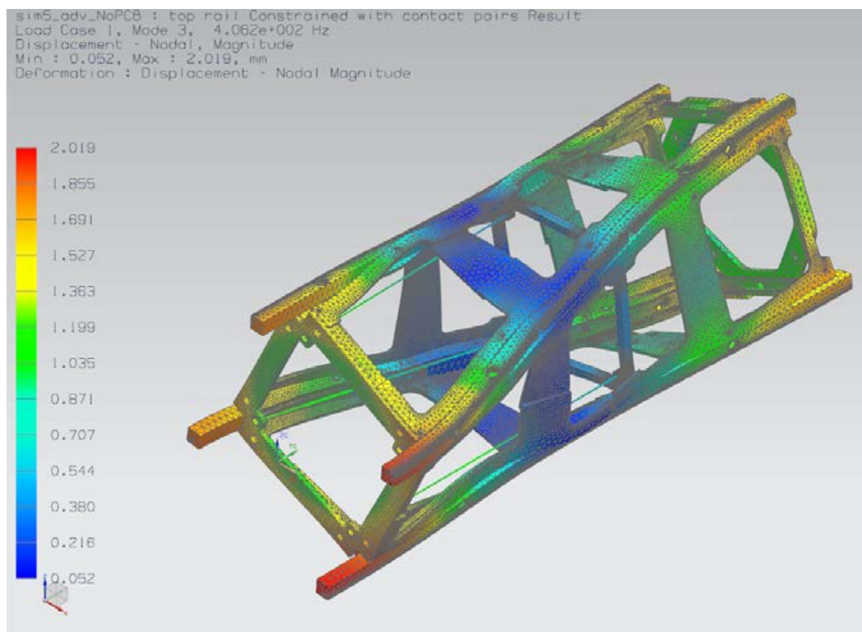

Figure 2.26: Mode 3, 406 Hz

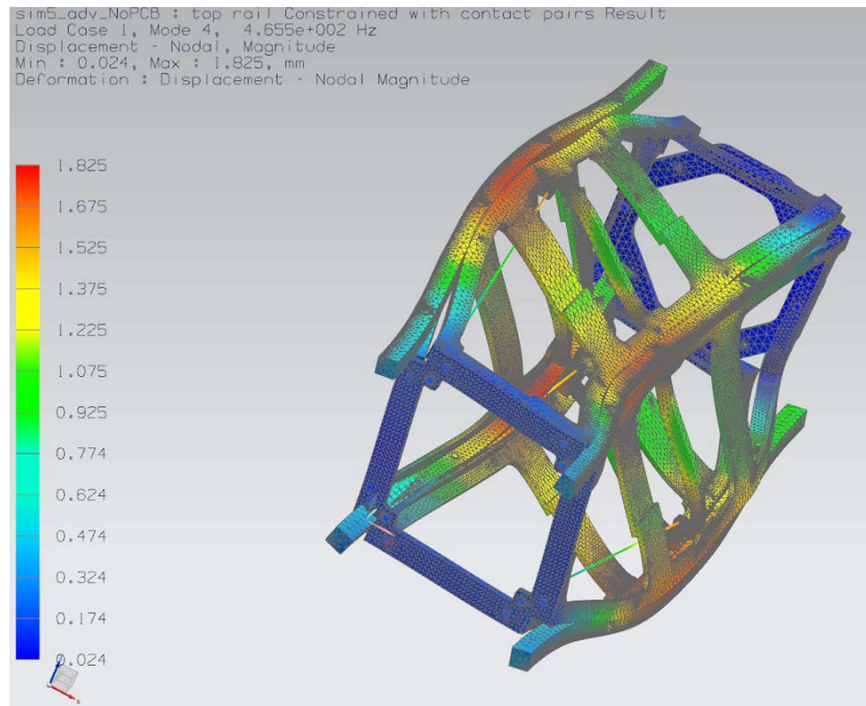

Figure 2.27: Mode 4, 465 Hz

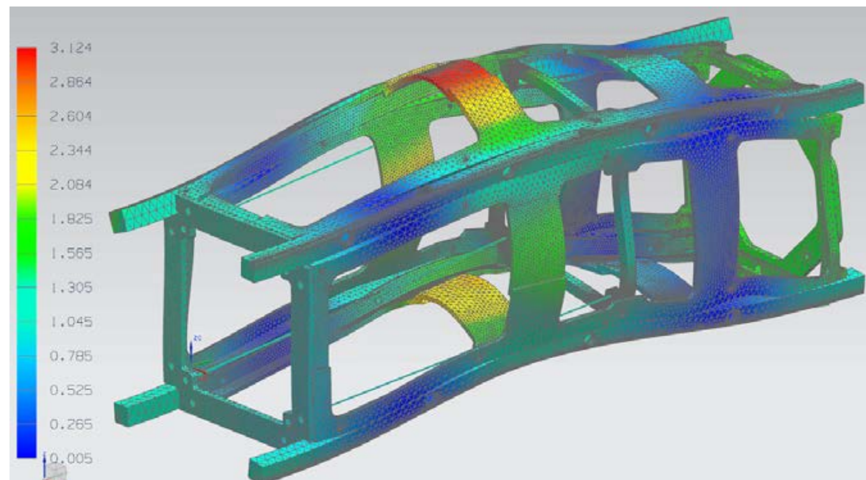

Figure 2.28: Mode 5, 701 Hz

The modal displacements shown in the previous five figures 32 through 37 since the satellite will be constrained in the launch container the structure will be limited in its displacement for the majority of the vibrational modes since the displacement will be restricted to ±500μm in the xy plane of the structure. Deformations as seen in figured 35 through 37 will not be possible without material failure of the aluminum structure.

2.5.2 Constrained at Rail Sides

The model for simulation was developed with the rail ends and sides constrained and contact boundary conditions developed to prevent the material from passing through the contact planes for each incident surface. The Simulation model with the constrained rail ends and the surface contact boundary conditions can be seen in Figure 2.29: Fully Constrained Structure.

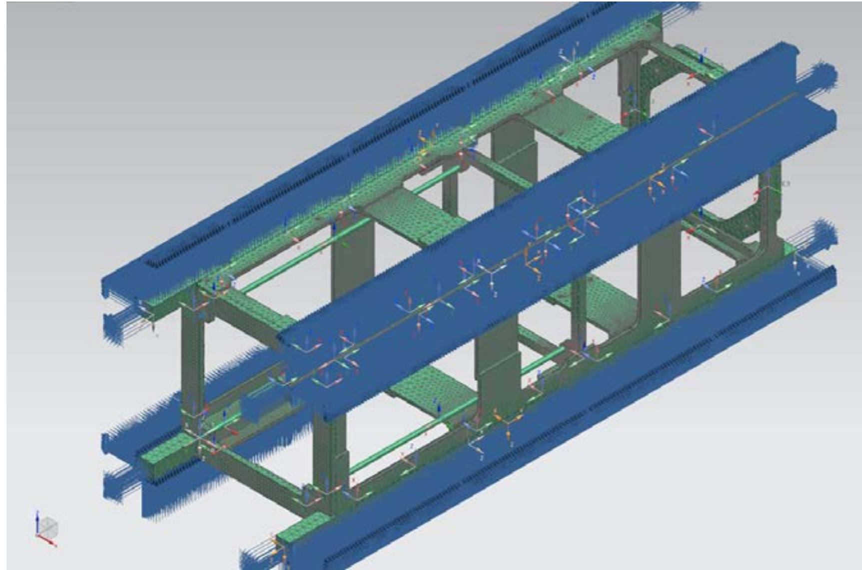

Figure 2.29: Fully Constrained Structure

2.5.2.1 Results

The deformation of the structure can be seen in the displacement however with the structure fully constrained the vibrational frequency mode is much higher than expected.

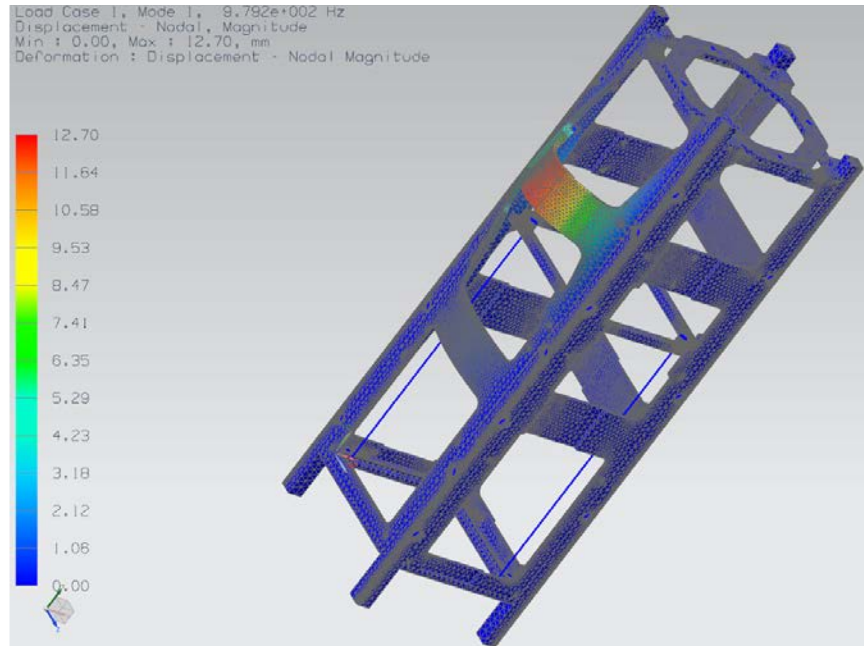

Figure 2.30: Mode 1, 979Hz

2.5.3 **Constrained at Rail Ends with PCB's**

The model for simulation was developed with the rail ends and sides constrained and contact boundary conditions developed to prevent the material from passing through the contact planes for each incident surface. The Simulation model had the printed circuit boards added to the structure however the problem exists that the vibrational mode and frequency of the printed circuit boards is very low and prevents the solver from finding the frequencies of the structural members.

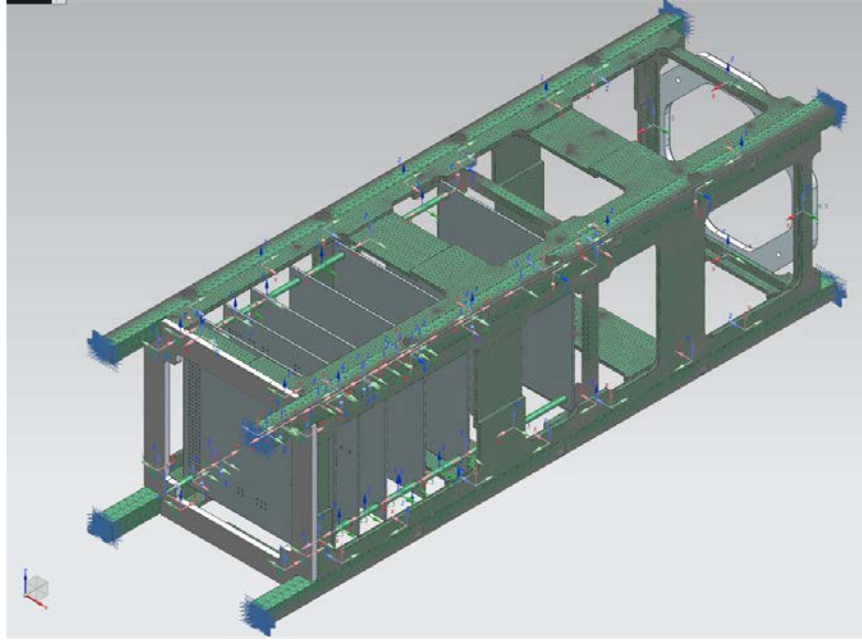

Figure 2.31: Structure with PCB and Constrained Rail Ends

2.5.3.1 Results

The deformation of the structure can be seen in Figure 2.32: Mode 1, 1.002 Hz the displacement of the printed circuit boards is quite small as expected however the frequencies at which they are vibrating is also very low approximately 1Hz which appears to be anomalous a number of techniques were attempted in order to remove these low frequency vibrations from the study, or to dampen them so that the primary frequencies of the structure could be observed with the PCB's installed in the system.

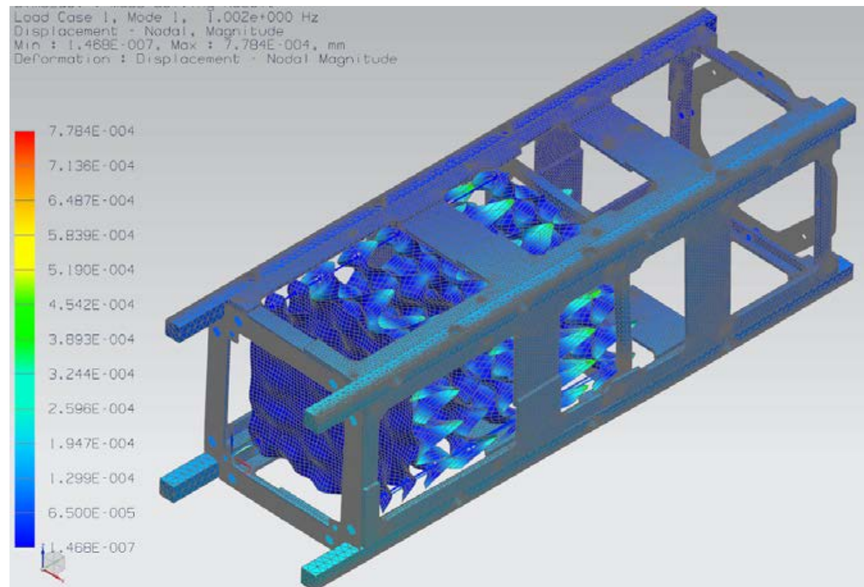

Figure 2.32: Mode 1, 1.002 Hz

2.6 PREVIOUS VIBRATION TESTING RESULTS

The results depicted in Appendix C 2012 Vibration Testing Results are from the previous satellite model which went through vibrational testing, this model shows similar frequency responses as the model under simulation in this study. However this new model has a significantly more rigid structure and therefore should also have higher frequencies than the previous model which underwent testing. The results from the previous testing campaign were used to help verify the validity of the simulation results prior to the next round of testing.

The three figures in the appendix show the X, Y, and Z plots of acceleration vs frequency, it can be seen from Figure C.3: X Plane Frequency Response and Figure C.4: Y Plane Frequency Response that the first fundamental frequencies are between 170Hz to 350Hz when compared to the simulation results in Figure 2.24: Mode 1, 306 Hz and Figure 2.25: Mode 2, 310 Hz the results are within expected ranges. The new structure which has been simulated using FEA in NX has been further rigidized from the model which underwent physical testing this can be source attributed to the increase in frequency response. The model in NX and the physical structure that underwent testing also have differing mass properties which could be attributed to the difference in vibrational response.

2.7 2014 VIBRATION TESTING RESULTS

The results shown in Appendix D 2014 Vibration Testing Results are from the most recent environmental testing performed on the ECOSat satellite. The satellite was instrumented with nine sensors looking at the rails, endplates, and radiation panels for frequency response, six additional accelerometers were used as control sensors; Table D-1: Sensor Legend cross references the sensors to the graphs can be found at the start of Appendix D. The satellite underwent vibration testing for each axis, the testing procedure consisted of performing a Low Level Sine (LLS) wave sweep at 0.5g from 5Hz to 2000Hz, followed by a random vibration test as outlined in Appendix A Random Vibration Specification followed by a second LLS wave sweep. The purpose of the first LLS is to develop a profile for the satellite with its instrumentation package, the second LLS is to ensure that the satellite configuration hasn't changed from the Random Vibration Test (RVT). The RVT is done to simulate the launch conditions for the satellite by exciting it with a controlled profile typically specified by the launch provider, in this instance it is specified by the CSDC.

The figures shown in the appendix represent all the data recorded from the testing campaign conducted in May 2014, from these graphs there are two important results to note. Firstly the results obtained in testing show strong correlation to the frequency response simulated in the NX environment. Secondly the magnitude of the testing results for the three axis show a similar response to that predicted by the FEA package.

However there are two noteworthy observations from the vibrational testing. First in Figure D.9: 1st Y-Axis Low Level Sine Response and Figure D.11: 2nd Y-Axis Low Level Sine Response it can be seen that sensor M2Y has a frequency response below the 90 Hz requirement set out by CSDC. Unfortunately the phase information for the testing results was not provided so this response cannot be confirmed as a fundamental frequency. It is assumed that the sub 90 Hz result is indeed a fundamental frequency response. The location of the sensor that corresponds to this measurement is on the corner rail of the satellite that contains the deployment switch. The section of the corner rail that houses the switch also has the longest distance between the end point of the rail and the closest fastener. Due to this it makes sense that the lowest frequency response would be observed at this point. The problem is compounded by the material missing due to the cutout for the switch and length between the rail end and nearest fastener.

The second noteworthy observation is in Figure D.14: 2nd Z-Axis Low Level Sine Response it can be seen that series 12 in the graph shows several concerning frequency responses which were not present in Figure D.12: 1st Z-Axis Low Level Sine Response. These large responses is due to the accelerometer detaching from the structure during either the random vibration test or the beginning of the 2nd LLS. Fortunately there was second sensor orientated in the same direction on the Z- plate, so there was additional data to corroborate results with.

If time and resources had allowed another set of tests would have been conducted for the Z-axis of the satellite to ensure that the structure had not been changed or modified by the random vibration test. Since this was not a viable option due to tight timelines it was decided that the satellite was not damaged since no physical damage was observed in the area in which the sensor was located. It was concluded that the satellite vibrational response data with the erroneous sensor reading was sufficient for the needs of the project.

After testing additional modeling was undertaken in an effort to reproduce the results and confirm the frequency response data. Also after lengthy discussion with experts in the use of NX for conducting FEA analysis for vibrational responses it was suggested that the model should be further simplified. This was in response to simulation times of the current model, computational resources required, and the number of elements in the model.

2.8 POST ENVIRONMENTAL TESTING SIMULATION RESULTS

A new model for the satellite underwent simulation upon returning to UVic, the model replaced the majority of the 3d meshes with 1d or 2d meshes. The driving factor behind this is an effort to have high fidelity models with reduced computation time. With the previous FEA model simulation times were around thirty minutes, after speaking with several experts in the field it became apparent that the simulations should be much lower and closer to a few minutes rather than dozens of minutes. The current model as depicted in Figure 2.33: No 3D Elements has yet to produce results that are consistent with those observed during environmental testing. However the simulation time has been reduced greatly to a few minutes and the model shows strong correlation to the frequency responses in the greater than 200Hz range.

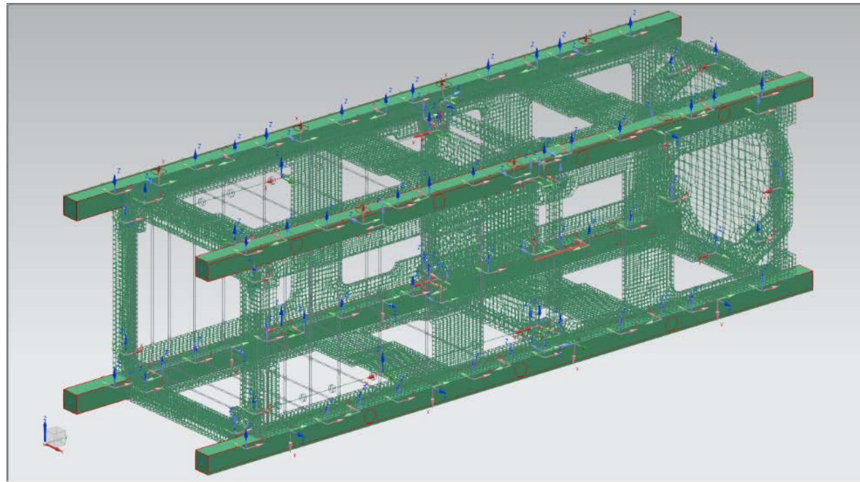

Figure 2.33: No 3D Elements

If Figure 2.34: Current Bulk and Figure 2.22: Bulk Element Data are compared it can be seen that the current element data is less than 20% of the previous simulation model and is only comprised of 2d and 1d elements. Whereas the previous model was dominated by 3d and 2d elements which enumerated over one million in total for the model.

Summary of Bulk Data cards written

NAME	NUMBER
CBAR	52
CBEAM	44
CONM2	8
CQUAD8	49484
CTRIA6	1751
EIGRL	1
GRID	152100
MAT1	2
MAT8	1
MATT1	2
PARAM	4
PBAR	1
PBEAM	2
PSHELL	4
RBE2	93
TABLEM1	3

Figure 2.34: Current Bulk Element Data

In order to increase the simulation accuracy applying 3d meshes to the corner rails is currently being considered in order to properly model the switch cutouts for the corner rails. The current model configuration uses 1d beam elements for the corner rails and as such lacks the detail for the switch cutout. This is currently the most likely attribution as to why the simulation is not showing the sub 90Hz vibrational response that is seen in the vibrational testing results.

2.9 CONCLUSION

The vibration analysis study covered in this section was conducted first since it has the largest bearing on the mechanical design of the structure and the mechanical structure has the strongest influence on the fundamental frequencies in each axis. These frequencies are of concern due to the 90 Hz or greater fundamental frequency requirement for each axis set out by the CSDC. [5]

The modeling of the vibrational modes of the satellite structure has the biggest impact on not only the design of the mechanical structure but also its interface to the electronic systems if it did not meet the required testing qualification levels.

The modeling and simulation of the ECOSat satellite structure and electronic circuit boards was successful in approximating the fundamental frequencies. The previous testing results were an excellent resource for the verification and qualification of the pre-environmental testing model. The use of these previous testing results for the current satellite structure

It was found from the simulations prior to testing in May 2014 that the first fundamental frequency appeared near or greater than 200 Hz in the XYZ axes of the structure. These simulation results were encouraging that the current design revision of the satellite would pass vibrational testing. The results obtained showed strong correlation to the results from testing at DFL as depicted in Appendix D. Several peaks can be seen in the range of 187 to 400 Hz in all three axes from the vibrational response data, this shows correlation to the simulation results previously discussed.

However there are two caveats one being a single frequency response which occurs at approximately 87 Hz, the phase data for the testing was not provided so unfortunately it cannot be confirmed if this is indeed the first mode. The second being a loss of a sensor during the final test of the Z-axis of the satellite. During either random vibrational testing or the beginning of the 2nd LLS sweep one of the Z-axis accelerometers became detached from the structure. Due to timeline and scheduling constraints we were unable to re perform the tests and it was deemed that our current test data was sufficient. The technicians at the DFL facility and other industry experts indicated that the loss of the sensor would be inconsequential to our overall assessment of the satellite frequency responses.

Additional modeling was undertaken after returning from testing in an effort to simulate the 87 Hz frequency response that was observed during testing. However as of yet the simulation results have not been able to reproduce the response. Additional techniques have been hypothesized and will be attempted in the future.

3 THERMAL MODELING AND TRANSFER SELECTION:

3.1 SUMMARY

A method for mitigating excessive heating in electronic components for a space based application was identified; additionally the material identified for the selected solution was tested against its manufacturer provided properties.

Much of the initial effort in this project was spent on researching possible heat transfer methods and analyzing their underlying mechanisms, this was required to insure that the system would be capable of functioning in the space environment as well as meeting the other parameters for the satellite such as form factor, mass, cost and development time. Once the heat spreader method for transferring the thermal energy had been identified as the most suitable candidate it was necessary to address the specific issues or caveats to implementing such a system. The drawback to the heat spreader thermal transfer solution is the bidirectional nature of its heat transfer. Ideally the system would be unidirectional so that the connected components could not accidently be heated if the heat sink becomes a higher temperature than the connected critical components.

For the heat spreader to function correctly it was required to identify a satellite component that could essentially function as a heat sink for the heat spreader and connected system components. The original thought was to connect directly to the radiator panels since they are the direct cooling method for the satellite. However the temperature delta's for the radiator panels are very high, since they have a small thermal inertia due to their low mass. From the previous work on the satellite using FEA it was identified that the structure of the satellite was a good candidate for acting as a heat sink due to its small temperature delta's and large mass.

The proposed solution to use a heat spreader consisting of pyrolytic graphite will be capable of meeting the mass, clearance, off gassing, and micro gravity constraints on the thermal management system. The pyrolytic graphite heat spreader is also a flexible structure making it easier to integrate with the electronic and mechanical systems. The equations developed in this study will be used in a subsequent study for more accurate modeling of the heat transfer in the FEA package.

3.2 INTRODUCTION

The purpose of this study was to analyze the current configuration of the ECOSat satellite and determine methods to improve the thermal safe operating area for system components which would either have improved performance by mitigating temperature delta's or those components which would have increased reliability with reduced temperature peaks. Various approaches were researched in order to converge on the most robust, reliable and efficient method for mitigating temperature fluctuations in the satellite systems. The caveat to finding an optimal solution to the thermal management of the satellite is the stringent volume and mass constraints which limit many traditional options as well as the requirement to loose less than 0.3% of total spacecraft mass, in addition to functioning in a micro gravity environment. Solutions were investigated with both empirical and analytic methods, NX was used to correlate results and provide simulations to emulate the in orbit temperature cycling of components. The results from this study will be implemented in the final design of the satellite to improve the temperature performance of all critically identified components and systems.

3.3 PROBLEM SPECIFICATION:

In the satellite several of the components have been identified as having marginal temperature operating zones or have extreme temperature variations which could lead to early failure or unnecessary thermal stress. [7] [8] [9] [10] [11] Many studies, reports, and articles have been written linking the failure of electronic systems and their components to issues surrounding temperature extremes and cycling for this reason our goal is to reduce these thermal stresses on the satellite systems. Since almost all the systems and their respective components have not been flight tested it is of great concern to mitigate such issues in order to provide a more robust design.

On the following page are two tables outlining the two extreme temperature situations the satellite will encounter during a one year orbital period. These tables were obtained from previous FEA thermal models of the satellite systems. The first is the "Hot Case" where the satellite was modelled having all its systems running at full power during the winter solstice which is when the satellite will be closest to the sun and receive the most solar heating. The second case is the "Cold Case" where the satellite was modeled as having all its systems in a minimum power state during the summer solstice which is when the satellite will be the farthest from the sun and receive the least solar heating. As can be seen by comparing Table 3-1: Hot Case and Table 3-2: Cold Case the components with the highest temperature or narrowest margins for their safe operating area are the: Communications Tx/Rx Board, Batteries, GPS, and Battery Charging Board. Additionally what can also been observed by comparing the two tables is the structure has some of the smallest temperature variability between the two cases as well it also has the

largest thermal inertia due to its mass and physical properties. For this reason the structure will be used as the "Heat Sink" for all the previously identified critical components, additional components may be identified during testing and added to the list as deemed necessary.

HOT CASE	Occurs on or around December Solstice(Dec 21). Sat is running on full power for all systems in this scenario.						
Affected Area	Max Temp		Operating Range	Pd	Margin	Conformity	Comments
	K	°C	°C	W	°C		
Voltage Reg Board	347	74	-55 to +125	2.68	51	Good	Boards would probably not reach this temperature. Model's method of coupling parts to one another could be improved for more accurate
Bat Charging Board	352	79	-25 to +125	2.13	46	Good	
GPS	347	74	-20 to +85	1.79	11	Good	
CPU/ADCS Board	346	73	-45 to +125	1.5	52	Good	Includes GPS
Comms Modem Board	351	78	-50 to +115	2.3	37	Good	
Comms Tx/Rx Board	374	101	-45 to +125	6.72	24	Good	
Payload	330	57	-20 to +85	0.7	23	Good	Max and Min both occur at points where the payload is coupled with the frame.
Spacecraft Body	336	63	-50 to +200	N/A	137	Good	Temp. is notably lower than board temps; suggests that further cooling of the board is possible.
Antenna	334	61	-30 to +90	N/A	29	Good	Occurs where the antenna is attached to the body
Batteries	334	61	-30 to +65	0.39	4	Marginal	assumes 40 mW dissipated per cell
Magnetorquers	333	60	-20 to +165	2.2	105	Good	Constant across hot and cold

Table 3-1: Hot Case

COLD CASE Occurs on or around June Solstice(June 21). Sat is running on lowest power for all systems in this scenario

Affected Area	Min Temp		Operating Range	PD	Margin	Conformity	Comments
	K	°C	°C	W	°C		
Voltage Reg Board	272	-1	-55 to +125	0.46	54	Good	Boards are still the warmest part of the craft. The close to the corners, where the bolts are attached, the cooler the boards are, in general.
Bat Charging Board	271	-2	-25 to +125	0.3	23	Good	
GPS	277	4	-20 to +85	0.3	-16	Good	
ADCS/CPU Board	271	-2	-45 to +125	1.5	43	Good	
Comms Modem Board	278	5	-50 to +115	2	55	Good	
Comms Tx/Rx Board	279	6	-45 to +125	1.6	51	Good	
Payload	268	-5	-20 to +80	0.6	15	Good	Both max and min temps occur at points where the payload is
Spacecraft Body	268	-5	-50 to +200	N/A	45	Good	Temperature is notably lower than board temperatures; Could probably be cooled further with more contact with the frame.
Antenna	275	2	-30 to +90	N/A	32	Good	Cold temperature occurs at attachment point, warmer as it goes outwards.
Batteries	271	-2	-30 to +65	0.11	28	Marginal	Within Spec, but significant capacity loss below 0C
Magnetorquers	270	-3	-20 to +165	2.2	17	Good	Constant across hot and cold

Table 3-2: Cold Case

3.3.1 Model Definition

The results presented in the previous tables were obtained from analysis preformed using Finite Element Analysis (FEA) this was accomplished by creating a study from the current solid model of the satellite seen below in Figure 3.1: Satellite External structure and Figure 3.2: Satellite Internal Structure. The level of detail of the satellite systems is quite refined; this must be simplified in order to perform a FEA analysis. The first render from the solid model Figure 3.1: Satellite External structure shows the satellite with all exterior components the perspective view depicts one full solar panel and a half solar panel and half radiator on the adjacent side the other two faces of the satellite which aren't visible are a mirror image of the displayed faces, minus the remove before flight pin shown on the left hand face.

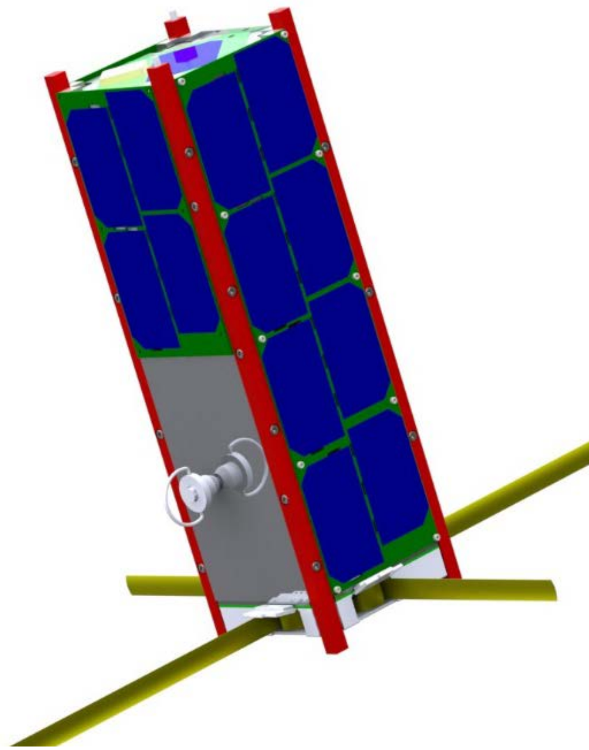

Figure 3.1: Satellite External structure

The second render below has the solar panel suppressed in order to display the internal level of detail of the satellite systems. Even though the image only shows a small section of the internal structure it is apparent that the current level of detail for the individual components and systems would make FEA lengthy and time consuming in order to accommodate the analysis a reduced detail model was created in the FEA environment NX only the critical elements of the satellite were retained in the simplified model.

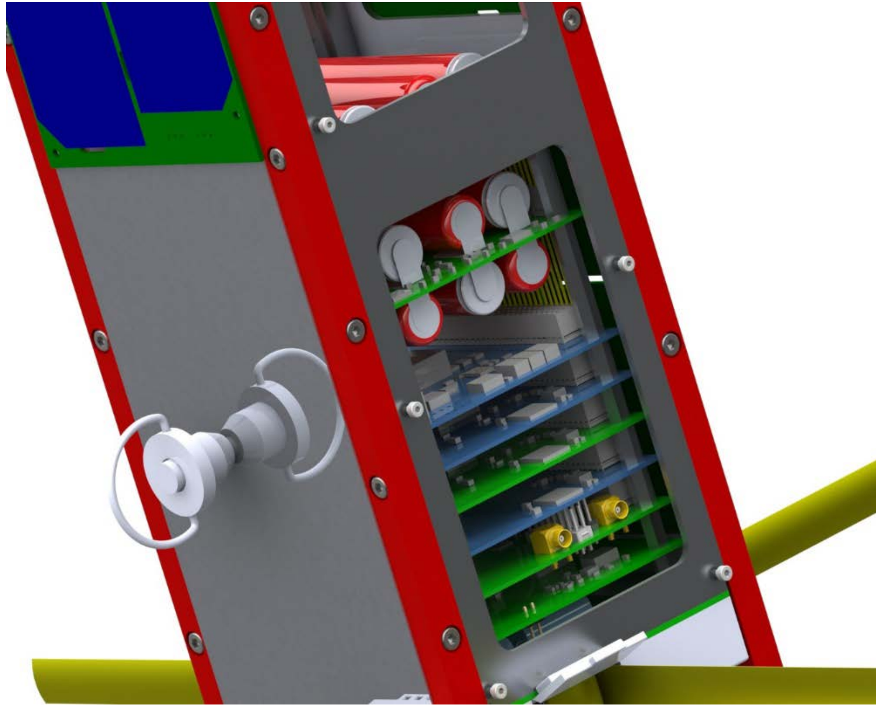

Figure 3.2: Satellite Internal Structure

The time required to analyze a fully resolved model of the satellite is not worth the increase in simulation accuracy. For the stated reasons a simplified model that combines many of the micro subsystems and boundary conditions has been created in order to expedite analysis as well as to simplify the result comprehension.

The current model has a reduced number of radiation elements specified; specifically for members of the satellite that have been identified as primary sinks and sources of radiation transfer such as the external surfaces of the satellite and the internal PCB Stack for the members which generate primary heat loads. Specifically the boards identified are the transmitter for the communication system and the power regulation boards since these two systems have been shown to have the highest power dissipation and therefore the largest heat load during prototype experimentation with the current satellite hardware.

The primary components for heat conduction in the satellite were identified as the structural members, the PCB stack, the radiator panels, and solar panels.

3.4 HEAT TRANSFER METHODS

The following section outlines the various approaches and techniques researched for the purpose of mitigating the thermal issues of the satellite. The summary at the end of the section will outline which approach was chosen and the details pertaining to the decision.

3.4.1 Bidirectional Heat Transfer

The following heat transfer methods conduct in both directions and have the same properties for either direction; there is no preference to the direction in which heat transfers.

3.4.1.1 Conventional Heat Pipe

Most heat pipes use a wick and capillary action to return the liquid from the condenser to the evaporator. The liquid is sucked up to the evaporator, similar to the way that a sponge sucks up water when an edge is placed in contact with a water pool. The wick allows the heat pipe to operate in any orientation; this property makes it ideal for space applications were gravity cannot be used to assist in the transfer of fluid.

3.4.1.2 Heat Spreader

A heat spreader is a heat exchanger that moves heat between a heat source, and a secondary heat exchanger whose surface area and geometry are more favorable than the source. Such a spreader is most often simply a plate made of copper, which has a high thermal conductivity. By definition, heat is "spread out" over this geometry, so that the secondary heat exchanger may be more fully utilized. This has the potential to increase the heat capacity of the total assembly, but the presence of the additional thermal junction will limit total thermal capacity. The high conduction properties of the spreader will make it more effective to function as an air heat exchanger, as opposed to the original (presumably smaller) source.

3.4.2 Unidirectional Heat Transfer

Conventional heat pipes transfer heat in either direction, from the hotter to the colder end of the heat pipe. Several different heat pipes act as a thermal diode, transferring heat in one direction, while acting as an insulator in the other

3.4.2.1 Thermosyphons

In a thermosyphon, liquid working fluid is vaporized by a heat supplied to the evaporator at the bottom of the heat pipe. The vapor travels to the condenser at the top of the heat pipe, where it condenses. The liquid then drains back to the bottom of the heat pipe using gravity, and the cycle repeats. Thermosyphons also act as diode heat pipes. When heat is applied to the condenser, there is no condensate available, and hence no way to form vapor and transfer heat to the evaporator. The fluid for the thermosyphon must be

carefully selected for the temperature range of the end application since the fluid must be able to phase change in order to efficiently operate.

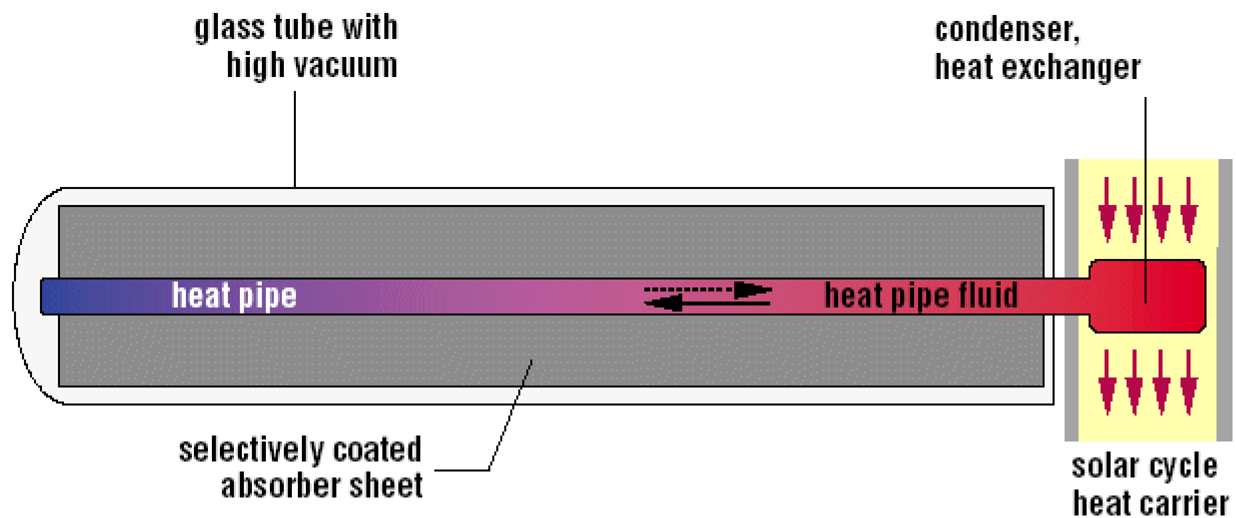

Figure 3.3: Thermosyphon

3.4.3 Variable Conductance Heat Pipes

Standard heat pipes are constant conductance devices, where the heat pipe operating temperature is set by the source and sink temperatures, the thermal resistances from the source to the heat pipe, and the thermal resistances from the heat pipe to the sink. In these heat pipes, the temperature drops linearly as the condenser temperature is reduced. For some applications, such as satellite or research balloon thermal control, the electronics will be overcooled at low powers, or at the low sink temperatures. Variable Conductance Heat Pipes (VCHPs) are used to passively maintain the temperature of the electronics being cooled as power and sink conditions change. [12]

VCHPs have two additions compared to a standard heat pipe: 1. A reservoir, and 2. A Non-Condensable Gas (NCG) added to the heat pipe, in addition to the working fluid. This NCG is typically argon for standard VCHPs, and helium for thermosyphons. When the heat pipe is not operating, the NCG and working fluid vapor are mixed throughout the heat pipe vapor space. When the VCHP is operating, the NCG is swept toward the condenser end of the heat pipe by the flow of the working fluid vapor. Most of the NCG is located in the reservoir, while the remainder blocks a portion of the heat pipe condenser. The VCHP works by varying the active length of the condenser. When the power or heat sink temperature is increased, the heat pipe vapor temperature and pressure increase. The increased vapor pressure forces more of the NCG into the reservoir, increasing the active condenser length and the heat pipe conductance. Conversely, when the heat sink temperature is decreased, the heat pipe vapor temperature and pressure decrease, and the NCG expands, reducing the active condenser length and heat pipe conductance.

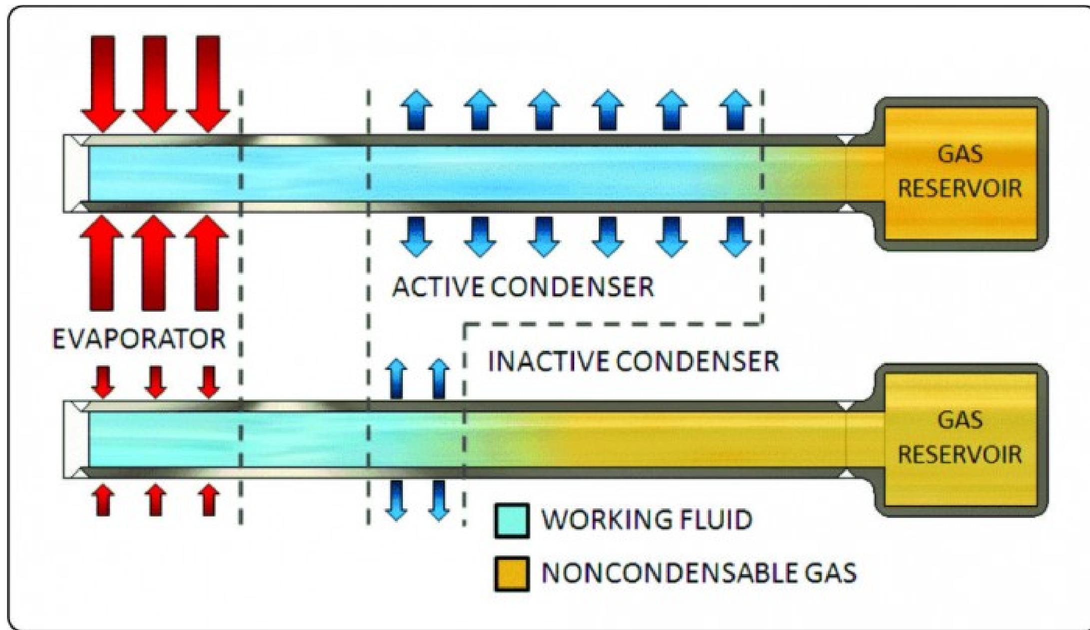

Figure 3.4: Variable Conductance Heat Pipes

3.4.3.1 Rotating Heat Pipes

The heat pipe is shaped so that liquid can only travel by centrifugal forces from the nominal evaporator to the nominal condenser. Again, no liquid is available when the nominal condenser is heated. However the system requires gravity to function in a unidirectional manner.

3.4.3.2 Vapor Trap Diode Heat Pipes

A Vapor Trap Diode (VTDHP) is fabricated in a similar fashion to a VCHP, with a gas reservoir at the end of the condenser. During fabrication, the heat pipe is charged with the working fluid and a controlled amount of a NCG. During normal operation, the flow of the working fluid vapor from the evaporator to the condenser pushes the NCG into the reservoir, where it doesn't interfere with the normal heat pipe operation. When the nominal condenser is heated, the vapor flow is from the nominal condenser to the nominal evaporator. The NCG is dragged along with the flowing vapor, completely blocking the nominal evaporator, and greatly increasing the thermal resistivity of the heat pipe. In general, there is some heat transfer to the nominal adiabatic section. Heat is then conducted through the heat pipe walls to the evaporator. In one example, a vapor trap diode carried 95 W in the forward direction, and only 4.3 W in the reverse direction. [13]

3.4.3.3 Liquid Trap Diode Heat Pipes

A Liquid Trap Diode (LDTHP) has a wicked reservoir at the evaporator end of the heat pipe, with a separate wick that is not in communication with the wick in the remainder of the heat pipe. During normal operation, the evaporator and reservoir are heated. The vapor flows to the condenser, and liquid returns to

the evaporator by capillary forces in the wick. The reservoir eventually dries out, since there is no method for returning liquid. When the nominal condenser is heated, liquid condenses in the evaporator and the reservoir. While the liquid can return to the nominal condenser from the nominal evaporator, the liquid in the reservoir is trapped, since the reservoir wick is not connected. Eventually, all of the liquid is trapped in the reservoir, and the heat pipe ceases operation.

3.4.3.4 Flat Heat Pipes

Thin planar heat pipes (heat spreaders) have the same primary components as tubular heat pipes: a hermetically sealed hollow vessel, a working fluid, and a closed-loop capillary recirculation system. In addition, a series of posts are generally used in a vapor chamber, to prevent collapse of the flat top and bottom when the pressure is lower than atmospheric.

They are primarily used when high powers and heat fluxes are applied to a relatively small evaporator. Heat input to the evaporator vaporizes liquid, which flows in two dimensions to the condenser surfaces. After the vapor condenses on the condenser surfaces, capillary forces in the wick return the condensate to the evaporator. Note that most vapor chambers are insensitive to gravity, and will still operate when inverted, with the evaporator above the condenser. In this application, the vapor chamber acts as a heat flux transformer, cooling a high heat flux from an electronic chip or laser diode, and transforming it to a lower heat flux that can be removed by natural or forced convection. With special evaporator wicks, vapor chambers can remove 2000 W over 4 cm^2, or 700 W over 1 cm^2. [14]

These thin planar heat pipes are finding their way into “height sensitive” applications, such as notebook computers and surface mount circuit board cores. These vapor chambers are typically fabricated from aluminum extrusions, and use acetone as the working fluid. It is possible to produce flat heat pipes as thin as 0.5 mm thinner than a credit card.

3.4.3.5 Loop heat pipe

A loop heat pipe (LHP) is version of the basic heat pipe that aims to increase performance by keeping the liquid and gas phases apart. [15] [16] Micro loop heat pipes have been developed and successfully employed in a wide sphere of applications both on the ground and in space.

3.5 HEAT TRANSFER METHOD SELECTION

After researching the possible methods for transferring thermal energy form components in the satellite to a sinking source the information was reviewed and a decision matrix was created in order to converge on the most appropriate design. The following table summarizes the design analysis for each of the methods outlined above.

Heat Transfer Method Selection Matrix									
	CHP	**HS**	**TS**	**VCHP**	**RHP**	**VTDHP**	**LTDHP**	**FHP**	**LHP**
Directional	0	0	1	1	1	1	1	1	0
Gravity	1	1	0	0	0	0	1	1	1
Mass	1	1	0	1	0	1	1	1	1
Longevity	1	1	1	1	1	1	0	1	1
Fabrication	1	1	0	1	1	1	0	0	0
Form Factor	0	1	0	0	0	0	0	1	0
Total:	**4**	**5**	**2**	**4**	**3**	**4**	**3**	**5**	**3**

Table 3-3: Heat Transfer Method Selection Matrix

After processing the various heat transfer methods through the selection matrix only two candidates remained for final selection, all methods that are unable to work without gravity were immediately removed regardless of final score. The Heat Spreader (HS) option and the Flat Heat Pipe (FHP) were found to be the two heat transfer methods which met the most requirements of the selection matrix. All though each method received the same final score they were marked in different categories, both methods were found to be gravity insensitive, require minimal mass, long service lifetime, and are able to work in the required form factor of the current satellite configuration.

For the HS method the disadvantage is the system is bidirectional that is to say it transfers thermal energy equally in both directions. This could potentially pose a threat to the satellite if the heat sink that the spreader is attached to becomes hotter than the device it is trying to cool. However if the structure of the satellite is used as the heat sink for the spreader it has a larger thermal inertia and has been modeled to show that it has minimal thermal fluxes compared to other systems in the satellite.

For the FHP method the disadvantage is the system requires specialized equipment to fabricate the physical structure as well as to evacuate the chamber and seal it, with the tight timeline and small budget of the team it would be very difficult to procure several custom made FHP's in time for the testing in spring 2014.

The final conclusion drawn from the selection matrix is the Heat Spreader method is the optimal choice for cooling components which are deemed to have critical temperatures or high heat fluxes.

3.5.1 Heat Spreader Material Selection

After selecting the method for transferring the thermal energy from the system components to the structure of the satellite a material and configuration for the spreader needed to be determined in order to finalize the solution for the thermal management of the satellite. Several materials were investigated such as aluminum, copper, and other metals which have high thermal conductivities however each of these solutions in order to be effective require a significant mass to provide the required thermal conductivity and capacity. An alternative solution was found using Pyrolytic Graphite the following table compares the properties of several materials proposed for use as a heat spreader.

Thermal Property Comparison				
	PGS	**Cu**	**Al**	**SiC**
Thermal Conductivity	1700.00 W/m-K	393.00 W/m-K	238.00 W/m-K	490.00 W/m-K
Specific Heat	712.00 J/kg-K	380.00 J/kg-K	270.00 J/kg-K	690.00 J/kg-K
Density	2210.00 kg/m^3	8900.00 kg/m^3	2700.00 kg/m^3	3200.00 kg/m^3
Thermal Expansion	1.6E-06 m/m-K	1.7E-05 m/m-K	2.3E-05 m/m-K	3.1E-06 m/m-K

Table 3-4: Heat Spreader Material Selection

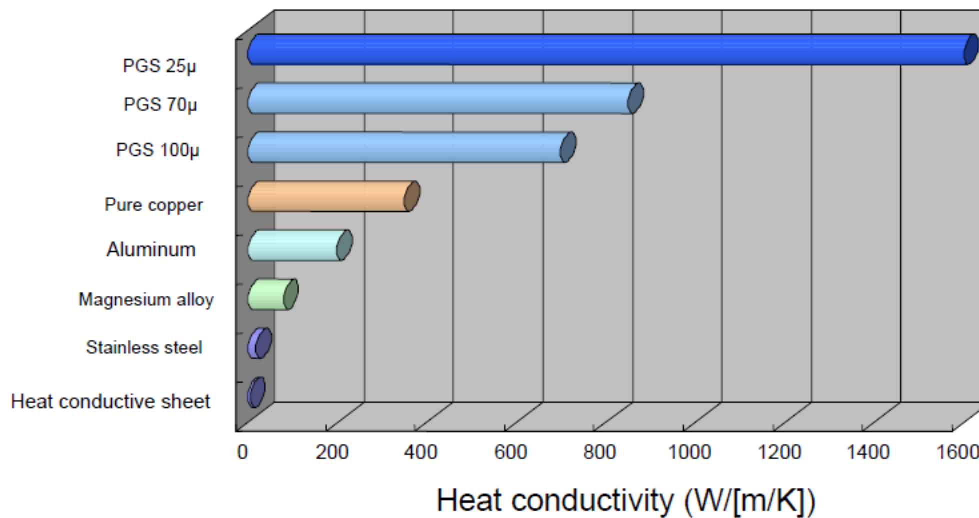

Figure 3.5: Heat Conduction of Each Material in the AB Plane

As can be seen from Table 3-4: Heat Spreader Material Selection and Figure 3.5: Heat Conduction of Each Material in the AB Plane the Pyrolytic Graphite Sheet (PGS) has the highest thermal conductivity, the largest specific heat, the lowest density, and the smallest thermal expansion making it an ideal candidate for the satellite thermal spreader. In addition the material is also flexible and easily manipulated to the form factor of the satellite since it is possible to cut the material using ordinary tools such as scissors, knifes, shears, or laser cutters.

3.5.1.1 What is Pyrolytic Graphite?

Pyrolytic Graphite (PG) is a unique form of graphite manufactured by decomposition of a hydrocarbon gas at very high temperature in a vacuum furnace. The result is an ultra-pure product which is near theoretical density and extremely anisotropic. This anisotropy results from the layered structure. As an example, PG exhibits a thermal conductivity consistent with the best conductors in the "AB" plane and lower than alumina brick in the "C" direction. Mechanical thermal, and electrical properties are generally far superior to conventional graphite's. Typical properties are listed below. PG is Available as plate, free-standing shapes (crucibles, boats, tubes, etc.), and as an impermeable coating on graphite and other substrates.

Pyrolytic Graphite Sheet (PGS) is an ultra-thin, lightweight, graphite film with a thermal conductivity high enough to release and diffuse the heat generated by heat sources such as CPU's, processors, power amplifiers and cameras. Developed by Panasonic engineers, this synthetically made material was named Pyrolytic Graphite Sheet or PGS. With a thermal conductivity up to four times greater than copper, PGS is extremely pliable and can be applied to heat-source shapes even in high-density mounting situations.

3.5.1.2 Properties of Pyrolytic Graphite:

3.5.1.3 Atomic Properties

Atomic Number: 6

Atomic Radius-Goldschmidt: 0.077 nm
Atomic Weight: 12.011 amu
Photo-Electric Work Function: 4.8eV
Thermal Neutron Absorption
Cross-Section: 0.0034 Barns

3.5.1.4 Physical Properties

Boiling point: 5000 C
Density @ 20 C: 2.25 g/cm^3
Melting point: 3650 C

3.5.1.5 Electrical Properties

Electrical Resistivity @ 0 C: 1.357 mΩ/cm
Cold Junction @ 0 C,
Hot Junction @ 100 C: +0.70 mV

3.5.1.6 Thermal Properties

Linear Expansion Coefficient @ 0 - 100 C : 0.6 - 4.3x10^{-6} m/m-K

Specific Heat @ 25 C : 712 J/kg-K

Thermal Conductivity, @ 0 - 100 C : 80 - 240 W/m-K

3.5.1.7 Mechanical Properties

Bulk modulus: 33 MPa

Hardness-Vickers: 0.5-1.0 kgf/mm^2

Elastic modulus: 4.80 GPa

However, the nature of the radiation damage to the graphite lattice places some fundamental limits on its useful lifetime in radiation shielding components. Increasing the crystalline perfection of graphite with higher production cost is suggested as one method of reducing the damage, but the actual life expectancy of a graphite component in a high radiation environment will depend upon the application and in particular effects such as exposure to neutron dose, level of external stresses and exposure to high energy particles from the sun.

If the neutron dose is considered independently as the limiting feature then it is reasonable to assume that development work might lead to materials of increased life expectancy. It may also be possible to make improvements in the microstructure, such as optimizing orientation, grain size and porosity distribution, but the problem with radiation damage in the crystallites seems to persist and may constitute an inescapable limitation.

For irradiation temperatures above 300 C the damage is due to defects which, if removed or decreased in number, will yield higher graphite lifetimes. One way of decreasing the defects which leads to reduced damage is by using heat treatment but this kind of treatment also reduces the strength of the graphite and makes it more expensive to manufacture. Results have shown that increased life can be obtained in highly orientated pyrolytic carbons, but in artificially manufactured graphite's the large internal strains will limit the life to a value dependent on the material, the irradiation temperature and dose.

3.5.1.8 Data and Correlation

Table 3-5: Pyrolytic Graphite Calculated and Empirical Properties shows the variation of structural and thermal properties of pyrolytic graphite with respect to temperature. [17] [18] [19] In Figure 3.6: Thermal Conductivity of PGS with Temperature depicts the variation of the thermal conductivity of pyrolytic graphite and in Figure 3.7: Specific Heat and % Thermal Expansion in the AB plane of Pyrolytic Graphite Vs Temperature structural properties with temperature.

Temp	Density	Elasticity Modulus		Poisson Ratio	Thermal Conductivity				Specific Heat	Ultimate tensile Strength	Thermal Expansion			
T	ρ	E emp	E calc	ν	K1 calc	K2 calc	K1 emp	K2 emp	C	Σμ	α - ab	α-ab%	α - c	α-c%
250 °K			5.28 GPa		6.30 W/m-K	2536.91 W/m-K	6.65 W/m-K		553.26 J/kg-K	7.06 MPa	1.6E-06 m/m-K	-0.02%	5.8E-06 m/m-K	-0.14 %
275 °K			5.29 GPa		5.77 W/m-K	2272.35 W/m-K	6.15 W/m-K		634.53 J/kg-K	7.22 MPa	1.6E-06 m/m-K	-0.01%	5.8E-06 m/m-K	-0.07 %
300 °K	2210.00 kg/m^3	5.35 GPa	5.30 GPa	0.14	5.32 W/m-K	2039.65 W/m-K	5.70 W/m-K	1950.00 W/m-K	712.25 J/kg-K	7.39 MPa	1.6E-06 m/m-K	0.00%	5.8E-06 m/m-K	0.00 %
325 °K			5.31 GPa		4.94 W/m-K	1835.90 W/m-K	5.30 W/m-K		786.51 J/kg-K	7.55 MPa	1.6E-06 m/m-K	0.01%	5.8E-06 m/m-K	0.07 %
350 °K			5.32 GPa		4.61 W/m-K	1658.37 W/m-K	4.90 W/m-K		857.38 J/kg-K	7.72 MPa	1.6E-06 m/m-K	0.02%	5.8E-06 m/m-K	0.14 %
400 °K		5.37 GPa	5.34 GPa		4.08 W/m-K	1371.80 W/m-K	4.09 W/m-K	1390.00 W/m-K	989.36 J/kg-K	8.04 MPa	1.6E-06 m/m-K	0.04%	5.8E-06 m/m-K	0.27 %

Table 3-5: Pyrolytic Graphite Calculated and Empirical Properties

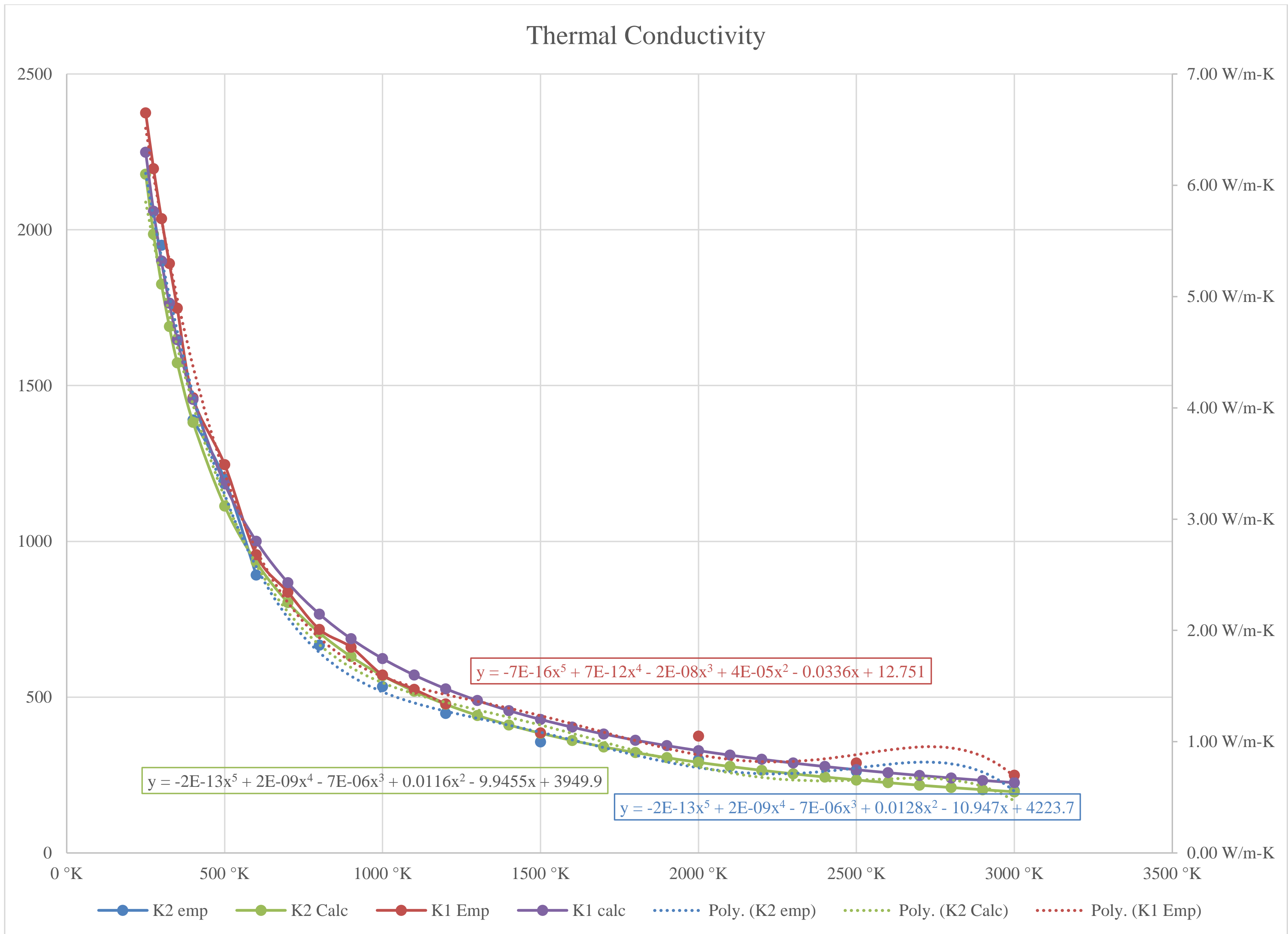

Figure 3.6: Thermal Conductivity of PGS with Temperature

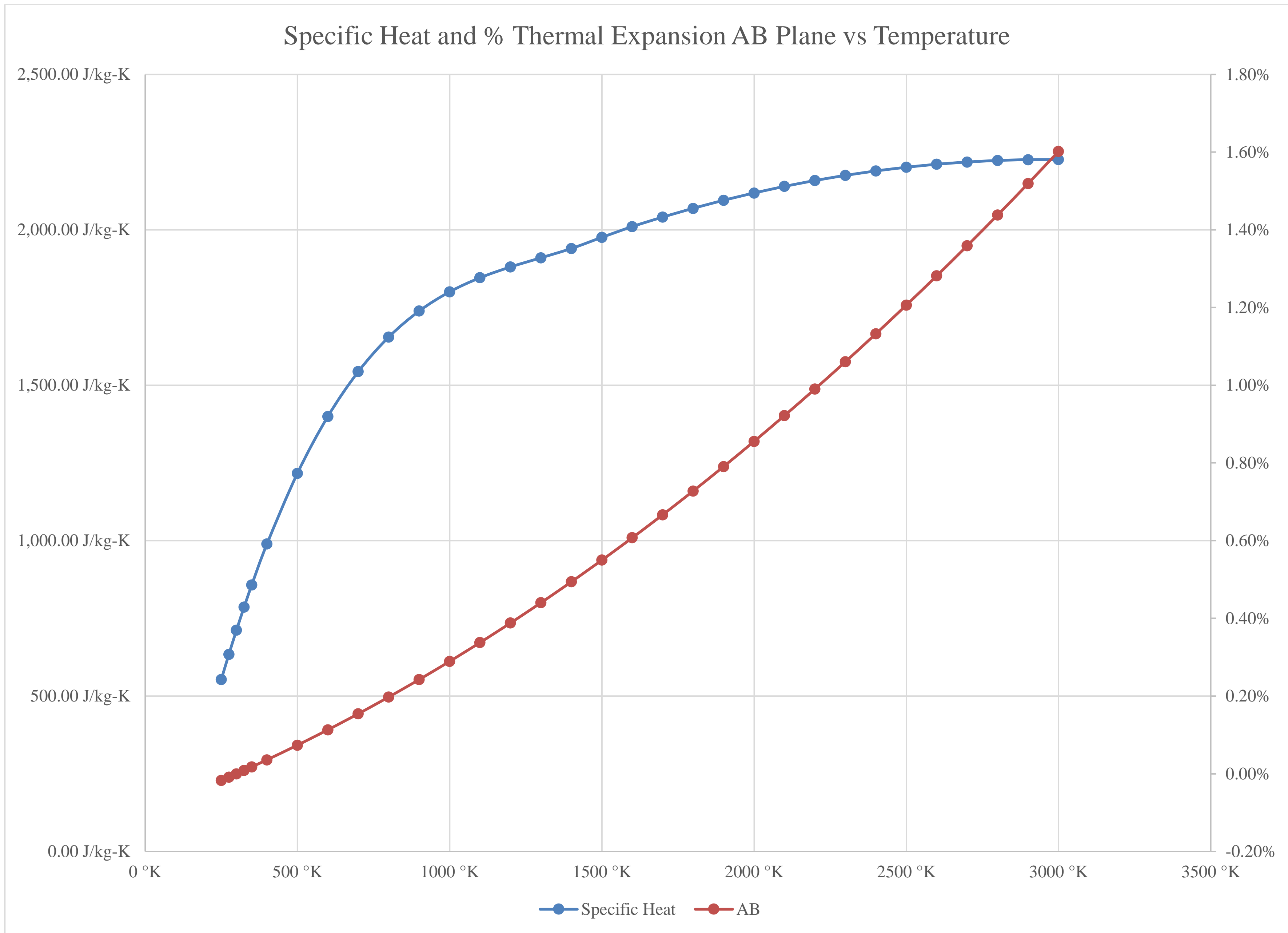

Figure 3.7: Specific Heat and % Thermal Expansion in the AB plane of Pyrolytic Graphite Vs Temperature

The calculated values in Table 3-5: Pyrolytic Graphite Calculated and Empirical Properties were ascertained by developing equations based on the empirical data from several manufacturers in order to provide high fidelity. Below is the list of the derived equations:

Thermal conductivity in W/m-K:

$$K_1 = 27.254 - 0.1315 * T + 2.3378 * 10^{-4} * T^2 + 2.5522 * 10^{-7} * T^3 + 1.1277 * 10^{-10} * T^4 - 1.825 * 10^{-14} * T^5$$

Equation 3.1: Thermal Conductivity of PGS in the C plane

K1 represents the thermal conduction through the thickness of the material the C plane.

$$K_2 = 7700.2 - 32.771 * T + 6.0693 * 10^{-2} * T^2 - 5.4398 * 10^{-5} * T^3 + 2.2946 * 10^{-8} * T^4 - 3.5965 * 10^{-12} * T^5$$

Equation 3.2:Thermal Conductivity of PGS in the AB plane

K2 represents the thermal conduction in the thickness of the material the AB plane.

Specific heat capacity c, in J/kg-K:

$$c = \begin{cases} -4740 + 4.9532T - 3.6093\times10^{-3}T^2 + 9.3068\times10^{-7}T^3 & 300 \le T \le 1500K \\ 12074 + 0.6876T - 1.16\times10^{-4}T^2 & 1500 < T \le 3000K \end{cases}$$

Equation 3.3: Specific Heat Capacity of PGS

Modulus of elasticity E, in GPa:

$$E = 5.24 + 3.1429\times10^{-5}T + 5.4286\times10^{-7}T^2$$

Equation 3.4: Modulus of Elasticity of PGS

Thermal expansion coefficient α, in m/m-K:

$$\left(\frac{\Delta\alpha}{\alpha}\right)_{a-dir} = \left(-9.3391\times10^{-2} + 2.9624\times10^{-4}T + 9.0036\times10^{-8}T^2\right)\times10^{-2}$$

Equation 3.5: Thermal Expansion of PGS relative to Alpha in the AB Plane at 300K

$$\alpha_{a-dir} = 1.6 \times 10^{-6}\left[1 + \left(\frac{\Delta\alpha}{\alpha}\right)_{a-dir}\right]$$

Equation 3.6: Absolute Thermal Expansion of PGS in AB plane

$$\left(\frac{\Delta\alpha}{\alpha}\right)_{c-dir} = \left[2.7174 \times 10^{-3}(T - 300)\right] \times 10^{-2}$$

Equation 3.7: Thermal Expansion of PGS relative to Alpha in the C Plane at 300K

$$\alpha_{c-dir} = 5.8 \times 10^{-6}\left[1 + \left(\frac{\Delta\alpha}{\alpha}\right)_{c-dir}\right]$$

Equation 3.8: Absolute Thermal Expansion of PGS in C plane

Ultimate tensile strength σ_u, in MPa:

$$\sigma_u = \begin{cases} 5.30 + 7.32 \times 10^{-3}T - 1.20 \times 10^{-6}T^2 & 300 < T < 2000K \\ 15.0 & T \geq 2000K \end{cases}$$

Equation 3.9: Ultimate Tensile Strength of PGS

Equations 1-2 and 4-7 are valid in the range 300-3000 K and Equations 3 and 8 are valid in the range 300-2500 K.

These equations were developed in order to provide additional resolution and refinement to the FEA project to properly evaluate the thermal energy transfer of the pyrolytic graphite in the satellite structure. As can be seen from Table 3-5: Pyrolytic Graphite Calculated and Empirical Properties and Figure 3.6:

Thermal Conductivity of PGS with Temperature the formulas show strong correlation between empirically found values and the calculated values derived from the equations the final equations coefficients will be modified once a manufacturer specific material is selected in order to closely match the materials profile for modeling purposes. In addition all the plots of the thermal conductivity for the pyrolytic graphite samples shows a tight grouping within the projected operating range for the satellite.

3.6 Manufacturer Specific PGS Selection

3.6.1 Momentive

Pyrolytic Graphite (PG) is a unique form of ultra-pure graphite manufactured by Momentive using hydrocarbon gas decomposition at high temperature in a vapor deposition furnace. The parameters listed in Figure 3.8 depicts the manufacturer specific properties. [20]

Typical Properties		
Density		2.18-2.22 g/cc
Flexural Strength	(a b)	18,000 psi (120 MPa)
Tensile Strength	(a b)	12,000 psi (80 MPa)
Compressive Strength	(a b)	15,000 psi (100 MPa)
Young's Modulus	(a b)	$3x10^6$ psi (20,000 MPa)
Coefficients		
Thermal Expansion	(a b)	$0.5x10^{-6}$ cm/cm/°C
	(c)	$2\text{-}x10^{-6}$ cm/cm/°C
Thermal Conductivity	(a b)	300 watts/meter °C
	(c)	3.5 watts/meter °C
Electrical Resistance	(a b)	$0.5x10^{-3}$ ohm-cm
	(c)	0.5 ohm-cm
Crystal Structure		Hexagonal
(C/2 Spacing)		(3.4Å)
Melting Pt. (Atmosphere)		Sublimes @ 3650°C
Purity		
Total		0.01% Maximum
Total Metallic		10 ppm
Outgassing		Negligible

Figure 3.8: Momentive PGS Properties

3.6.2 Minteq

PYROID® pyrolytic graphite is a form of graphite manufactured by Minteq using chemical vapor deposition. It is a carbon product grown atom-by-atom with superior thermal and electrical properties. The manufacturer specific properties can be seen in Figure 3.9 [21]

Physical Properties for PYROID® HT Pyrolytic Graphite

Property	Direction*	Metric Units	English Units
Density	--	2.22 g/cc	137 lb/ft^3
Tensile Strength			
Room Temperature	a	28,900 kPa	4,200 psi
Elastic Modulus			
Room Temperature	a	50 GPa	7.2 x 10^6 psi
Flexural Modulus			
Room Temperature	a	33,200 MPa	4.8 x 10^6 psi
Coefficient Thermal Expansion			
Room Temperature	a	-.60x10^{-6} cm/cm°C	-1.0x10^{-6} in/in°F
Room Temperature	c	25x10^{-6} cm/cm°C	44x10^{-6} in/in°F
Thermal Conductivity			
Room Temperature	a	1700 W/m°K	984 BTU/hr-ft-°F
Room Temperature	c	7 W/m°K	4.00 BTU/hr-ft-°F
Electric Resistivity			
Room Temperature	a	500 microhm-cm	197 microhm-cm
Room Temperature	c	0.6 ohm-cm	0.24 microhm-cm
Oxidation Threshold	a	650°C	1200°F
Permeability		Helium Leak Tight at 10^{-6} mmHg	

* a: Along basal planes (across surface)
c: Through basal planes (through thickness)

Figure 3.9: Minteq PGS Properties

3.6.3 Panasonic

PGS is a very thin, lightweight, flexible, graphite film with thermal conductivity higher than standard copper and aluminum. The manufacturer specific properties can be seen in Figure 3.10. [22]

Characteristics		Specifications			
Thickness		0.10 ± 0.03 mm	0.07 ± 0.015 mm	0.025 ± 0.010 mm	0.017 ± 0.005 mm
Density		0.85 g/cm³	1.1 g/cm³	2.1 g/cm³	2.10 g/cm³
Thermal Conductivity	a-b plane	600 to 800 W/(m·K)	750 to 950 W/(m·K)	1500 to 1700 W/(m·K)	1750 W/(m·K)
Electrical Conductivity		10000 S/cm	10000 S/cm	20000 S/cm	20000 S/cm
Extensional Strength		19.6 MPa	22.0 MPa	30.0 MPa	40.0 MPa
Expansion Coefficient	a-b plane	9.3×10^{-7} 1/K	9.3×10^{-7} 1/K	9.3×10^{-7} 1/K	9.3×10^{-7} 1/K
	c axis	3.2×10^{-5} 1/K	3.2×10^{-5} 1/K	3.2×10^{-5} 1/K	3.2×10^{-5} 1/K
Heat Resistance		400°C			
Bending (Angle 180, R5)		10000 Cycles			

Figure 3.10: Panasonic PGS Properties

3.6.4 Manufacturer Selection

Between the available manufacturers for Pyrolytic Graphite Sheet only Panasonic and Minteq have comparable specification, the PGS available from Momentive is only a fraction as conductive as the other two candidates. Since the properties for the PGS between the two companies is so similar the only debate was availability procuring Minteq PGS is slightly more difficult since it is only available directly from the company where as Panasonic is available from Digikey in Richmond, BC. The price points were similar and therefore since we already regularly order from Digikey the obvious choice was to select Panasonic as the preferred brand.

3.7 TESTING

After the manufacturer specific material was selected confirmation of the properties of the material was required in order to insure that the simulation of the PGS would be accurate reflection of the real world material.

3.7.1.1 Heat Transfer

Below is a test configuration with three strips of material each piece is 18mm wide by 180mm long and 100µm thick, each strip was painted matte black in order to produce a uniform surface reading for the infrared camera to register. The gray square located at the bottom of each material strip is a 10X10mm electric heater working at 8V and supplying 12W of total heating.

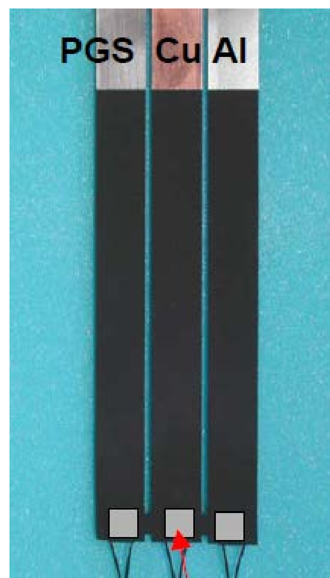

Figure 3.11: Heat Transfer Experiment

The experiment was conducted until a sample showed heat transfer to the end of the painted region, the experiment was replicated 5 times to ensure accurate results and replicability for future students. The experiment showed that after 10 seconds the PGS had transferred the thermal energy from the heater to the end of the sample, this is the expected result since PGS shows a much higher thermal conductivity then copper or aluminum below in Figure 3.12: Experiment Heating for 10 Sec.

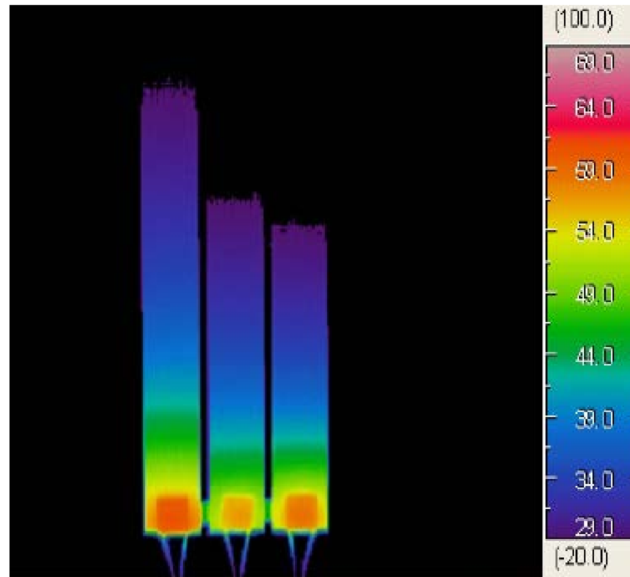

Figure 3.12: Experiment Heating for 10 Sec

Using the same experimental setup the goal was to test the cooling rate of the three materials and to verify the operation of PGS as a heat spreader. The three sample materials were brought to a temperature steady state at which the tip of each sample opposite the heater were all comparable in temperature relative to the resolution of the infrared camera. The experiment was conducted for 20 seconds after reaching steady state as can be seen in Figure 3.13: Experiment Cooling for 20 Sec the PGS is also faster at dissipating the heat than the copper or aluminum.

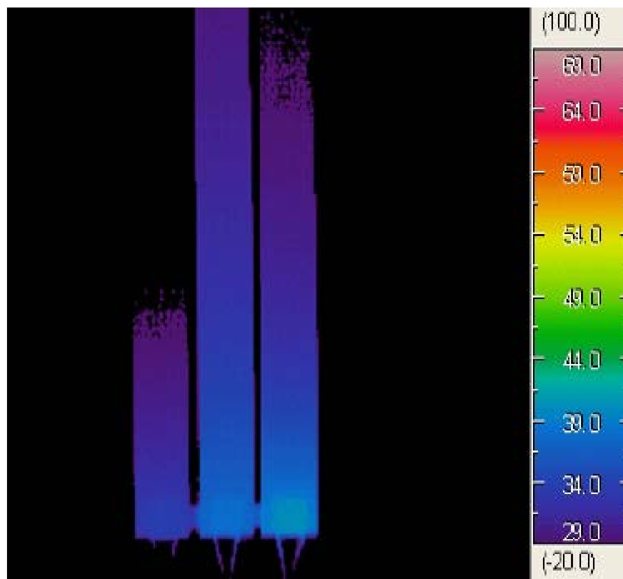

Figure 3.13: Experiment Cooling for 20 Sec

3.7.1.2 Heat Spreading

After confirming the materials operation as a heat transfer device it was also required to confirm its optimal selection as a heat spreading device since the material will be used to not only transport thermal energy away from heat sources but to efficiently distribute it to another heat sink. The following experiment consists of a 90x90x1mm sheet of copper, aluminum, and PGS. The experiment was conducted for 30 minutes using the same heaters as the first experiment the time frame was selected such that there was no detectable temperature variation from any of the samples. As seen in Figure 3.14: Heat Spreader Experiment it is clearly shown from the infrared camera that the PGS has the lowest surface temperature as well as the most uniform heat distribution, in addition it also shows that the heating element is 8.7 C° cooler than the copper sheet, and 10 C° cooler than the aluminum sheet this also indicates that the PGS has high heat dissipation.

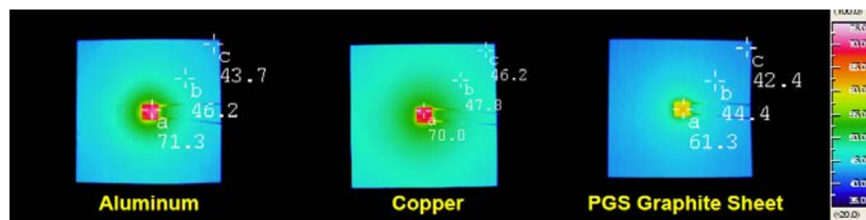

Figure 3.14: Heat Spreader Experiment

The empirical testing of the materials show above in Figure 3.12: Experiment Heating for 10 Sec, Figure 3.13: Experiment Cooling for 20 Sec, and Figure 3.14: Heat Spreader Experiment show strong correlation to the manufacture specified material properties, although exact numeric values for the thermal conductivity were not calculated for the experiments the results indicate that PGS is a far superior heat transfer material than the traditional copper or aluminum products tested.

3.8 CONCLUSION

This project was very insightful into the thermal modeling and characterization of the electronic systems in the satellite and how the thermal management for the critical system components can be achieved. Much of the initial effort in this project was spent on researching possible heat transfer methods and analyzing their underlying mechanisms for functioning, this was required to insure that the system would be capable of functioning in the space environment as well as meeting the other parameters for the satellite such as form factor, mass, cost and development time. Once the heat spreader method for transferring the thermal energy had been identified as a suitable candidate it was necessary to address the specific issues or caveats to implementing such a system. The drawback to the heat spreader thermal transfer solution is the bidirectional nature of its heat transfer. Ideally the system would be unidirectional so that the connected components could not accidently be heated if the heat sink becomes a higher temperature than the connected critical components.

For the heat spreader to function correctly it was required to identify a satellite component that could essentially function as a heat sink for the heat spreader and connected system components. The original thought was to connect directly to the radiator panels since they are the direct cooling method for the satellite however the temperature delta's for the radiator panels are very high, since they have a small thermal inertia due to their low mass. From the previous work on the satellite using FEA it was identified that the structure of the satellite was a good candidate for acting as a heat sink due to its small temperature delta's and large mass. An additional bonus to using the structure as the sink for the heat spreader is that the PGS can be connected to the critical system components and then fastened to the internal supporting structure. For integration with the PCB stack the system is very flexible in its ability to be modular and assembled outside of the satellite structure and integrated to the external structure when convenient. The heat spreader itself is also physically flexible which will aide during assembly and integration of the mechanical and electronic components.

The final step of the project was verifying the empirical results of the manufacturer specific PGS. From the testing conducted the material showed strong correlation to the data provided by the manufacturer, furthermore the equations that were developed in this project were then also integrated into the FEA environment to provide a greater accuracy in the modeling of the material for the transfer of thermal energy.

The future work on this project will be to work with the team to identify routing positions, geometry, and component specific connections based on the type of heat dissipation required in the satellite. This is required so the PGS heat spreader can be effectively connected to all sub-systems without interfering with

cabling, switching and other critical mission or system components. Once these issues have been resolved it will be possible to perform further FEA where the empirical equations developed in this study can be implemented to provide greater simulation accuracy.

4 HEAT SPREADER IMPLEMENTATION AND OPTIMIZATION:

4.1 SUMMARY

This project was successful in modeling a simplified form of the current satellite structure and performing the thermal analysis on the transmitter system with the heat spreader attached. The correlation between previous experimental data and the current simulations indicates that the results obtained from the NX FEA should be well correlated to the new testing results obtained at the end of May. Further work will be conducted on the model to increase its fidelity between the physical structure and the simulated model, additional structural members will be added to the model and the simulation process will be repeated.

The optimization and analysis process provided a solid base for creating a prototype design for each of the subsequent systems, as well as approximate sizing for the width of each individual heat spreader based on the required reduction in surface temperature.

The results from the optimization will be used as a starting point for determining the best configuration for all circuit elements. A number of simplifications were conducted in this study, mainly due to the complexity of the physical model and the dynamic relationship between each system. Further studies will be conducted looking into how the heat transfer is affected by factoring in the varying temperature of the satellite structure due to orbital heating cycles. The heat loads from other systems being coupled to the same structure will also need to be studied in order to determine the optimum heat spreader width for each system to minimize the temperature deltas in all systems as well as to minimize cross coupled heat transfer between subsystems since each heat spreader acts as a bidirectional heat transfer medium.

4.2 INTRODUCTION

In Thermal Modeling and Transfer Selection: section the method of thermal transfer was identified as using a heat spreader with pyrolytic graphite as its conduction material. The work in this section will focus on the simulation and analysis of the heat spreader for a specific coupling. The selected problem is to resolve the heating problems with the linear power amplifier on the transmitter. The heating problem identified with the batteries was rectified with the addition of a heating element and an aluminum bracket. This change to battery configuration ameliorated both the Hot and Cold case results for the batteries. The transmitter was selected since it has the smallest margin for the hot case condition as identified in Table 3-1: Hot Case additionally it also has the highest dissipated power of any system. The results of this work will be used to optimize the heat spreader design for the satellite. Since the thermal conductivity of the pyrolytic graphite material changes proportional to its thickness the sizing of the heat spreader for both

thickness and width will be conducted to reduce the case temperature of the electronic components. The optimization for this study will focus on the heat transfer for the passive heat spreaders. By optimizing the heat transfer between electronic components and the heat sink (Aluminum structure) further improvements for the overall system design can be realized.

By reducing the temperature of electronic components and optimizing for minimum temperatures deltas will help improve the durability of the satellite systems since there have been direct correlations between temperature cycles and mechanical fatigue and stress. [23] [24] [25]

To achieve this goal the equations developed in Section 3will be implemented into the FEA model of the satellite to more accurately predict the heat spreader capabilities. A simplified solid model of the satellite base structure and the PCB that houses the transmitter power amplifier will be created in the NX modeling environment. Several cases will be investigated in order converge on the optimal design parameters. This study will have the additional benefit that it will aid in determining the final configuration and location for the heat spreader mounting interface on the satellite structure.

4.3 PROBLEM SPECIFICATION

In the satellite several of the components have been identified as having marginal temperature operating zones or have extreme temperature variations which could lead to early failure or unnecessary thermal stress. [7] [8] [9] [10] [11] Many studies, reports, and articles have been written linking the failure of electronic systems and their components to issues surrounding temperature extremes and cycling for this reason our goal is to reduce these thermal stresses on the satellite systems. Since almost all the systems and their respective components have not been flight tested it is of great concern to mitigate such issues in order to provide a more robust design.

4.4 HEAT SPREADER MATERIAL SELECTION

See Section 3.5.1 for details on material selection.

4.5 SOLID MODEL

The base solid model for the heat spreader optimization was created to best represent the typical application for the satellite systems. Since there are several system level boards it is beyond the scope of this study to optimize the overall configuration of the heat spreader system. For simplicity the base model was used to represent the highest power dissipation load with a single Integrated Circuit (IC) that the satellite system has namely the power amplifier for the transmitter section of the communication system. The Aluminum mounting plate was kept at a constant temperature, the real system will have a varying temperature based on the orbit time and mission profile of the satellite. However for the base case of modeling and optimizing the heat spreader for the electronic systems this approximation will serve well for determining the ideal configuration.

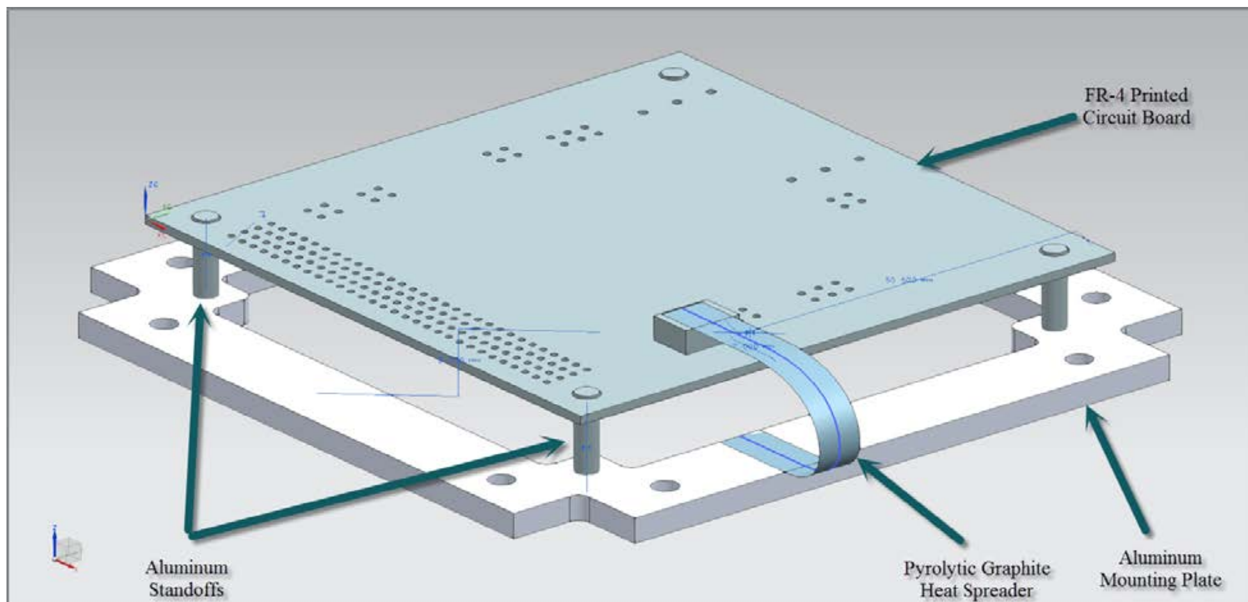

Figure 4.1: Solid Model of Electronic Component Mounting

The primary heat conduction paths will be through the Standoffs, the Pyrolytic Graphite Heat Spreader, and the ground connections in the 120 pin connector seen on the left half of the PCB in Figure 4.1: Solid Model of Electronic Component Mounting**.** The pyrolytic graphite sheet was modeled as a surface with no thickness, the finite element model of the material will have the parameters for varying the thickness of the material.

4.5.1 Additional Modeling

The original solid model that was created to simulate the thermal transfer characteristics of a printed circuit board did not feature the aluminum standoffs in the model. A coupling between the printed circuit board and the aluminum base plate was attempted however this did not result in creating a viable solution. It was required to recreate the model such that the solid models for the standoffs were underlying the beam meshes created to join the two modeling entities.

4.5.2 Optimization Caveat

After much investigation and research it did not seem possible to relate the "Thermal Conductivity" of the material to its thickness in order to perform a multi-variable optimization of the solution. Instead the material was optimized for two separate conditions with the end points of the thermal conductivity were optimized for the thickest and thinnest material, as per Table 4-1: PGS Thermal Conductivity by Thickness.

Thickness	Thermal Conductivity *W/m.K*
17um	1700
25um	1450
70um	900
100um	700

Table 4-1: PGS Thermal Conductivity by Thickness

4.6 FINITE ELEMENT MODEL

With the knowledge gained from the previous modeling and simulation work in NX on the vibrational and modal states of the satellite the simplified modeling for the thermal optimization went smoothly. The mesh types were chosen as 3D and 2D to represent the solid geometry of the system.

4.6.1 3D Meshes

For the 3D tetrahedral meshes three solid models were determined to require solid meshing the Aluminum Mounting Plate, the Integrated Circuit, and the Aluminum Standoffs. All meshes were created with the auto calculated mesh size using TET4 elements. After simulating results were analyzed for discontinuities that could be attributed to insufficient mesh density through the volume of the solids, none were found.

4.6.2 2D Meshes

For the 2D planar meshes two model elements were determined to be suitable candidates the Pyrolytic Graphite Sheet since it was modeled as a surface, and the printed circuit board since it also has a minimal thickness. Both Materials were modeled as orthographic types for their thermal parameters.

4.7 SIMULATION MODEL

4.7.1 Thermal Load

The thermal load for the system was determined based on the worst case scenario for the satellite systems, the largest single power dissipation of any system is the Power Amplifier for the transmitter section of the communication system which is capable of dissipating 650mA of current at 5V which translates to an approximate heat dissipation of 3.25W. The load case for the thermal study was applied to the volume of the transmitter with a uniform distribution.

4.7.2 Thermal Couplings

In order to calculate the thermal conductance between elements it is required to define a thermal coupling for their conductive properties. Since the NX environment calculates the area and temperature deltas all that is required is to determine the “Heat Transfer Coefficient”, this can be accomplished by simplifying Fourier’s Law.

Fourier's Law expresses conductive heat transfer as

Equation 4.1: Fourier's Law

$$q = \frac{k * A * dT}{s}$$

Where:

q = heat transfer (W, J/s, Btu/s)

A = heat transfer area (m^2, ft^2)

k = thermal conductivity of the material (W/m.K or W/m ^oC, Btu/(hr ^oF ft^2/ft))

dT = temperature difference across the material (K or ^oC, ^oF)

s = material thickness (m, ft)

Since the software solves for the temperature differences and the heat transfer area all that is required is to unitize the equation. By removing the temperature difference and simplifying the heat transfer area to a

ratio of the interface surface, and representing the material thickness as the interface thickness (gap between surfaces) the equation becomes:

Equation 4.2: Coefficient of Heat Transfer

$$h = \frac{k * A}{s} \frac{W}{m^2} °C$$

Where:

h = Coefficient of heat transfer (W/m^2.K or W/m^2 °C)

A = heat transfer area as a percentage of contact area (%)

k = thermal conductivity of the material (W/m.K or W/m °C)

s = material thickness (m)

Surface separation for coincident solids will be approximated as 10um

4.7.2.1 Aluminum Standoffs to PCB

The following calculation assumes that 75% of the Aluminum Standoff is contacting the surface of the Printed Circuit Board. The Thermal conductivity of the gap is estimated based on the proposed thermally conductive grease that will be used to fill the interface.

Equation 4.3: Aluminum Standoff to PCB Heat Transfer Coefficient

$$Heat\ Transfer\ Coefficient\ = \frac{15 \frac{W}{m} °C * .25}{100.0 * 10^{-6} m} = 18750 \frac{W}{m^2} °C$$

4.7.2.2 Aluminum Standoffs to Aluminum plate

The following calculation assumes that 50% of the Aluminum Standoff is contacting the surface of the Aluminum Mounting Plate. The Thermal conductivity of the gap is estimated based on the proposed thermally conductive grease that will be used to fill the interface.

Equation 4.4: Aluminum Standoff to Plate Heat Transfer Coefficient

$$Heat\ Transfer\ Coefficient\ = \frac{167 \frac{W}{m} °C * .5}{100.0 * 10^{-6} m} = 835000 \frac{W}{m^2} °C$$

4.7.2.3 IC to PCB

The following calculation assumes that 85% of the Integrated Circuit is contacting the surface of the Printed Circuit Board. The Thermal conductivity of the gap is estimated based on the proposed thermally conductive grease that will be used to fill the interface.

Equation 4.5: IC to PCB Heat Transfer Coefficient

$$Heat\,Transfer\,Coefficient\ = \frac{15\,\frac{W}{m}°C * .85}{500.0 * 10^{-6}m}\ = 136000\frac{W}{m^2}°C$$

4.7.2.4 Pyrolytic Graphite to IC

The following calculation assumes that 90% of the Pyrolytic Graphite Sheet is contacting the surface of the integrated circuit. The Thermal conductivity of the gap is estimated based on the proposed thermally conductive grease that will be used to fill the interface.

Equation 4.6: Pyrolytic Graphite to IC Heat Transfer Coefficient

$$Heat\,Transfer\,Coefficient\ = \frac{15\,\frac{W}{m}°C * 0.9}{10.0 * 10^{-6}m}\ = 1500000\frac{W}{m^2}°C$$

*The same Heat Transfer Coefficient was used for the interface to the aluminum mounting plate from the PGS.

4.7.3 Thermal Constraints

For a simplified modeling approach the constraints for the system were modeled as the aluminum mounting having a constant temperature of 25°C and the ground pins of the 120 pin connector having a constant temperature of 27.5°C.

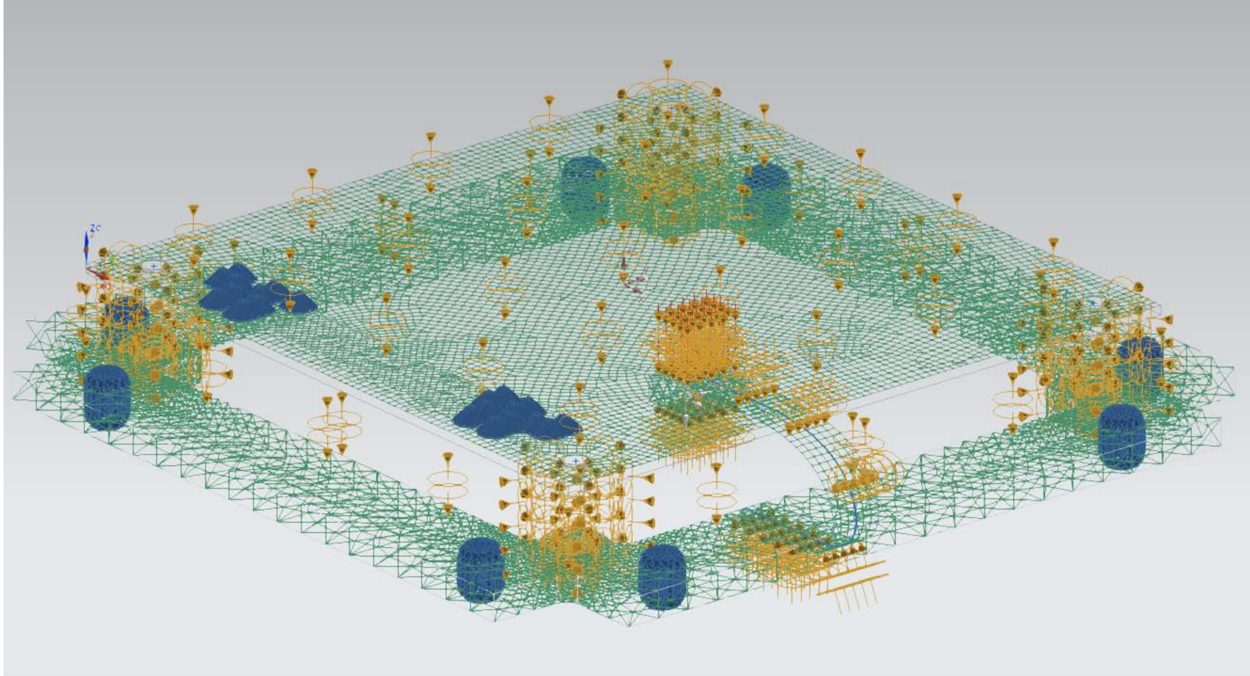

Figure 4.2: Simulation model with Constraints, Couplings, and Loads

4.8 FEA RESULTS

The results for the study were conducted in three parts, the initial case was conducted without a heat spreader added to the system, the second study had two sub parts for the two end points of the thermal conductivity for the Pyrolytic graphite in order to determine which would be the optimal for heat transfer based on thickness since the optimization could not be configured to model a change in thermal conductivity based on thickness.

4.8.1 Initial Findings No PGS

The first study performed was to identify the thermal response of the system if left as is without the addition of any thermal management via additional heat spreaders other than the sinks that currently exists in the structure via the standoffs and ground pins in the connectors. This will provide a baseline study for what the steady state thermal response of the system will be.

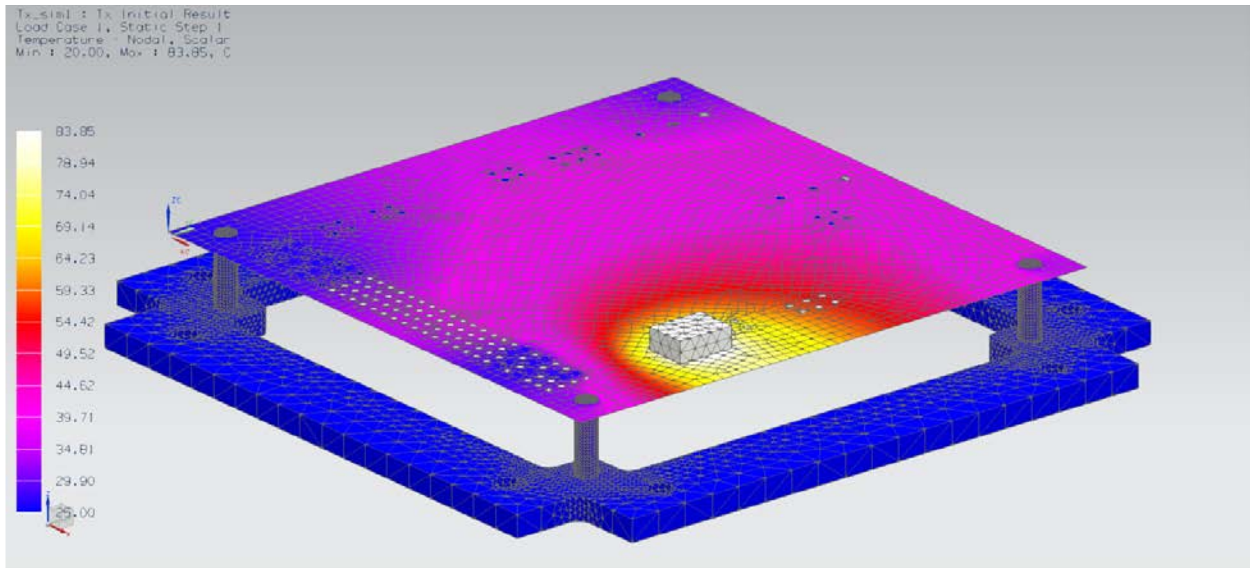

Figure 4.3: Nodal Thermal Results no PGS

From Figure 4.3: Nodal Thermal Results no PGS it can be seen that the integrated circuit reaches a maximum temperature of 83.85°C which is within the safe operating area of the transmitters power amplifier. The manufacturer specifies a maximum operating temperature of 85°C. However, the further thermal stress can be reduced the more reliable and robust the operation of system will be, therefore the system will benefit from employing additional cooling above the standard configuration to further reduce its temperature fluctuations and steady state temperatures.

4.8.2 Initial Findings with PGS

The following two studies were performed since an optimization configuration with the heat transfer coefficient of the Pyrolytic Graphite being dependent on the material or mesh thickness could not be realized, this study facilitated the choice of which thickness of heat spreader to use for the purpose of providing a starting point to begin the optimization strategy.

4.8.2.1 17um Thickness

The initial additional of a PGS heat spreader with a 100µm thickness and a conductivity of 1700 *W/m °C* from the results displayed in Figure 4.4: Temp Results with 17um PGS the temperature of the integrated circuit has been reduced by approximately 5 *°C* from the solution results with no heat spreader addition.

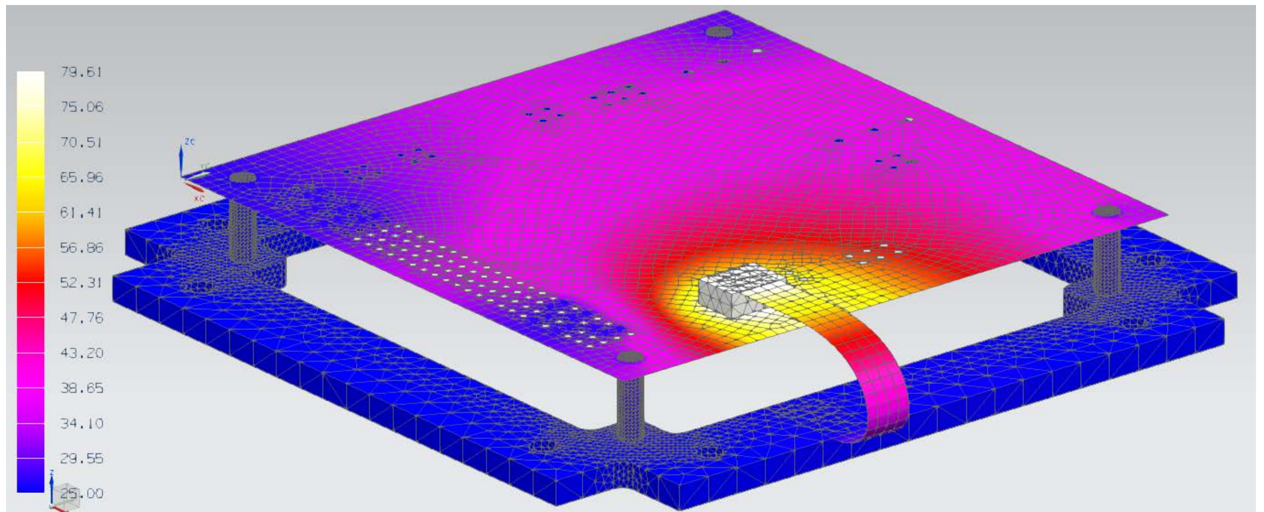

Figure 4.4: Temp Results with 17um PGS

4.8.2.2 100um Thickness

Since it was not possible to setup a study that would vary the thermal conductivity of the PGS material with thickness two initial studies were required in order to determine the optimum thickness to optimize for the model. The heat spreader 2D mesh thickness was then modified to a 100µm thickness and the material conductivity was changed from 1700 W/m °C to 700 W/m °C from the results displayed in Figure 4.5: Temp Results with 100um PGS the temperature of the integrated circuit has been reduced by approximately 18 *°C* from the solution results with no heat spreader addition, and reduced the temperature by an additional 13 °C over the 17 µm thick solution.

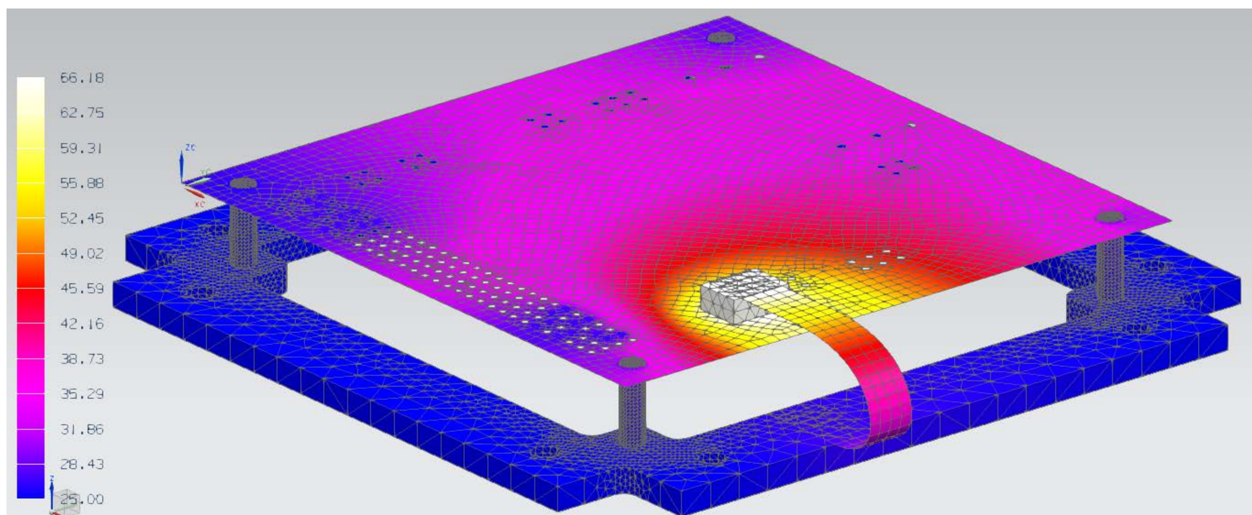

Figure 4.5: Temp Results with 100um PGS

4.8.3 Optimization Results

The optimization for the design results was set on reducing the temperature of the Integrated circuit in order to reduce the temperature induced stress on the part. The design constraint was set as a maximum temperature of 52 °C and the design parameter was configured as the width of the heat spreader. Since the optimal thickness of the heat spreader was already determined to be the 100 µm with a thermal conductivity of 700 W/m °C. From the results depicted in Table 4-2: Optimization Spreadsheet of the optimization study it can be seen that as the width of the PGS heat spreader is increased the temperature decreases proportionally.

Table 4-2: Optimization Spreadsheet

Design Objective Function Results							
Minimum Temperature	0	1	2	3	4	5	6
	66.17735	63.10743	63.76807	60.42097	57.94297	55.2156	54.63921
Design Variable Results							
Name	0	1	2	3	4	5	6
"Tx"::p14=3	3	3.86	3.6	4.632	5.5584	6.67008	7

The results from the study seem to indicate that as the heat spreader becomes wider than the IC there are diminishing returns on the reduction in IC and substrate temperature. A change in width of 0.86 mm yields a temperature reduction of 3.06 °C , which is a 28.6% change in width to yield a 4.6% change in temperature. Where as compared to the final design step where a change in width of 4mm yields a temperature reduction of 11.538 °C, which is a 133% increase in width to yield a 17.4% change in a temperature. The following two figures Figure 4.6: Nodal Temperature Design Cycle 2 depict the nodal temperature results for the solution.

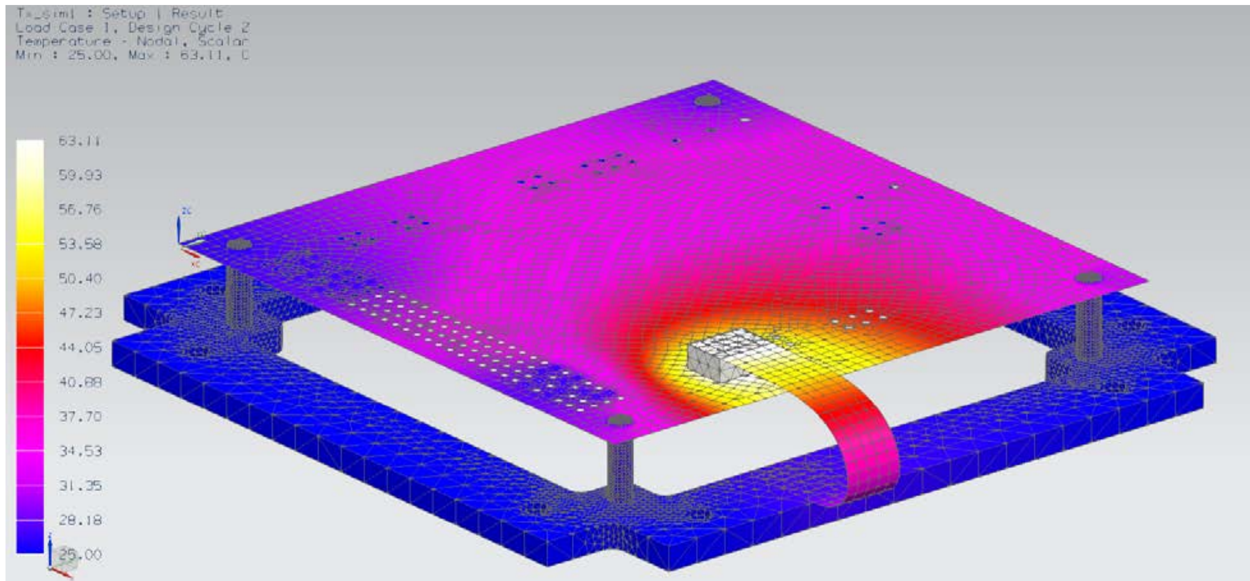

Figure 4.6: Nodal Temperature Design Cycle 2

4.8.3.1 Further Optimization

The optimization study was run a second time in order to confirm that the design was converging to a minimum value based on the width increase of the heat spreader. The design variable was increased for its available maximum size, this was done for two reasons:

1. To check the upper limit for the width of the heat spreader,
2. To determine the minimum achievable temperature for the system.

Table 4-3: Final Optimization

Design Objective Function Results					
Minimum Temperature	0	1	2	3	4
	54.63921	51.44976	52.22394	49.13031	47.36077
Design Variable Results					
Name	0	1	2	3	4
"Tx"::p14=3	7	8.86	8.4	10.632	12

From the graph depicted in Figure 4.7: Heat Spreader plot of Temperature vs Width it can be observed that the reduction in temperature based on width is following a steady decline.

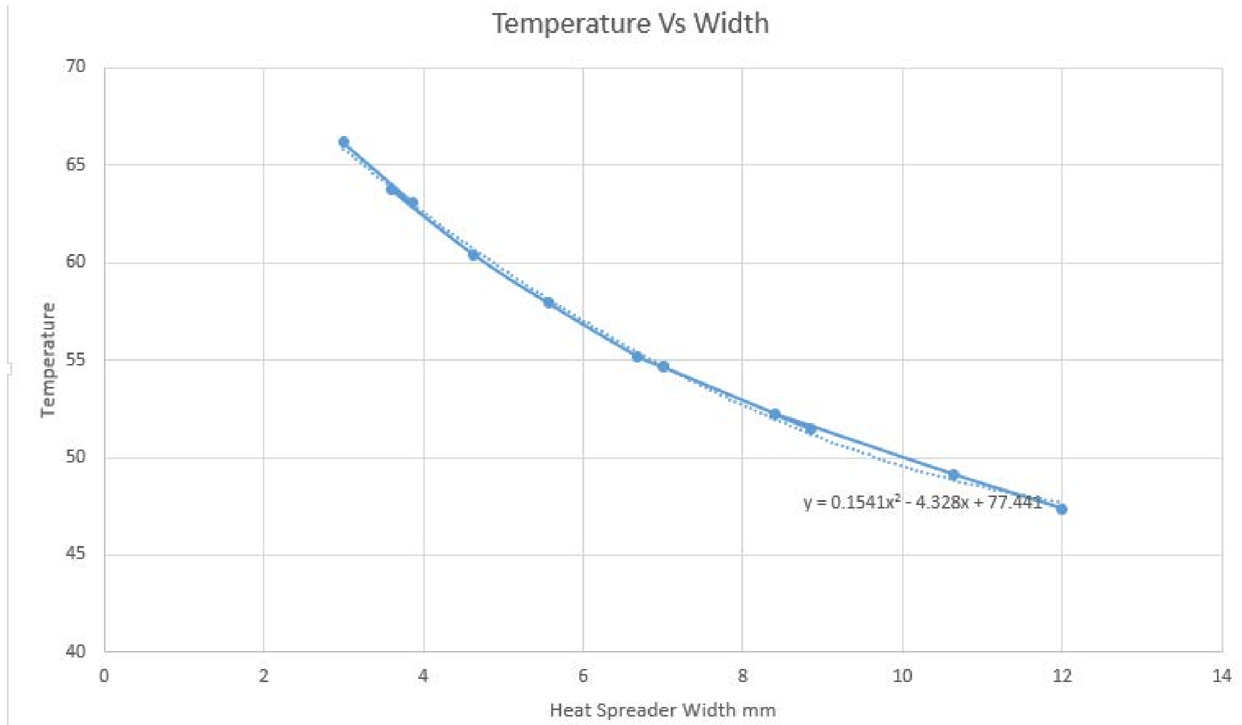

Figure 4.7: Heat Spreader plot of Temperature vs Width

The final nodal temperature plot can be seen in Figure 4.8: Final Nodal Temperature Plot. From the figure it can be seen that the nodal temperatures of the PGS are beginning to show a reduced temperature in the Y axis direction further indicating that a design with a width much greater than 12mm would show additional reductions in thermal relief for the IC.

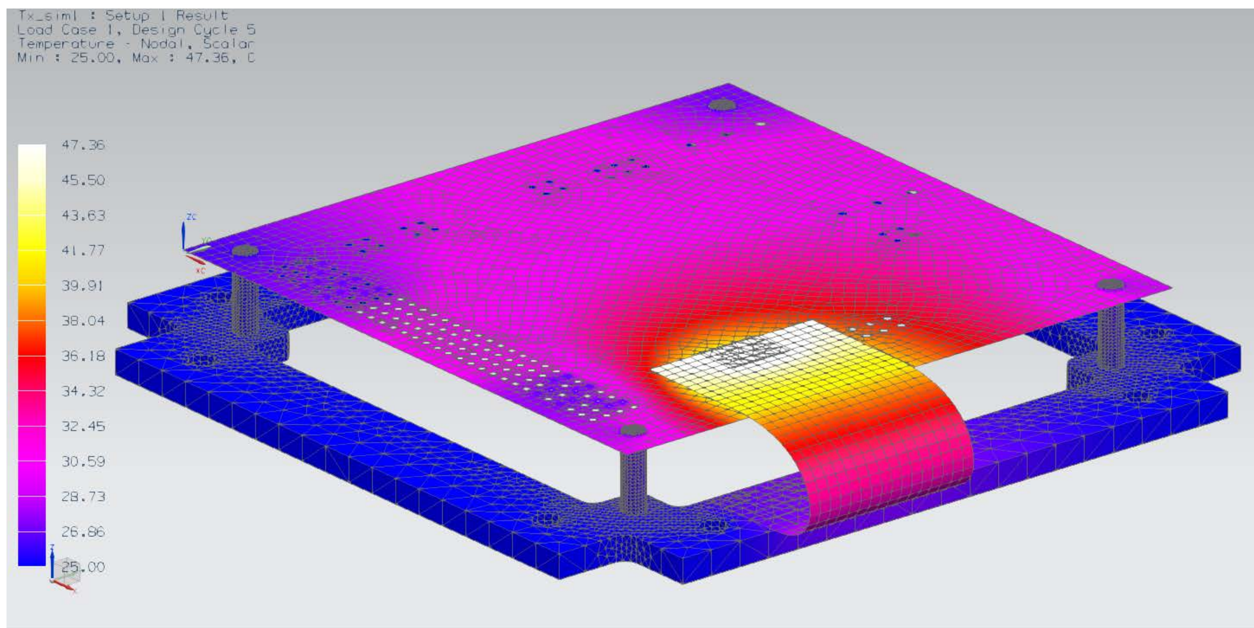

Figure 4.8: Final Nodal Temperature Plot

4.9 CONCLUSION

This project was successful in modeling a simplified form of the current satellite structure and performing the thermal analysis on the transmitter system with the heat spreader attached. The correlation between previous experimental data and the current simulations indicates that the results obtained from the NX FEA should be well correlated to the new testing results obtained at the end of May. Further work will be conducted on the model to increase its fidelity between the physical structure and the simulated model, additional structural members will be added to the model and the simulation process will be repeated.

There was a number of problems that required overcoming in order to properly simulate the model for this FE study, most of the obstacles were resolved by simplifying and trying new approaches to the model. Some of the bigger issues encountered were simple hardware limitations by the computer upon which the simulations were running. Other problems such as creating custom materials, optimizing physical relations, and modeling laminates were resolved on a trial and error basis.

The optimization results for the project proved very insightful into the effectiveness of the passive cooling system using Pyrolytic Graphite as a heat spreader medium. Again problems were encountered when creating the orthographic materials, as well as defining some of the contact resistance and heat transfer coefficients for the boundaries between modeling elements. However these proved to be excellent sources to further my understanding of thermal transfer properties and creating realistic models. The optimization and analysis process provided a solid base for creating a prototype design for each of the subsequent systems, as well as approximate sizing for the width of each individual heat spreader based on the estimated required reduction in surface temperature.

The results from the optimization will be used as a starting point for determining the best configuration for all circuit elements. A number of simplifications were conducted in this study, mainly due to the complexity of the physical model and the dynamic relationship between each system. Further studies will be conducted looking into how the heat transfer is affected by factoring in the varying temperature of the satellite structure due to orbital heating cycles, as well as heat loads from other systems being coupled to the same structure and determining the optimum heat spreader width for each system in order to minimize the temperature in all systems as well as to minimize cross coupled heat transfer between subsystems since each heat spreader acts as a bidirectional heat transfer medium.

5 SOLID MODELING FOR INTEGRATION

5.1 SOLID MODELING SUMMARY

The internal connections in the satellite were successfully modeled for connecting PCB systems via coax, and stranded cables. This was accomplished in a two part procedure where the cabling system was first created and clearance constraints were then evaluated in order to properly plan the routing of all the cable assemblies. The internal printed circuit board stack is depicted in Figure 5.1: Printed Circuit Board Stack Before the two images below show some of the changes to the Printed Circuit board stack before and after adding the electrical cable routing Figure 5.2: Printed Circuit Board Stack After the structural components and enclosure have been excluded from the pictures below in order to see the internal printed circuit board stack ups.

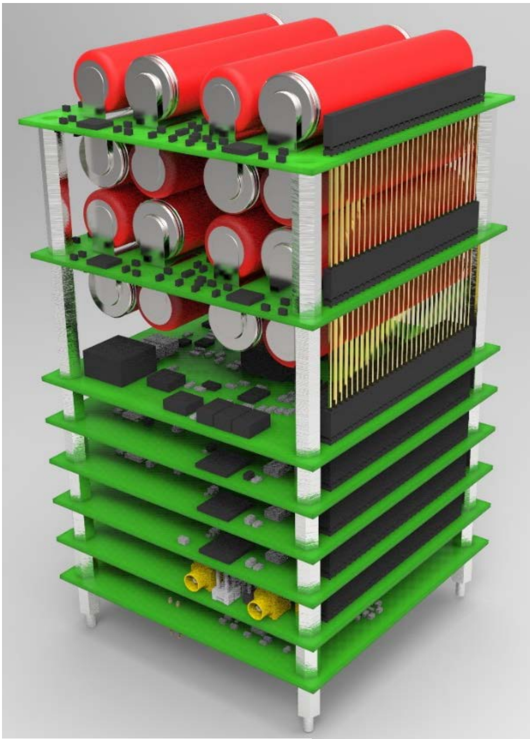

Figure 5.1: Printed Circuit Board Stack Before

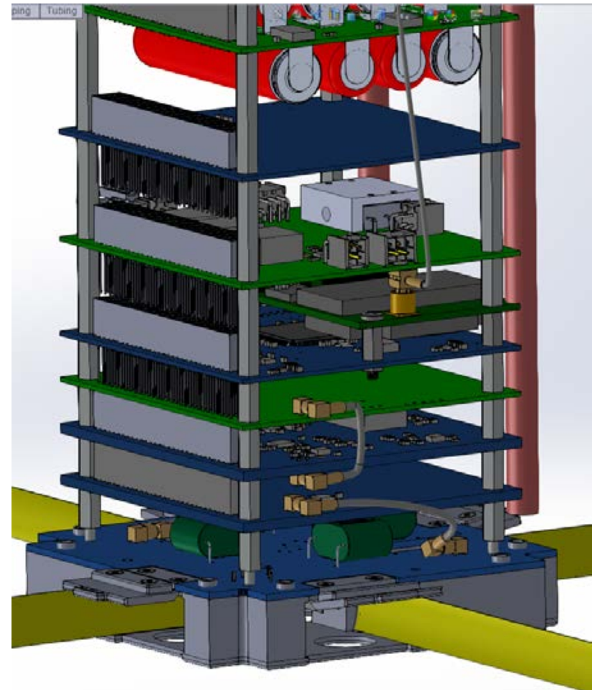

Figure 5.2: Printed Circuit Board Stack After

By comparing the two figures above, several subtle design changes can be noted. The configuration of the coax communication ports on the PCB second from the bottom in Figure 5.1**.** In the new design the connectors were moved to opposite sides of the PCB in order to simplify cable routing and facilitate a cleaner design from an assembly and integration perspective. This one of several design changes, several of the mechanical members that support the upper sections of the PCB stack also had to be modified in order to meet clearance

requirements. Omitted from Figure 5.2 above are the electrical connections for the solar panels, this was done for clarity as they obscured the coaxial connection to the other subsystems which were of greater concern from an assembly and integration standpoint than the stranded solar panel connectors.

5.2 INTRODUCTION

The physical constraints and clearances of the satellite are such that without accurate and in-depth solid modeling of the satellite mechanical structure prior to assembly and integration it would be impossible to guarantee its success. The depth of the modeling extended to including not only structural members of the system but also the individual electronic components, connectors, IC's, as well as cabling, and fasteners. It was only with this level of detail that it was possible to mitigate many of the fitment issues which arise during the integration phase of any project. Due to the tight timelines and limited resources of the project it was required to be successful on the first attempt without any substantial design changes or the reordering of any parts.

Two pieces of software had to be linked in order to accomplish this task. The first being SolidWorks which is the primary solid modeling software used by the team for creating the overall mechanical structure which must house all the electronics as well as act as the interface to the launch vehicle. The second piece of software is Altium. Altium is an Electrical Computer Aided Design software suite which is able to capture circuit schematics and translate these into physical designs via PCB design.

It was possible for these two programs to work efficiently with one another by using "STEP" files as the transitionary phase between the two programs. Both software suites were able to import and export files using the STEP file type which helped in translating parts and systems from the electrical world to the mechanical world and vice versa. This was not without its challenges but it did provide a method for guarding against unforeseen clearance constraint issues.

In addition to this all the electrical routing connections needed to be captured between the electronic systems. Since this constituted physical cabling which would be assembled and integrated once the electronics were housed in the mechanical structure it was essential to ensure that:

1. The cabling and connectors had clearance internally in the structure
    a. The bend radius of the cables was within the tolerance of the manufacturer.
    b. The cable with connectors were possible to fabricate
2. The cabling assemblies could be inserted into the structure to connect the system either before or after the electronics and mechanical systems had been assembled.

This section details the use of tools and functionality to achieve a high level of knowledge with respect to the "Electrical" and "Routing Toolbox" plugin for SolidWorks. This will extend to creating connectors and components using Excel spreadsheets for driving designs and providing connectivity in the assembly. The software was also used to create manufacturing and assembly drawings for the cable and wiring harness for the completed cabling assemblies. These drawings were used to pre-construct and integrate the cables into the satellite. Some of the features used were tools and resources to create cabling assemblies and manufacturing drawings, excel spreadsheet driven routing designs, and creating and modifying parts for electrical routing between systems.

The following sections are the detailed design steps for the creation of the cable routing and assemblies.

5.3 Electrical Component Creation

The first step in using the "Routing Toolbox" in SolidWorks is enabling the plugin; once the routing plugin has been "Enabled" the routing toolbar will appear.

There are three toolbars added to the user interface when the plugin is enabled "Electrical, Piping, and Tubing" only the "Electrical" routing tools were explored in this project.

In order to begin creating electrical connections and routing cable ways SolidWorks must have a library of routing components to use to enable connectivity in the assembly model. This is facilitated using the "Routing Library Manager", after a solid model of a component is created or downloaded from a manufacturer electrical connection properties must be added to the solid part. The current solid part must be open and an active model as seen in Figure 5.3: Solid Part Model the active part is a RF connector made by Linx Technologies which is used for multiple connections in the assembly model.

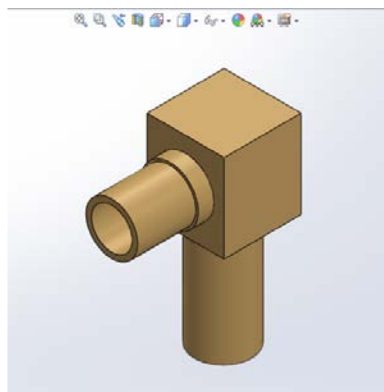

Figure 5.3: Solid Part Model

The “Routing Library Manager” can be access from the “Routing” menu. Once the library manager has been started from the menu it is possible to use the “Routing Component Wizard” on the “Home Page” in order to add electrical component properties to existing solid models. However the wizard is only capable of working with Solid Parts it cannot work with solid assemblies that must be accomplished using another process if desired, for this project only Solid Parts were used not Assemblies. Once the “Routing Component Wizard” has been started the selection of component type can be made. The user has the option of choosing “Electrical, Miscellaneous, Piping, or Tubing” the “Electrical” type connector was used exclusively in this project.

The “Component Type” window is then prompted to the user. The user then has a choice of a number of electrical routing components to add connection information to. The following menu provides the user with the ability to add Electrical routing information to “Clips, Conduits, Conduit Adapters, Conduit Crosses, Conduit Elbows, Conduit Tees, Connectors, Ribbon Cable, or Splices” the majority of the project used Connectors with some Clips for constraining routing paths.

The C-points connection menu is then presented to the user for adding “C-Points” which describes the direction and location of “Wire, Cable, Ribbon Cable, or Harness” connections relative to the modeled component. At least one C-Point is required for any routable component.

Clicking the add button takes the user to the solid model part and request the user to select a ‘Circular Face or Edge, Face or Plane and Point or Vertex” to indicate the point in which you would like the C-Point to be connected to as seen in Figure 5.4: C-Point Added as depicted in the figure the Cpoint has been added to the circular face of the model.

The “Parameters” for the model consist of the maximum size cable or wire that will be attached to the CPoint as well as it minimum defaults length known as the Stub length as well as any internal wire length and if there is a 2d schematic pin ID for providing cable management information. In order to properly connect wiring and cables to the model the maximum size must be of a total outside diameter less than the maximum specified in the Cpoint parameters.

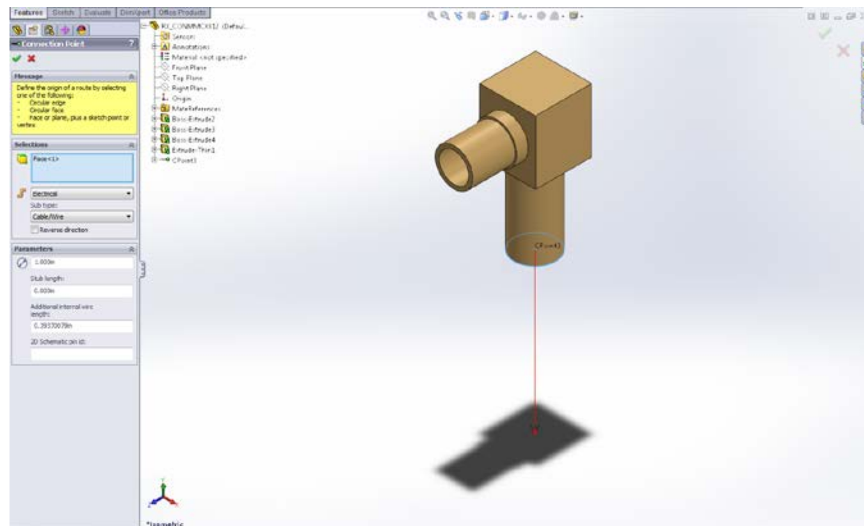

Figure 5.4: C-Point Added

After specifying the “C-Points” for the solid model the user must then provide the “Mate References” for the part as seen in Figure 5.5: Mate References Added . The mate references are used to provide information as to how the parts are mated together; this facilitates the part having pre-defined mates in order for the part to snap together when using the routing package. It should be noted that “Mate References” are not required for parts however it greatly simplifies the routing procedure. As a note SolidWorks does not condone the mating of parts using the traditional mating dialogue for parts in a routing assembly. It is highly recommended to use the Mate References function in order to route electrical components.

Clicking the add button takes the user to the solid model part and request the user to select the mating references for the model. It should be noted that the “Reference Name” for the mate must be the same for all models that are required to be mated via reference. In addition for the mates to function and properly mate the definition for the mates must match such as the “Mate Type” and the “Alignment” of the mates the order in which the mate is performed must also match that is to say that the “Primary, Secondary, and Tertiary” mate references must be the same type and alignment in order for the models to mate via reference. Additionally the mates have a precedence that is to say that SolidWorks will attempt to use the Primary mate over the secondary and tertiary mates if using one of the lower order mates causes a higher order mate to break. With that in mind the most important mate property should be made the primary and all others done in subsequent order.

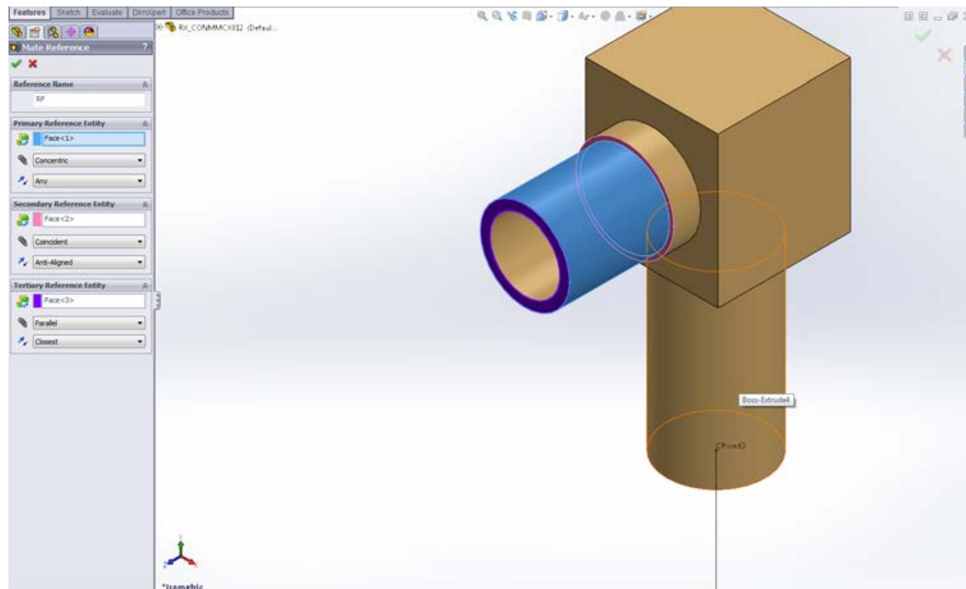

Figure 5.5: Mate References Added

It should be noted that the mating by reference procedure also took quite a lot of trial and error partially due to the naming issue for mate references and defining the mates properly for achieving the desired degrees of freedoms with mating components. One caveat which is not covered in the help files or tutorials discovered was having multiple mate locations in a single assembly or part, since there are a number of circuit boards in the project which have the several connection points if all the reference mates are called the same SolidWorks has a problem with properly mating with each reference. The problem is such that it attempts to reuse the same location multiple times if the mate for the parts is not robust enough, that is to say if the mates are not constrained sufficiently. This was a problem that took significant time to resolve.

Once the component has had the Cpoint and Mate Reference information added, the next step in the Routing component wizard is to add part information for other design configuration, it is highly recommend to use a design table if such functionality is required. The model also request information about the part such as the PartNo, description, material and manufacturer. Only the PartNo and saved name of the solid model are used for additional design elements the rest is information for manufacturing.

The final step is naming the part and indicating the library location as well as the library files in XML format, the component name will be used for referencing the part in subsequent design documents as well as being used in the feature tree of SolidWorks. The library folder location and library file must be specified if one is not specified the default SolidWorks location will be used.

This problem was encountered much later on once several parts had been created. SolidWorks doesn't provide a dialogue or menu for creating an XML library for parts in this process, you can specify a new location for a library for a personal project otherwise it will use the default location which can be problematic if you have a design that is being used by multiple users and is held on a network share. This will be covered later in the report where I address creating a library.

Up to now this has dealt with creating an Electrical model that will be used for attaching cabling however there is also no dialogue option for creating a part using the library wizard for one in which you don't want to attach a cable. This was another problem encountered when using the routing plugin. Since often the other connector that is being mated to whether male or female is directly mounted on a circuit board or part it does not need a "Cpoint" for cable attachment simply a "Mate Reference" the problem is such that when using the Routing Library Manager and the Connector Wizard there it is not possible to create a component without a CPoint they are required for all electrical parts. However a solution was discovered, initially the parts were created using the wizard and then the CPoints deleted afterwards from the feature tree for the part.

Upon further investigation in the SolidWorks help files it was discovered that you can directly add mate reference information to any part using the function in SolidWorks. This menu can be found under the Insert menu item, using this scheme parts which only required a reference mating can be created without the unneeded additional electrical information.

As can be seen in Figure 5.6: Mate Referenced Non Cable Part the part feature tree contains Mate References but there is no CPoint in the model, additionally the part was created with mate references in order to work in conjunction with the part previously displayed in Figure 5.5: Mate References Added it should be observed that the primary mate reference is the concentricity of the two parts followed by a coincident mate and a parallel mate with the circular outer and inner faces of the solid model respectively.

Figure 5.6: Mate Referenced Non Cable Part

An additional side note if this part is saved to the same Part library location as the ones created with the wizard tool it will appear in the "Design Library" folder in SolidWorks as seen in Figure 5.7: Design Library with the remainder of the created electrical parts. The "RX_Con… and TX_CON…" parts were created using this technique. In this manner if there are mounting locations in the design for parts that have not been added they can be mated to the solid assembly or solid part and then further electrical routing components can be connected to it.

MMSD-2
RX_CONMMCX002
RX_CONMMCX012
Solar Cell Connector
TX_CONMMCX002

Figure 5.7: Design Library

5.4 Library Creation

In order to efficiently manage a routing design in SolidWorks it is required to have design libraries for not only the routing components but also for the wiring and cables that connects them. By having a standardized library it greatly reduces the creation time for routes since information is automatically added to the design such as the cable diameter, minimum bend radius, color, and part number. This information is used later on when both routing and when creating manufacturing documents.

Once again using the "Routing Library Manager" as described in the previous section it is possible to create "Wire and Cable Libraries" first I'll commence with a wire library. Under the "Cable and Wire

Library Wizard" the user is prompted to select the type of action. I will address the three options and then show the differences between Wire and Cable libraries. The menu for selecting the desired operation is shown below, we will start by "Creating a New Library".

SolidWorks provides you with the ability to create either an Excel spreadsheet library or an XML library for all three types of parts "Cables, Wires, and Ribbon Cables" the libraries can be created as blanks and edited afterwards with another program such as Microsoft Excel. This is the preferred method since the Entry methods in SolidWorks is slow, the additional benefit is that SolidWorks will only use information in the library file in the columns below the key name titles. This provides the user with the ability of adding additional information above these column headers for other designer, users, or engineers to use in future work.

It should also be noted that if excel libraries are created as seen in Figure 5.8: Cable Library Excel that all the wiring and cable libraries will be stored in the same document on different sheet tabs, however if XML libraries are created they are each contained in their own document. That is to say that the Cable, Wire, Core and Ribbon Cable libraries will be independent files. From a user perspective it is easier to navigate a single excel document then it is to look at several independent files. With that being said in order to use these design libraries in subsequent routing tools it is required to be in XML format to be used within the SolidWorks tool package. This requires the designer or engineer to import the latest cable library file from excel into SolidWorks when creating the project in order to convert it to an XML library with the most current information, I believe this feature should be improved to work with the excel files directly.

	A	B	C	D	E	F	G
1	Cablename	PartNo	Descriptic	Outer Diameter	NoOfCore	Min Bend Radius	
2	RG-178U	83265 Coax	Belden te	0.110236	4	1	
3	RG-174	8216 Coax	Belden PV	0.0708661	4	1	
4							
5							
6							
7							
8							
9							
10							
11							
12							
13							
14							
15							
16							
17							
18							
19							

RibbonCable | Wire | Core | **Cable** | Sheet1

Figure 5.8: Cable Library Excel

The above depiction in Figure 5.8: Cable Library Excel shows the key names of the column headers that SolidWorks uses to identify properties of the components. This file was generated by creating a blank library and then adding information to each section using excel. In a similar manner information was also added to the Wire and Core tabs of the spreadsheet. In Figure 5.9: Core Library the relation between the Cable library and the core library can be seen via use of the Cablename keyword the minimum bend for cabling can be driven by core elements or by the overall cable parameters depending on the design preferences.

	A	B	C	D	E	F	G	H
1	Cablenam	Wirename	Size	Outer Dia	Colour	DispColou	Min Bend	Seal
2	RG-178U	Copper	26	0.019	Black	#FF00000C	0	Unset
3	RG-178U	Polyethyl	Unset	0.06	Black	#FF00000C	0	Unset
4	RG-178U	Copper Br	Unset	0.02	Black	#FF00000C	0	Unset
5	RG-178U	PVC	Unset	0.011236	Black	#FF00000C	0	Unset
6	RG-174	Copper	30	0.012	Black	#FF00000C	0	Unset
7	RG-174	Teflon	Unset	0.033	Black	#FF00000C	0	Unset
8	RG-174	Copper Br	Unset	0.01	Black	#FF00000C	0	Unset
9	RG-174	Core4	Unset	0.02	Black	#FF00000C	0	Unset

RibbonCable | Wire | Core | Cable | Sheet1

Figure 5.9: Core Library

The following shows how to import a previously created excel library into SolidWorks for use with routing tools such as the "from-to" dialogue. Once again using the "Cable Wire Library Wizard" under the "Routing Library Manager" it is possible to import an excel spreadsheet to be converted into an excel spreadsheet; the user must select the import function.

When proceeding the user is prompted with selecting the cable library location and providing information as to what the key names are for the header information if the library was generated with SolidWorks initially then the names do not need to be changed.

Once the library has been imported the dialogue window will show the user the imported information in this example a Cable library as seen in Figure 5.10: Library Information and Format was imported as such both the cable and core information is displayed as well the format in which the file will be saved it is possible at this window to change the file format from excel to XML and save the library. The user can also select from the dropdown menu what library tab is being looked at, Cable, Wire, or Ribbon Cable and each one can be subsequently saved to its on XML library for use with SolidWorks.

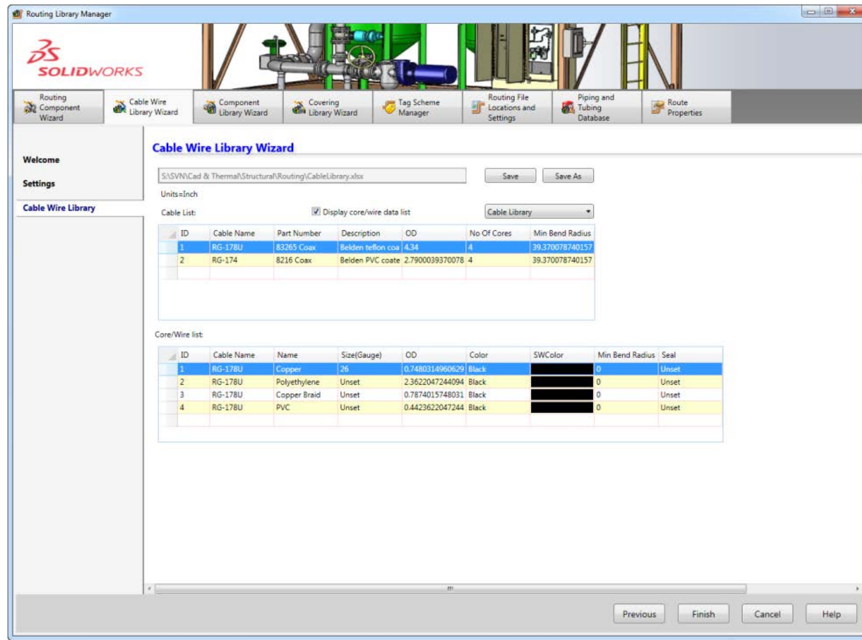

Figure 5.10: Library Information and Format

The last step for in the manipulation of libraries for both components and cables is opening an existing XML library, for instance if throughout the design process new components were created and saved to an XML design library it is possible to open said library and save them as an excel file for editing outside of SolidWorks. The following shows how to open a previously created XML library. Once again using the "Cable Wire Library Wizard" under the "Routing Library Manager" it is possible to open an XML library to be converted into an excel spreadsheet; the user must select the open function. In Figure 5.11: Opened Existing XML Library depicts the information that SolidWorks would read from the specified library, for a cable library it would show both cabling and core information.

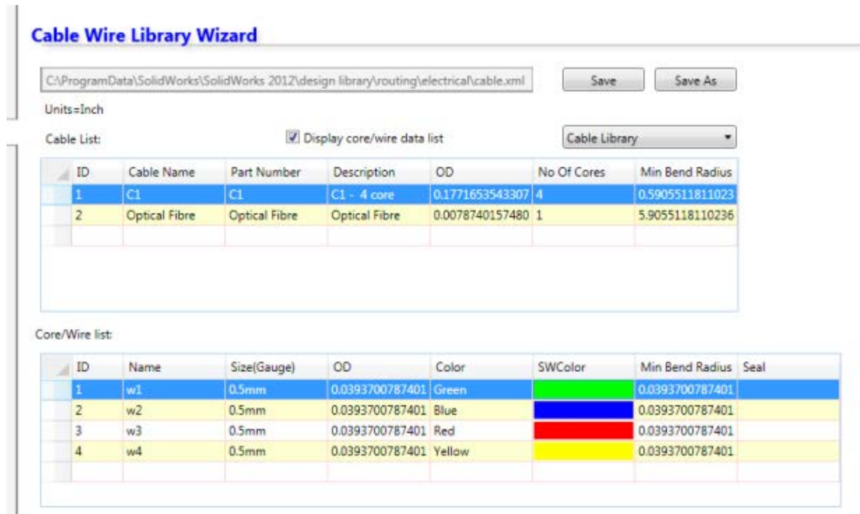

Figure 5.11: Opened Existing XML Library

It should be noted that SolidWorks will only open the libraries that are specified in its default location, however this location can be changed in “Routing File Locations and Settings” tab in the “Routing Library Manager” this provides the user the choice of having the preferred libraries in an alternate location as well as changing the default unit type. These setting can also be saved and loaded in order to provide the user with customized settings for each project or assembly.

The procedures for importing, creating, and opening Cable Wire libraries can also be applied to Component Libraries the process is identical with some differences in the key names used for the various libraries the dialogue for using component libraries using the Routing Library Manager.

5.5 ROUTING

Once components have been created for electrical routing the designer has several choices for creating routes it is possible to drag and drop components to initiate a route, import a from to excel sheet listing the components and routing information, or to use the Auto-Route feature between components that have already been placed with Cpoints. The simplest and most streamline options for a good design is to use the from-to option however all three options were explored in this project.

5.5.1 Drag and Drop

The drag and drop feature is the simplest to understand and implement the user grabs a component from the electrical component library and drops it onto an assembly containing parts with reference mates already established as can be seen in Figure 5.12: Drag and Drop Routing the component MMSD-2 was selected from the design library and dropped onto a component in the assembly design in this case IPL1-02.

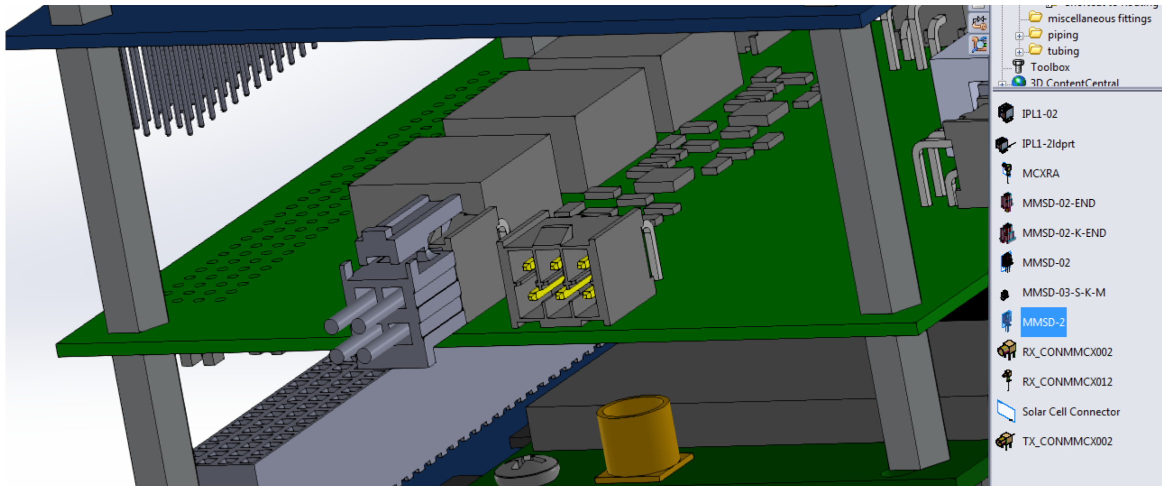

Figure 5.12: Drag and Drop Routing

After the part has been successfully dropped into the assembly and mated with another part the “Route Properties” window will prompt the user to define the name of the “Routing Subassembly” the “Routing Template” to be used, as well as the electrical properties “Sub type Harness, cable, wire” also the “Outside Diameter” of the route.

After the parameters have been entered and the ok button selected the user is prompted to the “Auto Route” window where the user can select between “Auto-Route, Edit (drag), and Re-route Spline” the auto-route function can only be used if there is another CPoint in the assembly in which to connect to, otherwise the Cpoints can be dragged in a linear direction.

If the user wishes to create the route manually using the “Spline or Line” option from the “Electrical Routing Toolbar” the user is then able to route from the Cpoint and terminate the route at any point in which a reference can be inferred or related. The difficulty with creating such routes is the inference of points due to perspective as can be seen in Figure 5.13: Spline Placement the route appears to be connected to the top circuit board on the battery terminal.

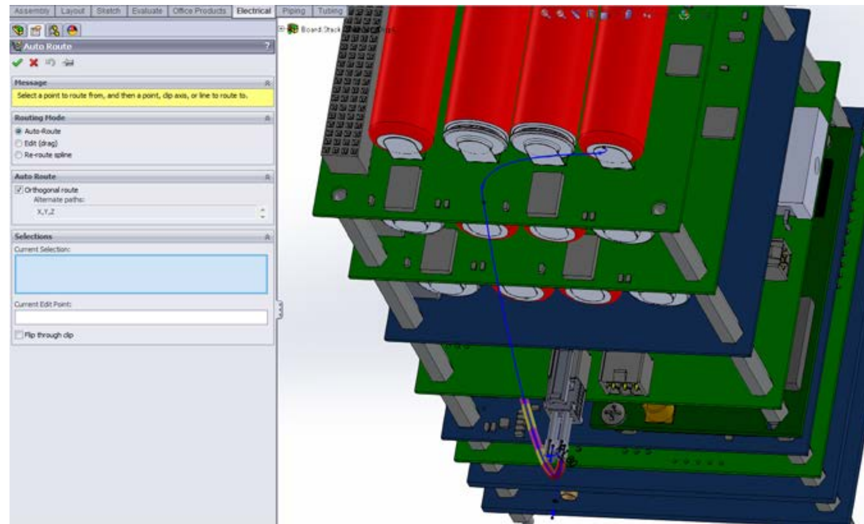

Figure 5.13: Spline Placement

However due to the unintuitive perspective of the model the route is actually going underneath board and into the plane as seen in Figure 5.14: Spline Errors the spline is also passing through other components causing clearance infractions**.** The problem with perspective in the model is why free drawing splines is discouraged.

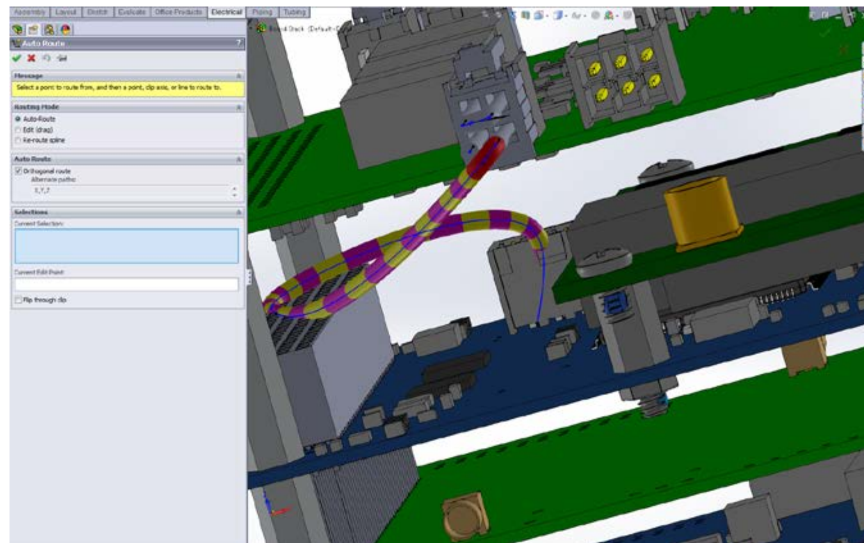

Figure 5.14: Spline Errors

One simple fix to the issue of manually drawing a route is to specify the end points this can also be accomplished using drag and drop methods by terminating the auto route window for the first component and then “Insert Connectors” into the existing route there by providing two end points to route between the tool is found under the “Electrical Routing Tab”. Once the end points of the route have been established it is easier to draw orthogonal routes using the spline or line function as seen in Figure 5.15:

Route with Two End Points by constraining the end points of the spline it is possible to draw a route by hand that remains in the plane and does not go through other components.

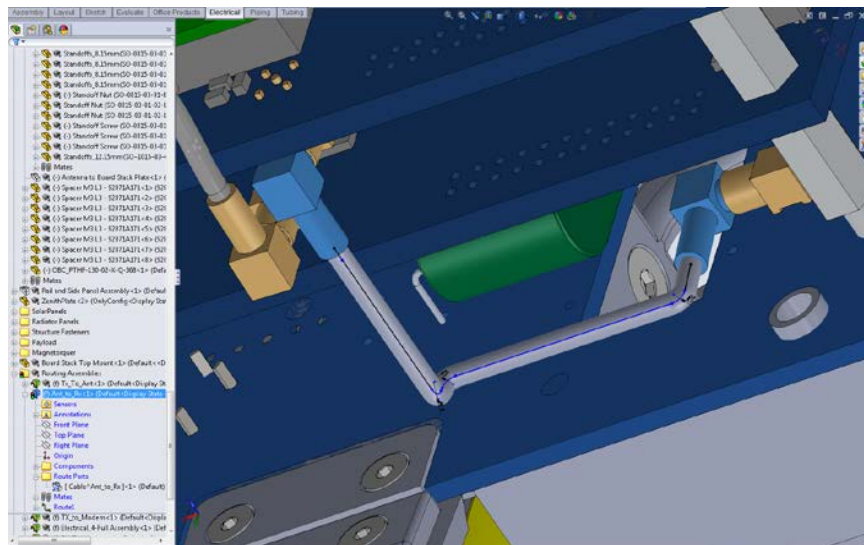

Figure 5.15: Route with Two End Points

5.5.2 From-To List

The preferred method for creating a route is to use a from to list which can found under the “Electrical Routing Toolbar” the “Start by From/To” tool initiates the dialogue window seen in Figure 5.16: From-To Dialogue

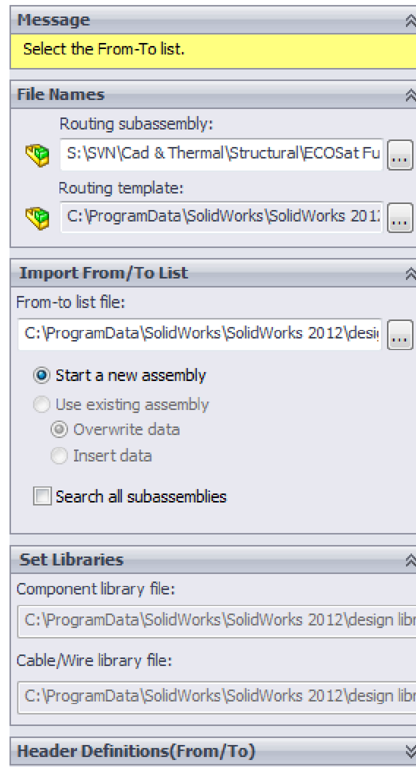

Figure 5.16: From-To Dialogue

This dialogue requires a from to list to be loaded that has information contained in the "Component Library File" and "Cable/Wire Library file" these were covered earlier in the document and discuss the creation of the components in xml format for the use with this tool. In Figure 5.17: From-To List Excel shows a typical example of a listing of parts with references to and from the end points as well as specifying individual cable pin outs. In this manner there is much more design control and authority over the routing and creates a more robust design with far easier placement of parts and routes since the ends become constrained.

	A	B	C	D	E	F	G	H	I	J	K
1											
2	**Wire**	**Cable**	**Core**	**Spec**	**From Ref**	**Pin**	**Partno**	**To Ref**	**Pin**	**Partno**	**Colour**
3	S1W	C1	W1	C1	motor1	1	db15-plug	con2	3	db9-plug	
4	S2W	C1	W2	C1	motor1	2	db15-plug	con2	5	db9-plug	
5	S2t	C1	W3	C1	motor1	4	db15-plug	con2	2	db9-plug	
6	W5	C1	W4	C1	motor1	3	db15-plug	con2	4	db9-plug	
7	W11			9982	motor1	5	db15-plug	con3	1	5pindin-plug	
8	W6			9982	motor1	6	db15-plug	con3	1	5pindin-plug	

Figure 5.17: From-To List Excel

5.6 ROUTE CHECKING

In order to properly model the routing of the cable and wire assemblies it is critical to ensure that the geometry does not compromise the properties of the cables and that they are able to be bent into the shapes that the splines and lines are depicting. This can accomplished using another of the spline evaluation tools in the SolidWorks toolbox.

Once a Route is edit mode right clicking on the “Spline or Cable” will provide the user with the options for “Minimum Radius, Curvature Combs, Inflection Points, Control Polygons, and Spline Handles” using these tools it is possible to evaluate the geometry of the spline and modify it accordingly to meet the cable requirements.

It also possible to move control points in the spline, rotate spline entities, create fixed lengths for the route, add relations to objects, and insert further spline points or tangency control.

In Figure 5.18: Spline Evaluations the Tangency Control Arms can be seen by the blue arrowed polygons in the image, the Minimum radius is indicated by the yellow circle with a dimensional arrow showing the radius at the minimum points, and the blue combing is indicating “Curvature Combs” of the spline so that the rotation of the curvature about the routing direction can be observed. Using these tools it is possible to properly evaluate the routed spline to ensure it meets the requirements of the cable manufacturer. It is also possible to increase the density of the comb and the amplification of the scale in order display small and large curvatures of individual splines.

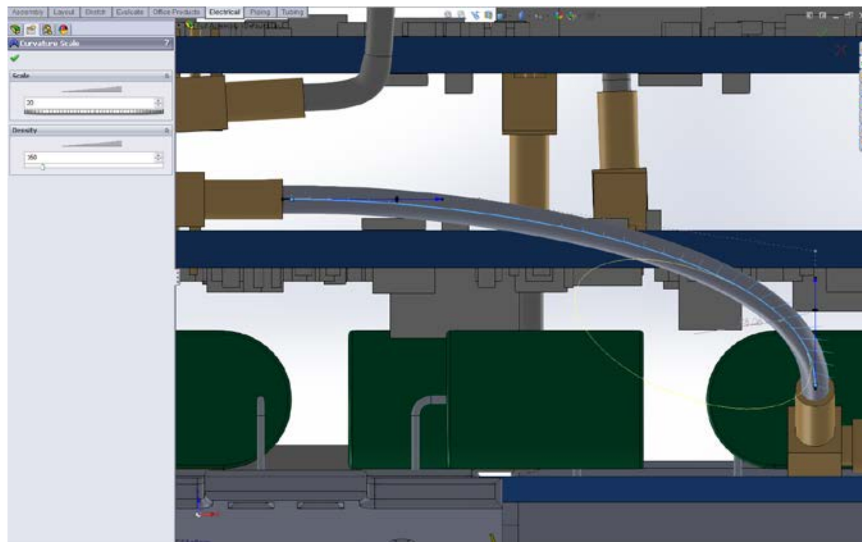

Figure 5.18: Spline Evaluations

5.7 MANUFACTURING DRAWINGS

Once routes have been created it is a relatively easy matter to create drawings for manufacturing the cables prior to assembly, this is another feature of the routing toolbox plugin for SolidWorks. By right clicking on a "Routing Assembly" in the SolidWorks feature tree by selecting the "Flatten Route" option in the menu will prompt the user with the a dialogue window by selecting the "Annotation" type will create a drawing that is not scale but will show all the additional information to manufacture the wiring assembly such as the number of connectors, their part number, the length of wire and its part number. This is providing that they have been defined in the cabling and component libraries that the parts were sourced from. The information depicted in Figure 5.19: Annotation Schematic shows the detail provided in the fabrication drawing the relative orientations of the connectors with respect to each other, the parts names of the components used as well as the total length of wire required to complete the wiring assembly.

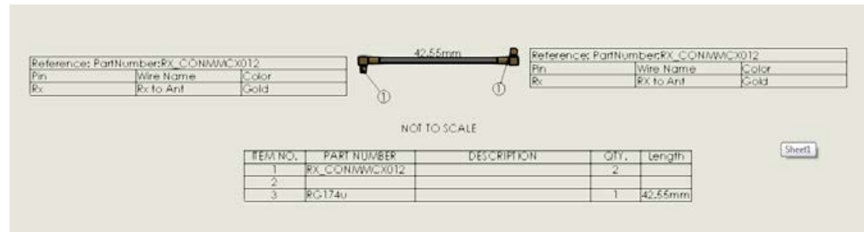

ITEM NO.	PART NUMBER	DESCRIPTION	QTY.	Length
1	RX_CONMMCX012		2	
2				
3	RG174u		1	42.55mm

Figure 5.19: Annotation Schematic

The physical construction of the cabling assemblies was undertaken using the annotation schematics as a primary reference source the cables were also checked against the physical model once partially complete. If the schematic in Figure 5.19 is compared to Figure 5.20 the accuracy of the schematic can be seen. All cables constructed were successfully assembled and integrated into the structure without unexpected complications or clearance constraints.

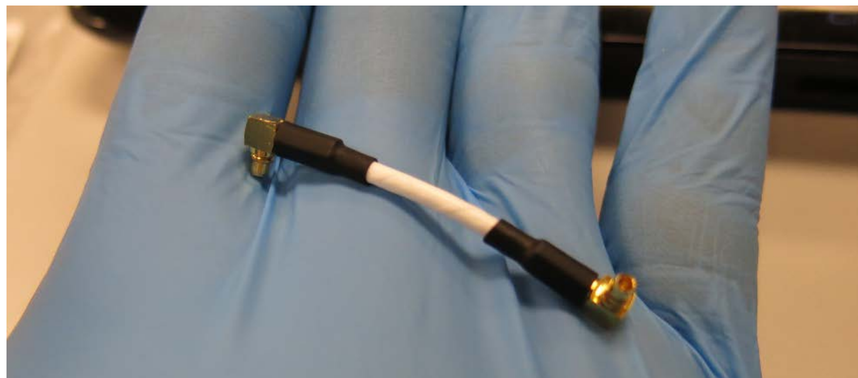

Figure 5.20: RG174u Cable

5.8 CONCLUSION

The modeling of the electrical routing and the parts creation was successful in identifying problem components and coming up with design changes and mitigation strategies to ameliorate the assembly and integration process. The electrical routing accomplished in this project was needed in order to properly identify clearance issues in the design as well as to plan and adjust the mechanical layout of the model to suit cable path ways. Furthermore this provided the team with a guide to the electrical assemblies in the satellite and how to access connectors for both assembly and disassembly when troubleshooting problems.

Much modeling was conducted surrounding the creation; categorization and indexing of parts for this project as well as how to use excel sheet and libraries to drive the design of the project. These libraries created will be used many subsequent times for further modeling. A number of problems were encountered throughout this project specifically in regards to working in the assembly, and interfacing with the SolidWorks plugins.

A significantly larger amount of time was spent on this project then initially anticipated this is largely due in part to the lack of information, the complexity of the model, and the creation of 3d splines in a large assembly.

5.8.1 Problems Encountered

5.8.1.1 Model Dependency

Due to the integration of this project with the ECOSat team many of the sub models required updating prior to commencing the routing project. This meant updating all of the current designs in the PCB editing software and creating 3D models of the systems to then bring them into the SolidWorks environment. This was done as a step file which was then converted into an assembly in order to be mated to other system boards and the external structure of the satellite. This was required prior to being able to commence the majority of the routing work on the project with the exception of the creation of library components, and “from-to” routing lists.

5.8.1.2 Assembly size

Due to the large part count of the assembly and sub-assemblies it was computationally intensive at most times to manipulate the model. This is due to the electrical routing requiring the models to be fully resolved in order to detect mating properties and create routes. This resulted in a large graphical load on the system which caused lag and graphical artifacts in the modeling environment. These graphic artifacts resulted in difficulties with aspect ratio and perspective when creating 3d splines.

5.8.1.3 Information Resources

A number of problems arose when working on this project, the primary being lack of information on the tools and resources being used. There was no formal training or tutorials on the use of the toolboxes and plugins apart from YouTube videos from other users. The unfortunate part is often it is the small or behind the scene details that are left out, specifically things pertaining to the creation of parts, their mating definitions, requirements for part resolution.

One issue that was encountered frequently is the fact that the project is done in a large assembly, therefore the majority of the parts are resolved as lightweight or draft which causes many issues when trying to mate electrical components where the part has to be fully resolved in order to use the "Reference Mating" created for the electrical components. The reference mating properties is suppressed for parts that are not fully resolved.

Since all the videos I was able to find used pre-defined components from the SolidWorks library or parts that the user already created. Due to this the part and library creation required significantly more time using trial and error testing; resolving problems without many resources to aid in the process, the help files were often found to be cryptic or lacking specific information on how to setup or use the tools.

5.8.1.4 Creating Routes

Initially multiple ways of creating electrical routes was explored, "On the Fly, Drag and Drop, From-To Lists" many issues arose when initially trying to do "On the Fly" and "Drag and Drop" routing particularly how to make two connectors use the same cabling route. That is to say how to make one cable or wire with a connector on either end. This alone consumed countless hours since often the individual parts of the route would create relations to the assembly and have locked nodes which would cause the "3D Spline" of the route to create wild routing paths going through the model where the two end points would be connected.

The final conclusion was that due to the complexity of the model, and that all the routes took place in three dimensions which makes drawing the routes using freehanded splines difficult and unintuitive due to the perspectives. The only feasible option which did not results in undesired results was to use "From-To Lists" which uses an Excel spreadsheet that is imported into SolidWorks and creates an XML description reference of the route. Specifically the list describes the end connectors and the wires or cables that have been predefined in the library files to route the end connectors together.

5.8.1.5 Creating Libraries

Another serious delay in the project was how to create component libraries for electrical parts, wiring, cables, and how to relate pins to the various parts. Again all the tutorial videos found simply had libraries

with preconfigured components and parts. Alternatively the demonstration would show a quick excel sheet but they would lack explanation as to how or why they had the entries they did as well as how to relate the items in the sheet to the actual location of the solid part models used in SolidWorks.

6 FINAL REMARKS AND FUTURE WORK

6.1 FINAL REMARKS

A fully functional satellite was designed and manufactured in May 2014, prior to presentation and testing during the final stage of the Canadian Satellite Design Challenge Competition. Here, the satellite was subject to ground vibration testing. The team then went on to win the second and final phase of the CSDC and won the national competition by being placed first in all three rounds of the competition.

In reverse order of the sections laid out in this thesis, the system was first assembled. The mechanical systems were integrated and the structure for the satellite was constructed. This was done to develop a detailed procedure for assembling and integrating all the structural members of the satellite chassis prior to introducing any additional complexity from the electrical components. This was done in part to develop a well-defined assembly procedure, as well as to identify any possible constraints or problems during the assembly phase which may present itself during the integration of the electrical systems. The final mechanical structure was also evaluated and validated using the 3D solid model of the satellite for consistency not only in dimensions but also for its mass properties. All values were within the specified tolerances of mass and tolerance budgets.

In parallel, the electrical systems were integrated, each system was initially tested for conformity to design specification. After individual testing, the electrical system was assembled into its vertical stack configuration and checked against the solid model for discrepancies and congruence with the estimated tolerance stack up. The tolerance on the standoffs for each section is ±.05 mm with 10 standoffs that led to concerns with alignments. However the tolerances negated one another in the final assembly and the mounting holes aligned precisely with the model predictions.

Once the electrical and mechanical systems were assembled and validated using the solid models, the two systems were integrated for a preliminary test fit to ensure proper mating and clearances. Once the systems were verified to be compatible, the assembly procedure for the remaining cabling and external components was pursued. This consisted of the solar panels, RF cabling, and antenna connections.

After final integration and assembly, the satellite was checked against its solid model for mass properties and center of mass. The fully assembled satellite was found to be within ± 2% of all model predictions.

The satellite was then packaged and prepared for shipping to undergo testing at the David Florida Lab (DFL) in Ottawa. Once at DFL the satellite was instrumented with accelerometers, the placement was decided after consulting with the lab technicians and other industry experts that were available at the time

of testing. Due to clearance constraints, sensors could only be mounted at the center of the radiator panels, and on the ± Z faces. Fifteen sensors were used for analyzing the fundamental frequencies of the satellite, three were used for control and the remaining twelve were used for measurements on the satellite.
The system was then excited both with random frequency as specified in Appendix A and a low-level sine wave sweep from 5 Hz to 2 KHz. These tests were repeated for each axis of the satellite, such that the orientation of the satellite was in line with the linear motion of the shake table. The results were tabulated and analyzed with the assistance of the technicians and experts at the competition. The testing results showed strong correlation with the dynamic modeling that was performed using the numerical tools. There was one outlying frequency which was not seen in the dynamics simulation prior to testing. Unfortunately the phase information for the measurements was not provided and therefore we could not verify if the frequency was an actual mode or simply a mode from the support structure.

The testing was an overall success with the ECOSat satellite passing its initial testing as well as passing the post environmental testing showing that the satellite was still functional following the ground vibration tests. It is concluded the design, the construction, assembly, integration, and testing of the satellite was completed successfully.

6.2 FUTURE WORK

Further vibrational modeling and testing is required in order to increase the fidelity of the model as well as to obtain higher correlation between testing results and model predictions. Work has already begun on improving the model by increasing the fidelity between the simulation model and the solid model, as well as simplifying elements of the vibrational model so that it is less computationally intensive. One issue which arose with the previous vibrational model was the long computation times approximately 30 minutes and high demand on computer resources approximately 30GB of RAM with another 30 to 60 GB of temporary hard drive space. After discussion with many industry professionals it came to light that the model could be greatly simplified by replacing the 3D elements of the model with 1D and 2D elements. A proper testing procedure needs to be finalized, this is especially important for deciding on the placement of the sensor locations. The corroboration of the simulation results to testing results requires understanding the relationship between the location of sensor placement and frequency response, this aspect of instrumentation was made clear during the vibrational testing of the satellite.

The thermal and vacuum testing of the satellite is still yet to be tested. Unfortunately at the time of our environmental testing the use of the Thermal Vacuum chambers was not permissible due to other testing and maintenance. This aspect of the environmental testing leaves a large unknown as to how the satellite will correlate to its modeling. More work is required for simulating the thermal models of the satellite, as

well as developing a proper testing procedure so that simulation results can be correlated to the obtained testing results. Much of the work left in the thermal modeling of the satellite is to accurately model the cross coupling of heat transfer through the structural members of the satellite that are being used as a heat sink.

Further design work could also be conducted in ameliorating the mechanical and electrical system for full system integration. Some of the problems encountered during final assembly of the satellite with the coaxial connectors and the insertion of the bus connectors could be improved with small design changes to the location of the connectors and the board outlines of the printed circuit boards.

Current work on the design revisions of the satellite is progressing and the recommended changes are being implemented for the next revision.

7 REFERENCES

[1] Canadian Satellite Design Challenge Management Society Inc., "Home," Canadian Satellite Design Challenge, 2014. [Online]. Available: http://www.csdcms.ca/. [Accessed 20 10 2014].

[2] Canadian Satellite Design Challenge, "CSDC Rules and Requirements," 10 2012. [Online]. Available: http://geocentrix.ca/images/CSDC_Files/CSDC_Rules_2a.pdf. [Accessed 17 10 2014].

[3] International Telecom Union, "Committed to connecting the world," ITU, 15 05 2014. [Online]. Available: http://www.itu.int/en/Pages/default.aspx. [Accessed 03 10 2014].

[4] United Nations, "Committee on the Peaceful Uses of Outer Space," United Nations, 11 06 2014. [Online]. Available: http://www.oosa.unvienna.org/oosa/COPUOS/copuos.html. [Accessed 05 10 2014].

[5] Canadian Satellite Design Challenge, "Information for Teams," 2014. [Online]. Available: http://csdcms.ca/images/Documents/CSDC_DIETR_3a_RELEASED_2014-10.pdf. [Accessed 11 10 2014].

[6] D. P. Schreurs, "Warpage of Printed Circuit Boards," Mechanical Engineering Computational and Experimental Mechanics, Eindhoven, 2005.

[7] M. Pecht, "Why the traditional reliability prediction models do not work – is there an alternative?," *ElectronicsCooling,* vol. 2, pp. 10-12, 1996.

[8] D. Das, "Use of Thermal Analysis Information in Avionics Equipment Development," *ElectronicsCooling,* vol. 5, pp. 28-34, 1999.

[9] M. Osterman, "We still have a headache with Arrhenius," *ElectronicsCooling,* vol. 7, pp. 53-54, 2001.

[10] P. Lall, M. Pecht and E. Hakim, "Influence of temperature on Microelectronics and System reliability," CRC Press, New York, 1997.

[11] D. Humphrey, L. Condra, N. Pends, D.Das, C. Wilkinson and M. G. Pecht, "An Avionics Guide to Uprating of Electronic Parts," *IEEE Trans,* vol. 23, no. 3, pp. 595-599, 2000.

[12] Advanced Cooling Technologies, Inc, "VCHPS FOR PASSIVELY CONTROLLING TEMPERATURE," Innovations in Action, March 2013. [Online]. Available: http://www.1-act.com/vchps-for-passively-controlling-temperature/. [Accessed 5 October 2013].

[13] W. Anderson, " Variable Conductance Heat Pipes for Variable Thermal Links," in *42nd International Conference on Environmental Systems (ICES 2012)*, San Diego, 2012.

[14] P. Dussinger, "High Heat Flux, High Power, Low Resistance, Low CTE Two-Phase Thermal Ground Planes for Direct Die Attach Applications," in *GOMACTech*, Las Vegas, 2012.

[15] Ku, J.; Ottenstein, L.; Pham, T.; Douglas, D.;, "Multi-Evaporator Miniature Loop Heat Pipe for Small Spacecraft Thermal Control," in *NASA Space Technology Conference*, College Park, 2007.

[16] Ku, J.; Paiva, K.; Mantelli, M.;, "Loop Heat Pipe Transient Behavior Using Heat Source Temperature for Set Point Control with Thermoelectric Converter on Reservoir," NASA. Goddard Space Flight Center, Greenbelt, 2011.

[17] F. P. Incropera, D. P. Dewitt, T. L. Bergman and A. S. Lavine, Fundamentals of Heat Mass Transfer, Hoboken: Wiley, 2011.

[18] J. Ohmori, T. Kobayashi, M. Yamada, H. Iida and T. Horie, "Mechanical behavior of graphite first wall during disruptions," *Fusion Engineering and Design,* vol. 9, pp. 201-205, 1989.

[19] H. Shinno, M. Kitajima and J. M. Okada, "Thermal stress analysis of high heat flux materials," *Journal Of Nuclear Materials,* Vols. 155-157, pp. 290-294, 1989.

[20] Momentive, "Pyrolytic Graphite," Momentive, 10 6 2013. [Online]. Available: http://www.momentive.com/products/main.aspx?id=22873. [Accessed 24 8 2013].

[21] MiNTEQ, "Pyrolytic Graphite," MiNTEQ, 9 2013. [Online]. Available: http://www.mineralstech.com/Pages/Minteq/Pyrolitic-Graphite.aspx. [Accessed 24 8 2013].

[22] Panasonic, "Thermal Protection: Pyrolytic Graphite Sheet," Panasonic Industrial, 12 6 2013. [Online]. Available: http://na.industrial.panasonic.com/products/circuit-thermal-protection/thermal-protection/pyrolytic-graphite-sheet-pgs. [Accessed 20 8 2013].

[23] C., Mauney, "Thermal Considerations for Surface Mount Layouts," 20 20 2010. [Online]. Available: http://focus.ti.com/download/trng/docs/seminar/Topic%2010%20-%20Thermal%20Design%20Consideration%20for%20Surface%20Mount%20Layouts%20.pdf. [Accessed 20 08 2013].

[24] Y. A. S. Y. Hirokazu Tanaka, "Confirming Reliability of Printed Circuit Boards with Temperature Cycle and Thermal Shock," ESPEC Corp, Hudsonville, 1996.

[25] Electronics Cooling, "Conduction heat transfer in a printed circuit board," Scientific Research Publishing, Philadelphia, 1998.

[26] The Aluminum Association Inc., "Aluminum Standards and Data," Make it From, 2006. [Online]. Available: http://www.makeitfrom.com/material-data/?for=6061-T6-Aluminum. [Accessed 15 8 2013].

[27] Electro Optical Industries Inc, "Material Emissivity Properties," 9 2013. [Online]. Available: http://snap.fnal.gov/crshield/crs-mech/emissivity-eoi.html. [Accessed 20 8 2013].

[28] K. Azar and G. J. E, "Experimental Determination of Thermal Conductivity of Printed Wiring Boards," in *Twelfth IEEE SEMI-THERM Symposium*, Austin, 1996.

[29] American Society for Metals, Aluminum: Properties and Physical Metallurgy, Russel Township: American Society for Metals, 1984, pp. 1-57.

[30] P. Teertstra, "Calculating interface resistance," Electronics Cooling, Philadelphia, 1997.

Appendix A RANDOM VIBRATION SPECIFICATION

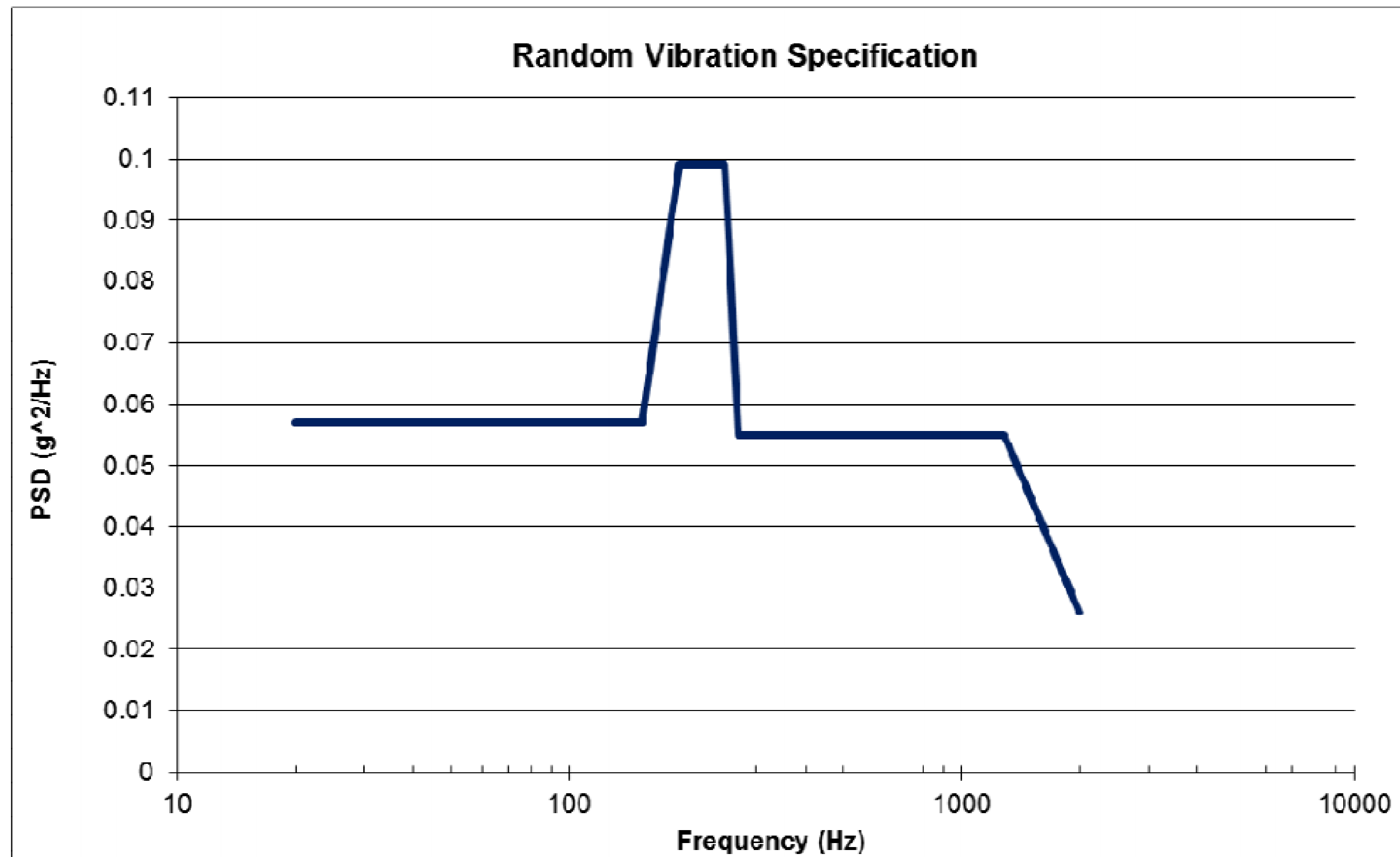

Figure A.1: Random Vibration Specification

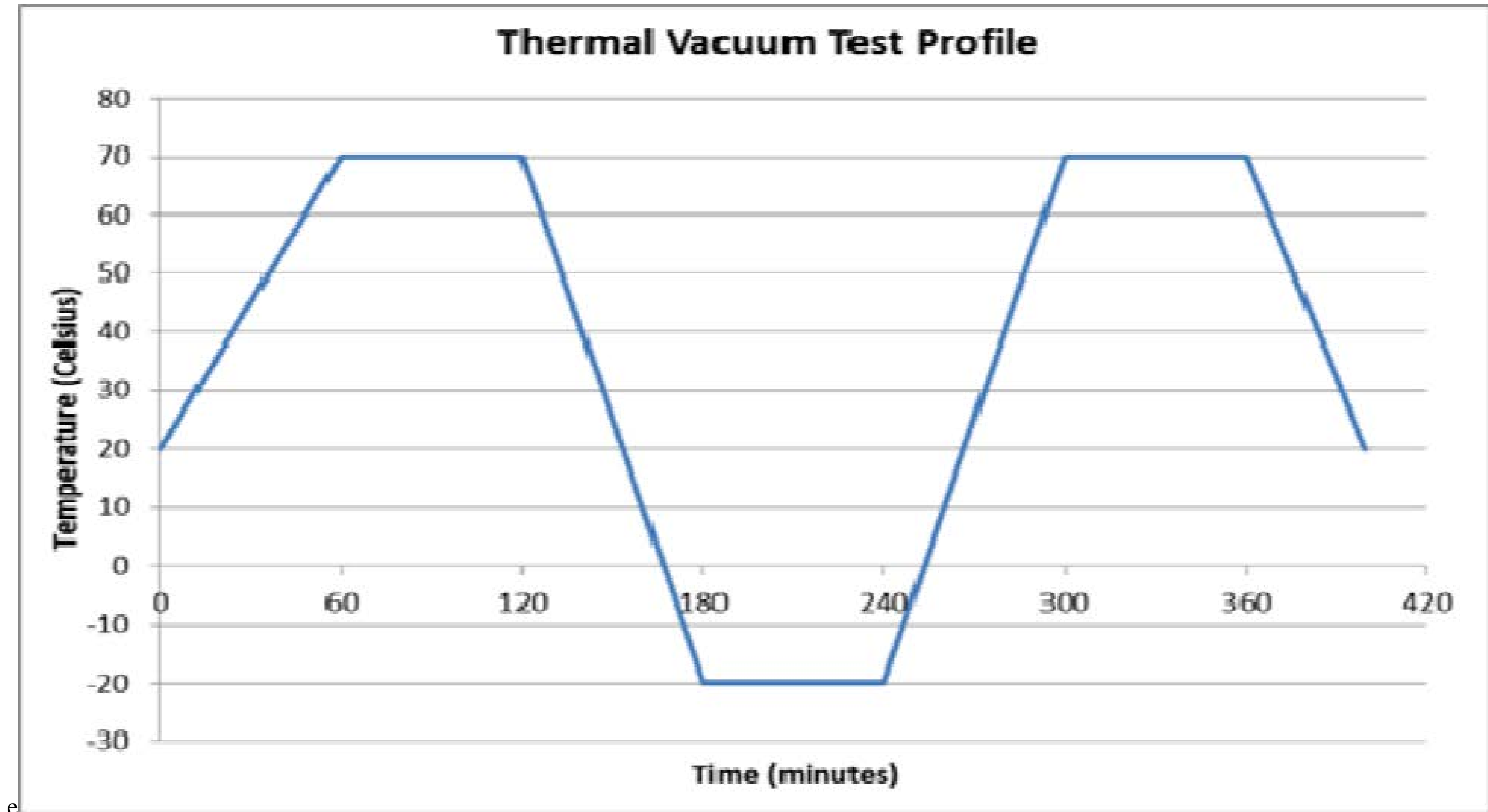

e

Figure B.2: Thermal Vacuum Test Profile

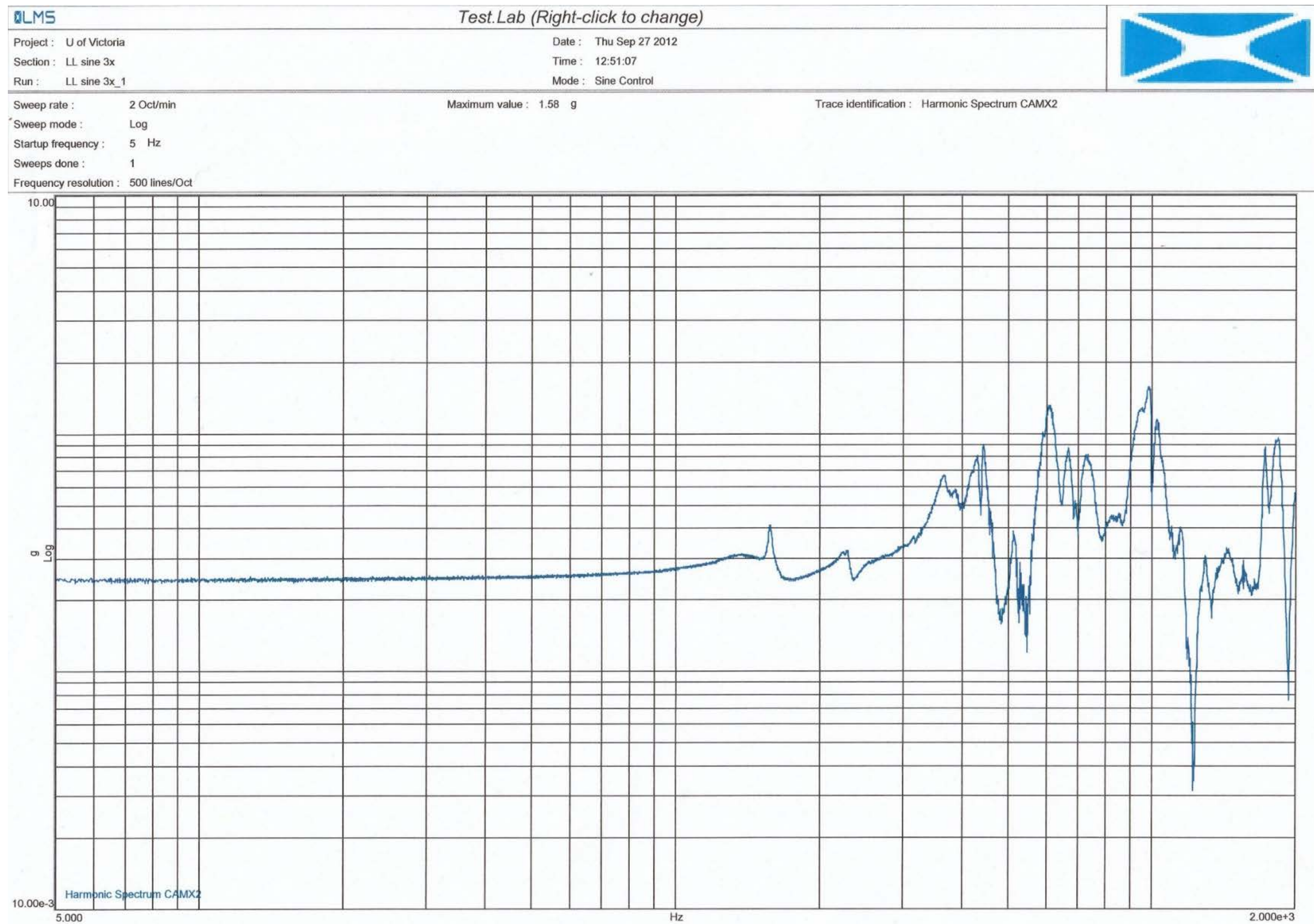

Figure C.3: X Plane Frequency Response

LMS

Test.Lab (Right-click to change)

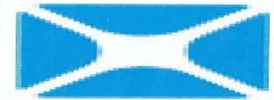

Project : U of Victoria

Section : LLsine 3y

Run : LLsine 3y_1

Date : Thu Sep 27 2012

Time : 09:57:25

Mode : Sine Control

Sweep rate : 2 Oct/min

Sweep mode : Log

Startup frequency : 5 Hz

Sweeps done : 1

Frequency resolution : 500 lines/Oct

Maximum value : 1.86 g

Trace identification : Harmonic Spectrum CAMX2

10.00

g
Log

1.000e-3

Harmonic Spectrum CAMX2

5.000

Hz

2.000e+3

Figure C.4: Y Plane Frequency Response

LMS

Test.Lab (Right-click to change)

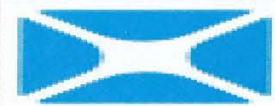

Project : U of Victoria
Section : LLsine 3z
Run : LLsine 3z_1

Date : Thu Sep 27 2012
Time : 11:59:43
Mode : Sine Control

Sweep rate : 2 Oct/min
Sweep mode : Log
Startup frequency : 5 Hz
Sweeps done : 1
Frequency resolution : 500 lines/Oct

Maximum value : 1.98 g

Trace identification : Harmonic Spectrum CAMX2

10.00

g
Log

1.000e-9

Harmonic Spectrum CAMX2

5.000 Hz 2.000e+3

Figure C.5: Z Plane Frequency Response

Appendix D 2014 VIBRATION TESTING RESULTS

The following table cross-references the name and axis of measurement for the instrumentation package that was affixed to the satellite during testing in May 2014. The first six sensors were used as control inputs the last nine were used for the measurement of the satellite

Table D-1: Sensor Legend

Sensor Name	Series #
MC1X	1
MC1Y	2
C1Z	3
MC2X	4
MC2Y	5
C2Z	6
M1X	7
M2Y	8
M3Z	9
M4X	10
M5Y	11
M6Z	12
M7X	13
M8Z	14
M9X	15

Figure D.6: 1st X-Axis Low Level Sine Response

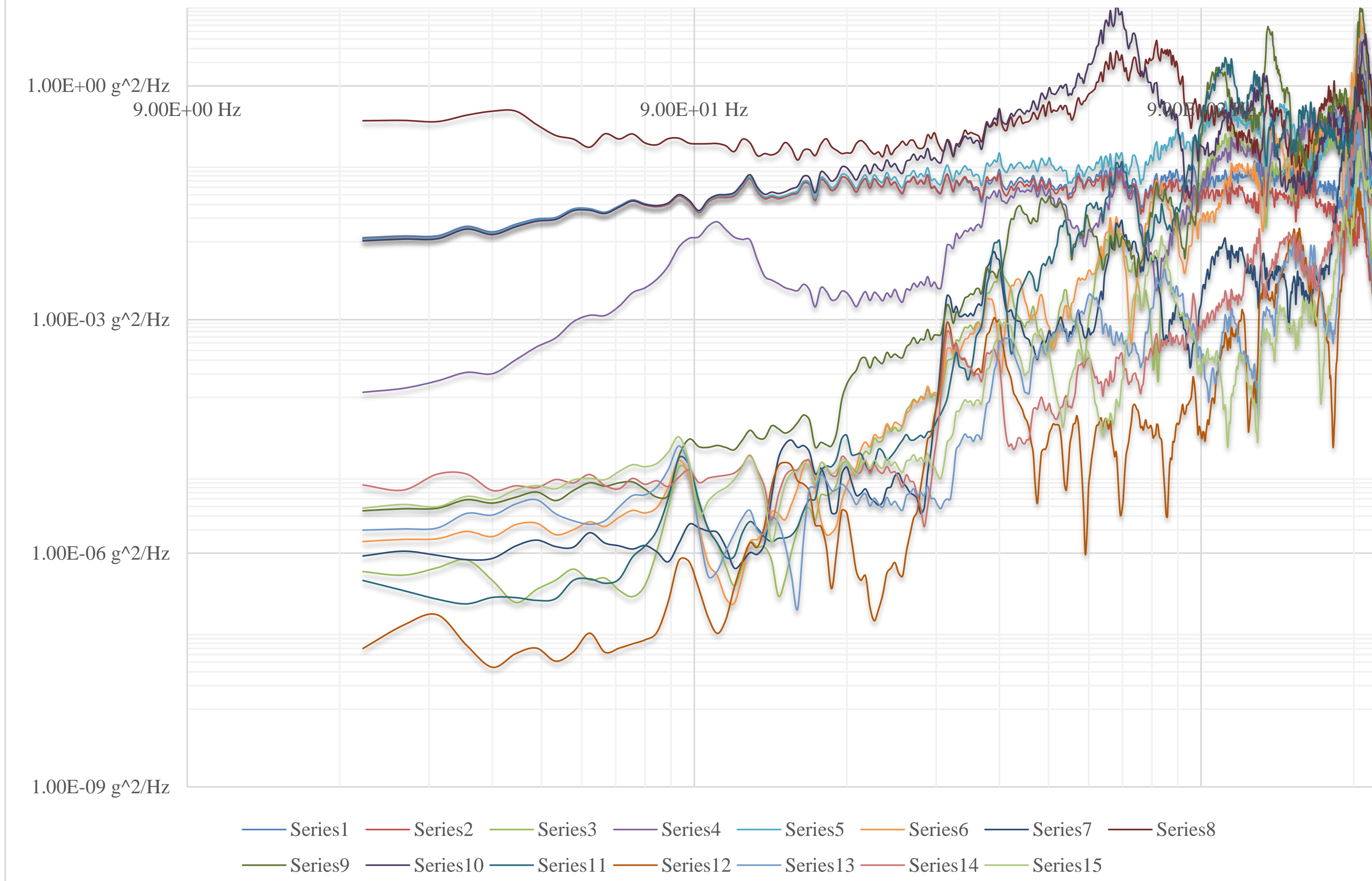

Figure D.7: X-Axis Random Vibration Response

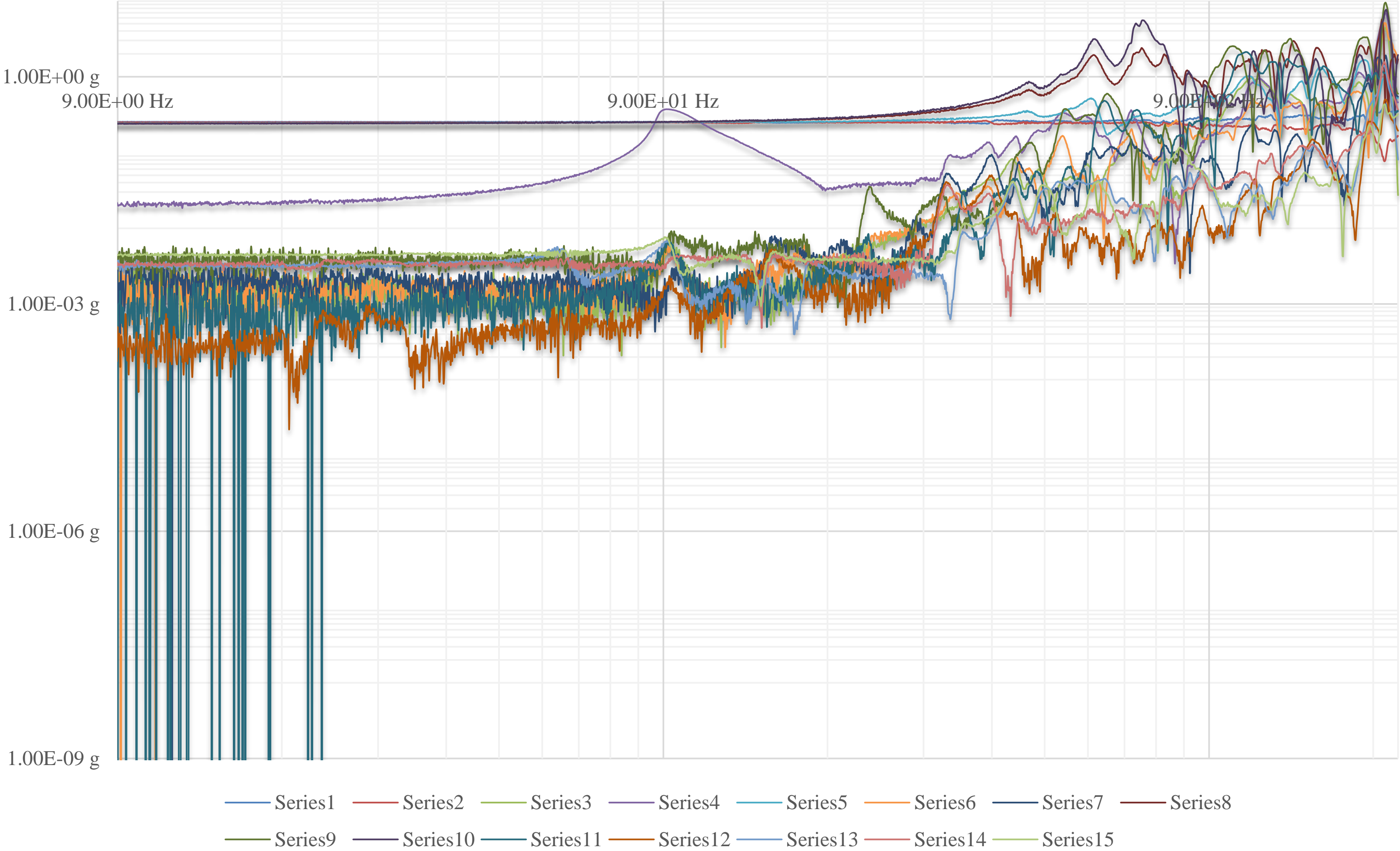

Figure D.8: 2nd X-Axis Low Level Sine Response

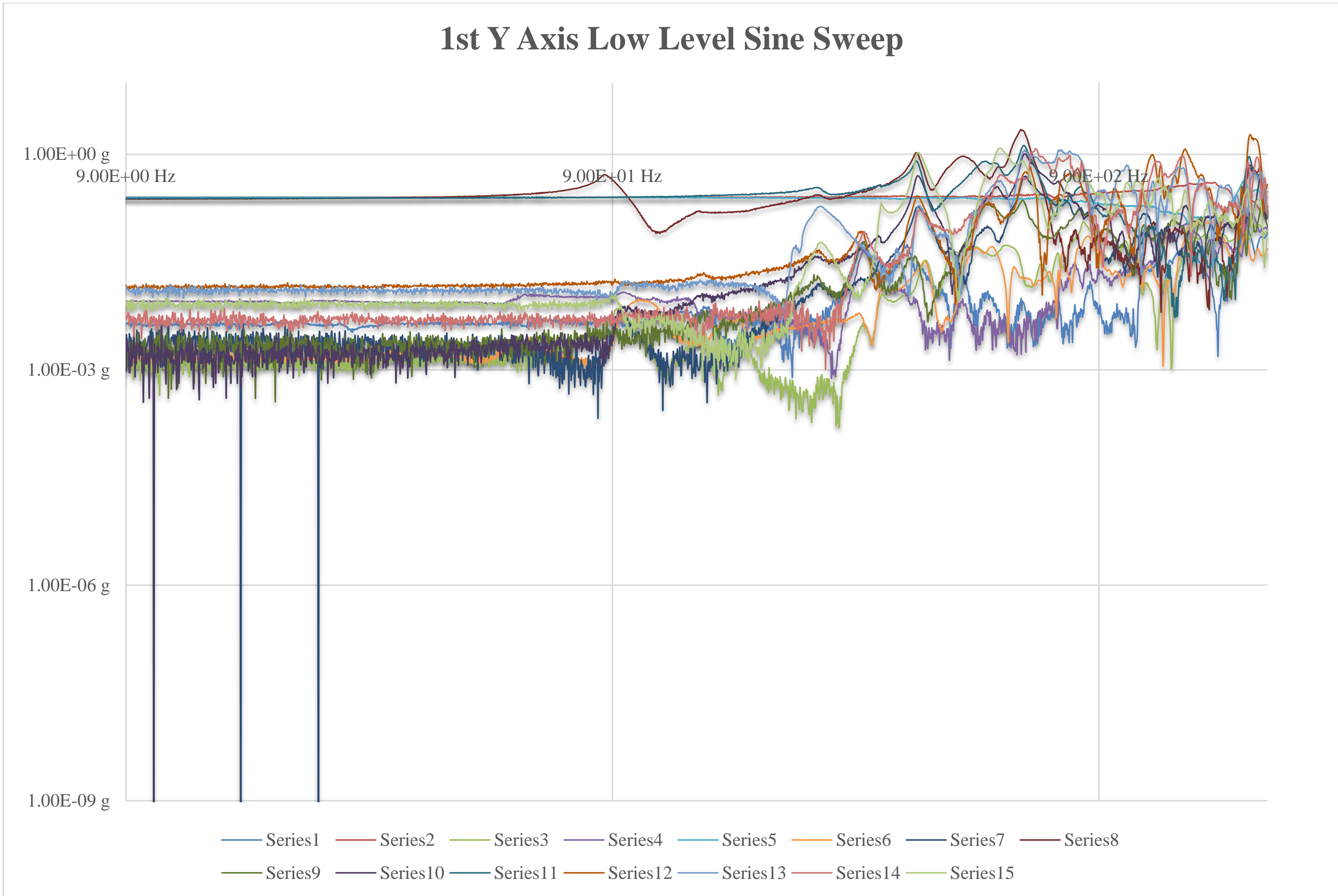

Figure D.9: 1st Y-Axis Low Level Sine Response

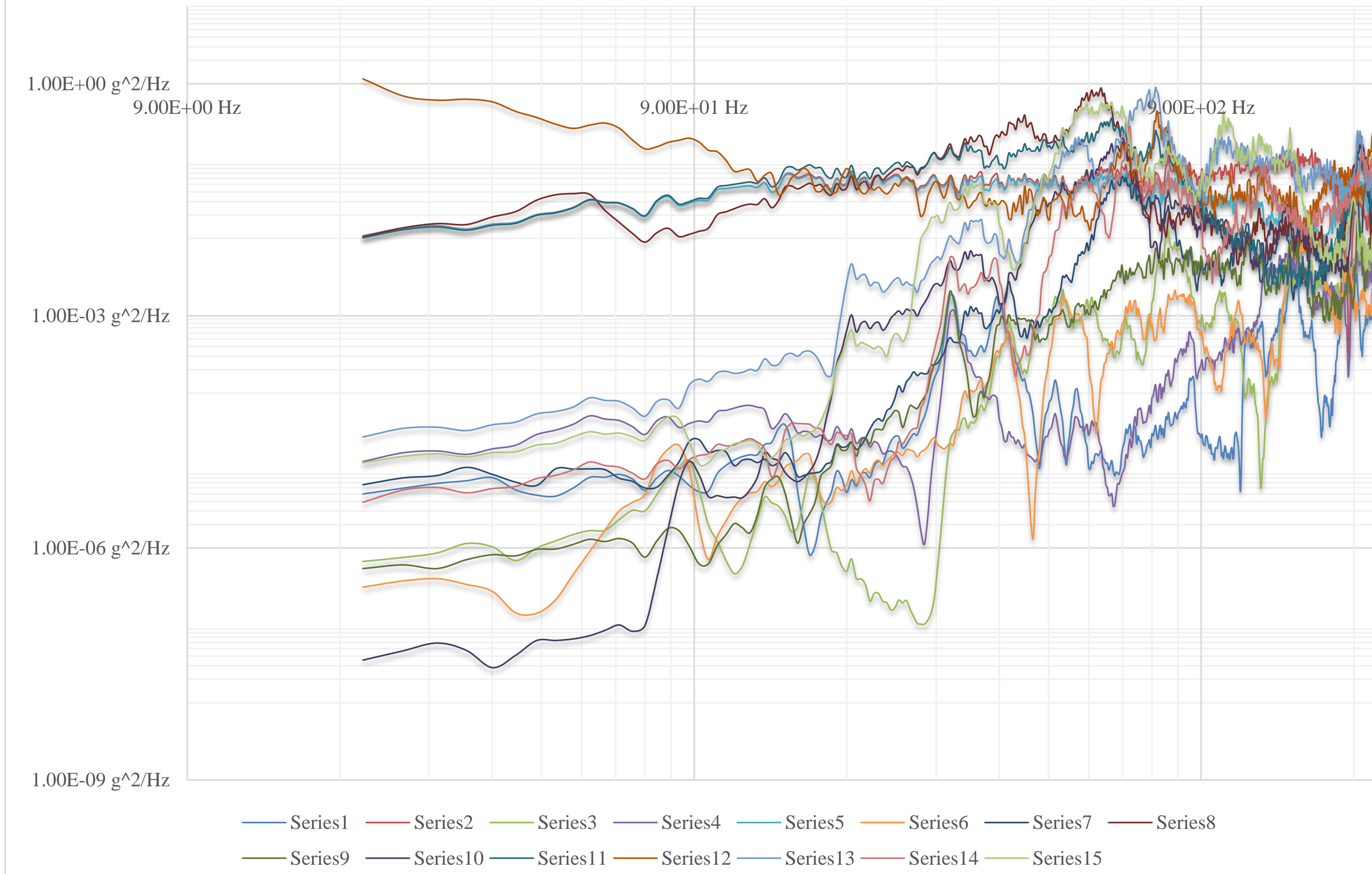

Figure D.10: Y-Axis Random Vibration Response

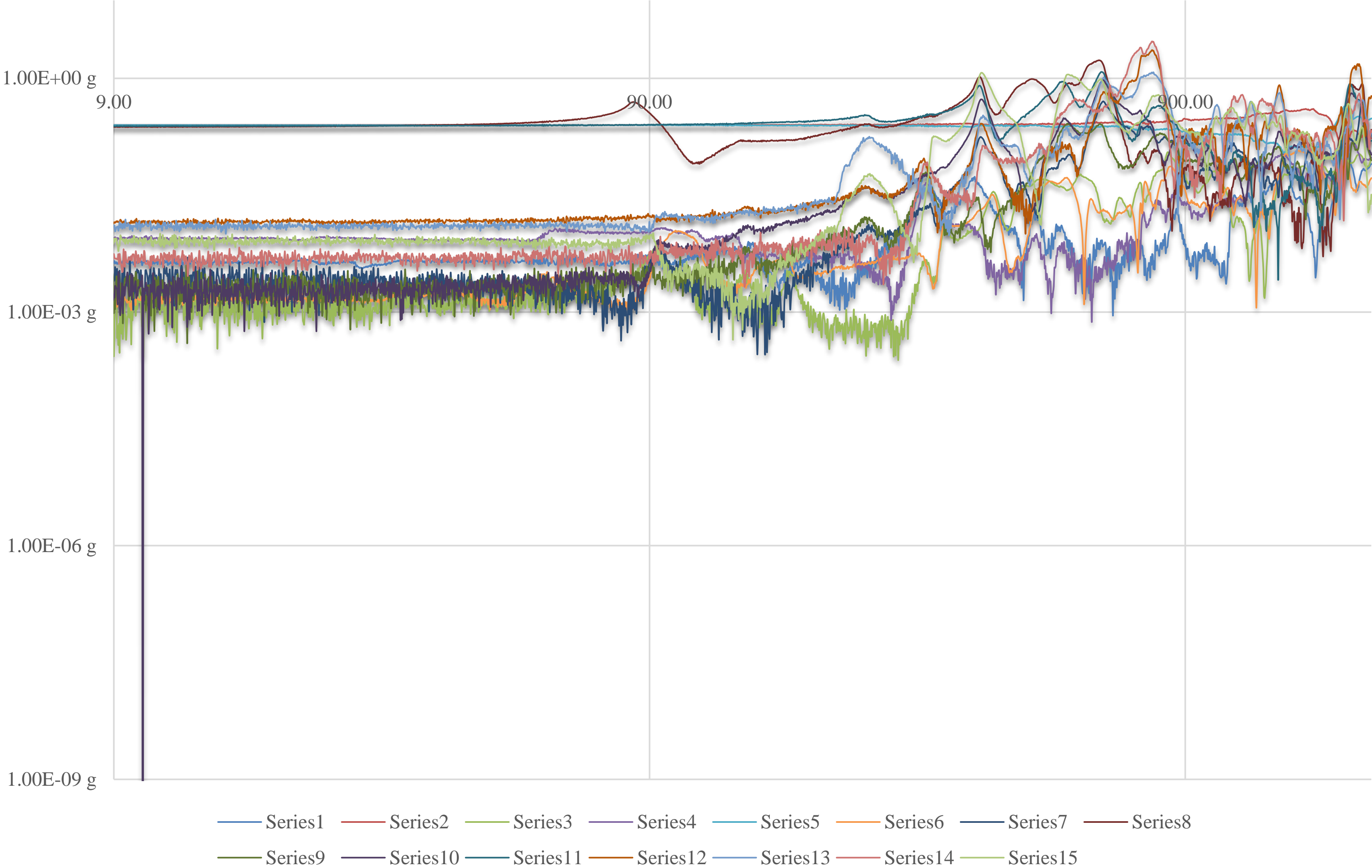

Figure D.11: 2nd Y-Axis Low Level Sine Response

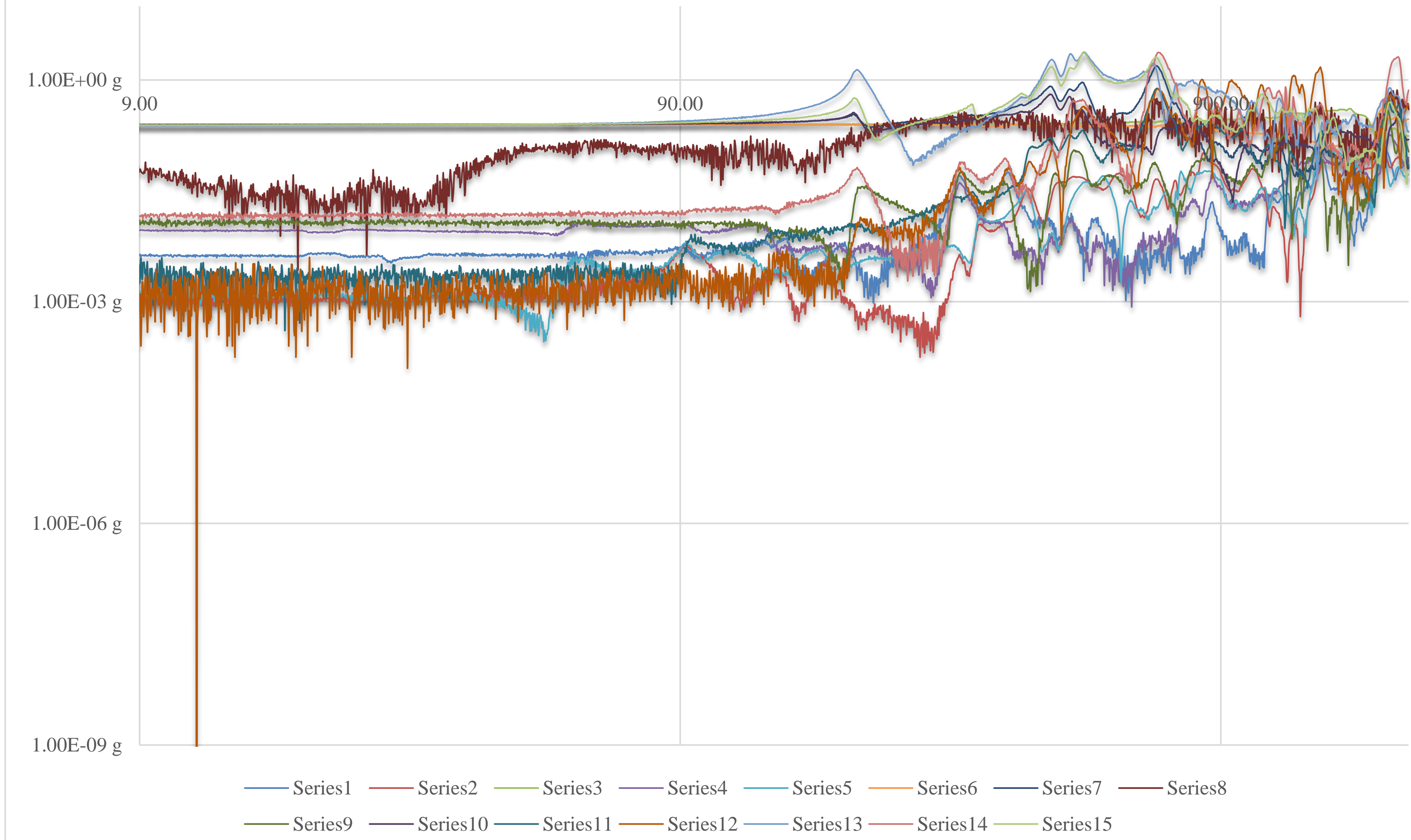

Figure D.12: 1st Z-Axis Low Level Sine Response

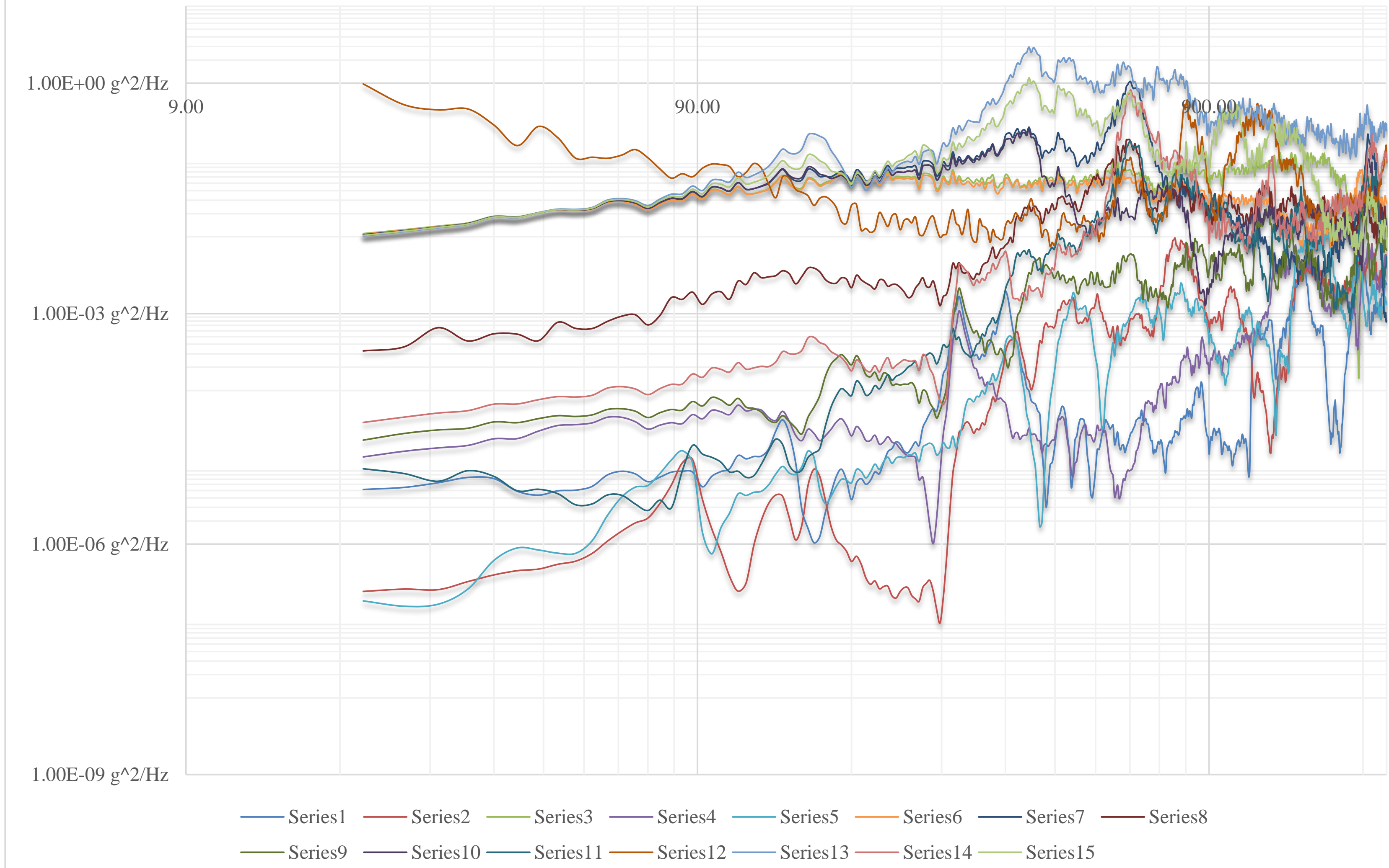

Figure D.13: Y-Axis Random Vibration Response

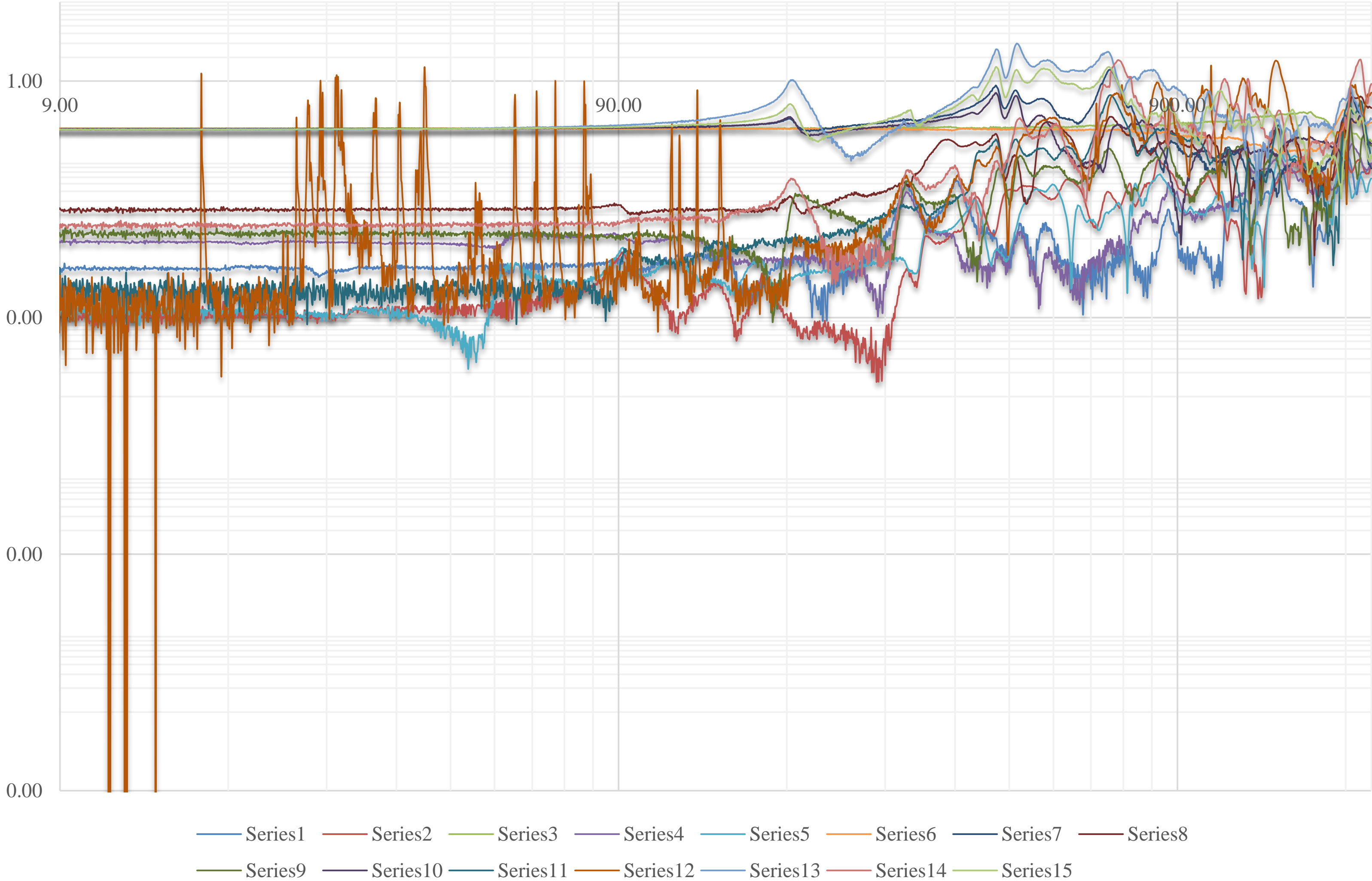

Figure D.14: 2nd Z-Axis Low Level Sine Response